Inertial Sensors in Estimating Spatio-Temporal Parameters of Walking: Performance Evaluation and Error Analysis

by

Shuozhi Yang

A thesis submitted to the
Mechanical & Materials Engineering
in conformity with the requirements for
the Degree of Master of Applied Science

Queen's University
Kingston, Ontario, Canada
August 2011

Abstract

The portability, ease of use and improved accuracy of miniature inertial sensors brought by current microelectromechanical system (MEMS) technology has inspired researchers to develop human movement monitoring system with body-fixed sensors. Although a large number of studies have attempted to explore the use of miniature inertial sensors in estimating walking speed for the past two decades, there still remain some questions regarding applying inertial sensors in estimating walking speed under different walking conditions and for different subject populations. In this thesis, I focus on evaluating and improving the performance of a shank-mounted mounted inertial measurement unit (IMU) based walking speed estimation method. My research can be divided into four parts. The first part was a systematic review regarding the state of the art of current development of the inertial sensor based walking speed estimation method. A total of 16 articles were fully reviewed in terms of sensor specification, sensor attachment location, experimental design and spatial parameter estimation algorithm. In the second part, a comprehensive performance evaluation was conducted, which included the treadmill and overground walking experiments with constraint on the walking speed, stride length and stride frequency. A systematic error was observed in the error analysis of this study, which was adjusted by subtracting the bias by linear regression. In the third part, a post-stroke subject

overground walking experiment was carried out with an improved walking speed estimation method that reduced the systematic error caused by previous false initial speed assumption. In addition to walking speed estimation, the gait asymmetry for post-stroke hemiparetic gait was also evaluated with the proposed method. The last part was the sensor error model analysis. We elaborately analyzed and discussed the estimation errors involved in this method in order to completely understand the sensor error compensation in walking speed estimation algorithm design. Two existing sensor error models and one newly developed sensor error model were compared with the treadmill walking experiment, which demonstrated the effect of each sensor error component on the estimation result and the importance of the sensor error model selection.

Acknowledgments

I would like to sincerely thank the people who made this thesis possible.

It is difficult to overstate the help, both in research and life, I received from my supervisor, Dr. Qingguo Li. Since the first day of my grad school, his knowledge, experience, inspiration, enthusiasm and kindness have been invaluable to me. He is very thoughtful and always comes up with cool ideas about research that eventually led me to the completion of this thesis.

I wish to thank Dr. Qingguo Li, Dr. Brenda Brouwer, Alison C Novak, Jun-Tian Zhang, Chris Mohr and Annemarie Laudanski, who provided me great help in the preparation of my papers written in my grad school. Also thanks to Dr. Kelvin Deluzio, Scott Brandon, Stacey Acker, Allison Clouthier, and all members in JAM, who gave me the opportunity to be exposed in different aspects of biomechanical researches.

Special thanks to my parents, Hua Yang and Jianxi Ren. They bore me, raised me, supported me, taught me and loved me throughout my life. Lastly, I am grateful for my girlfriend, Huan Jin, for her understanding, support and love in these years.

Co-Authorship

While the primary responsibility for this thesis rests with the author, Shuozhi Yang, others have contributed to the studies described herein. I would like to gratefully acknowledge my collaborators as co-authors on the following manuscripts and conference proceedings:

Chapter 3

- S. Yang and Q. Li. Ambulatory walking speed estimation under different step length and frequency. In IEEE/ASME International Conference on Advanced Intelligent Mechatronics, pages 658–663, 2010.

- S. Yang and Q. Li. IMU-based ambulatory walking speed estimation in constrained treadmill and overground walking. Computer Methods in Biomechanics and Biomedical Engineering, 2011. First Published on: 02 February, 2011.

Chapter 4

- S. Yang, A. Laudanski and Q. Li. An ambulatory spatio-temporal analysis system for post-stroke hemiparetic gait using shank-attached IMUs. Medical Engineering & Physics, 2011. (Submitted)

Chapter 5

- S. Yang, J.T. Zhang, A.C. Novak, B. Brouwer and Q. Li. Inertial sensors in estimating walking speed and inclination: an evaluation of sensor error models. Medical & Biological Engineering & Computing, 2011. (Submitted)

Table of Contents

List of Tables

List of Figures

Glossary

ANOVA Analysis of Variance.

CABGCS Constant Acceleration Measurement Biases in Global Coordinate System.

CABSCS Constant Acceleration Measurement Biases in Sensor Coordinate System.

COM Center of Mass.

DOF Degree of Freedom.

FF Foot Flat.

HD Heel Down.

HS Heel Strike.

IMU Inertial Measurement Unit.

MEMS Microelectromechanical System.

MSE Mean Squared Error.

RMSE Root Mean Squared Error.

SD Standard Deviation.

SL Stride Length.

SLR Stride Length Ratio.

SSR Stance/Swing Ratio.

TO Toe Off.

ZUPT Zero Velocity Update.

Chapter 1

Introduction

1.1 Motivation

Walking is the main form of human locomotion and the most frequently performed daily activity, and human gait analysis is commonly utilized in biomechanical research, clinical assessment of abnormal gait, development of prostheses, orthoses, exoskeletons, and energy harvester. In many aspects of human gait studies, walking speed has long been recognized as an essential measure of human walking performance and widely used in pathological gait assessment. In clinical studies, the walking speed is generally defined as the average velocity of human body in the direction of progression. Traditional instrumentation of measuring walking speed varies from stopwatch to camera-based motion capture system, which suffer from either low accuracy or complicated setup. Recent development of microelectromechanical system (MEMS) offers the possibility of measuring gait parameters using body-fixed miniature inertial sensors, i.e. miniature accelerometers and gyroscopes. With the acceleration and angular velocity data collected by the inertial sensor, the motion of the specific

body segment where the sensors are attached can be estimated accordingly, which can further be used to determine the walking speed.

1.2 Objective

The primary objective of this research is to evaluate the performance of a shank-mounted inertial sensor-based walking speed estimation method under different constrained walking conditions and with post-stroke hemiparetic gait. A secondary objective is to analyze the errors involved in this method and improve the performance based on the error analysis.

1.3 Contributions

Since most of my researches have been published in, submitted to or in preparation for conference proceedings or scientific journals, I summarize the contributions as follows.

1.3.1 Systematic review for inertial sensor based walking speed estimation method.

Focusing on inertial sensor based walking speed estimation method, a systematic review was done in four major electronic engines/databases: PubMed, ISI Web of Knowledge, SportDiscus and IEEE Xplore. The sensor specification, sensor attachment location, experimental design and spatial parameter estimation algorithm were completely reviewed. This work is in preparation for submission to a scientific journal.

1.3.2 Validation of the shank-mounted IMU based walking speed estimation method.

A comprehensive evaluation of a shank-mounted IMU based walking speed estimation method was performed under constrained walking conditions, which included both treadmill and overground walking experiments with different constraints on the walking speed, step length and step frequency. This work has been partially reported in the Proceedings of the 2010 IEEE/ASME International Conference on Advanced Intelligent Mechatronics (AIM) [1] and fully published in Computer Methods in Biomechanics and Biomedical Engineering [2].

1.3.3 Investigation of the feasibility of applying the method on post-stroke hemiparetic gait.

The concept of using two IMU's, one on each shank, to estimate the walking speed and the gait asymmetry information simultaneously was investigated with post-stroke subjects in the 10-meter walking test (10MWT). Improvements of the algorithm was made to correct the estimation error resulted from the approximation of the initial sensor velocity. This work has been submitted to Medical Engineering & Physics [3].

1.3.4 Improvement of the accuracy of the algorithm and analysis of the sensor errors.

A comparison study between three sensor error models, including two common sensor error models used in inertial sensor based gait analysis method and one newly developed sensor error model, was experimentally conducted to analyze the effect of the

sensor error compensation method on the estimation result. The selection of sensor error model was elaborately discussed in this study. This work has been submitted to Medical & Biological Engineering & Computing [4].

1.4 Organization of Thesis

The outline of the thesis is as follows. The next chapter first provides a complete review of existing walking speed estimation methods from the literature. Chapter 3 evaluates a shank-mounted IMU based walking speed estimation algorithm from our previous study. Chapter 4 investigates the feasibility of using an improved walking speed estimation algorithm in the application of assessing post-stroke hemiparetic gait. Different IMU sensor error models used in the algorithm are discussed and evaluated in Chapter 5. Chapter 6 concludes and outlines future work.

References

[1] S. Yang and Q. Li. Ambulatory walking speed estimation under different step length and frequency. In *IEEE/ASME International Conference on Advanced Intelligent Mechatronics, 2010.*, pages 658–663, 2010.

[2] S. Yang and Q. Li. Imu-based ambulatory walking speed estimation in constrained treadmill and overground walking. *Computer Methods in Biomechanics and Biomedical Engineering*, 2011. First published on: 02 February, 2011.

[3] S. Yang, J.T. Zhang, A.C. Novak, B. Brouwer, and Q Li. An ambulatory spatio-temporal analysis system for post-stroke hemiparetic gait using shank-attached imus. *Medical Engineering & Physics (Submitted)*, 2011.

[4] S. Yang, A. Laudanski, and Q. Li. Inertial sensors in estimating walking speed and inclination: an evaluation of sensor error models. *Medical & Biological Engineering & Computing (Submitted)*, 2011.

Chapter 2

Inertial Sensors in Human Walking Speed Measurement: A Systematic Review

Abstract

Self-selected walking speed is an important measure of the ambulation ability and the gait rehabilitation level and commonly measured in various clinical gait experiments. Miniature inertial sensors, i.e. accelerometers and gyroscopes, have been gradually introduced to walking speed estimation and attracted a lot of attentions for the the past two decades, because of their small size and low weight. With the intention to understand the state of the art of current development, a systematic review was done in the following electronic engines/databases: PubMed, ISI Web of Knowledge, SportDiscus and IEEE Xplore. Sixteen journal articles and papers in proceedings focusing on inertial sensor based walking speed estimation method were fully reviewed.

The existing methods can be categorized by sensor specification, sensor attachment location, experimental design and spatial parameter estimation algorithm. Further system development and performance evaluation is desired for practical applications.

2.1 Introduction

With the development of microelectromechanical system (MEMS), the use of miniature inertial sensors, i.e. accelerometers and gyroscopes, in human biomechanical studies has drawn huge attentions because of their portability, self-containedness and promising performance in providing motion information [1]. Instead of measuring human gait features via traditional instruments with limited accuracy, e.g. stopwatch, or complex camera based motion tracking system, inertial sensors with appropriate algorithms are capable of accomplishing specific biomechanical research tasks, such as physical activity monitoring and ambulatory ability assessment [2].

Self-selected walking speed has long been recognized as a proxy measure of ambulation quality and is used to quantify the progress of gait rehabilitation [3, 4, 5, 6]. Since 1990s, many studies have been conducted with the focus of estimating human walking speed or stride length with inertial sensors. In 1995, Aminian *et al.* [7] developed a walking speed estimation method based on the patterns present in the body acceleration signals. Two neural networks were utilized to process the acceleration signals collected from the back (3 orthogonal directions) and the heel (forward direction). Although Aminian's attempt successfully estimated a wide range of walking speeds with maximum error of 16%, large amounts of training time and training data are required in order to achieve more accurate speed estimation. Later studies focused more on processing the inertial sensor data based on physical principles. For

example, Miyazaki [8] proposed a gyroscope based stride length estimation method using a symmetric single-segment human gait model. In this method, each leg was simplified as a single segment while the angle of the leg segment was determined by integrating the angular velocity measurement from the gyroscope attached to the thigh. A walking speed estimation algorithm using both the accelerometer and gyroscope measurements was first introduced by Tanaka *et al.* in 2004 [9]. Their algorithm was basically the same as the method proposed by Miyazaki [8]; however, in addition to the simplified gait model, Tanaka *et al.* used the thigh acceleration to establish the initial condition for the thigh angle calculation. Instead of using neural network or gait model, a direct walking speed estimation method is to obtain comprehensive inertial information from an inertial measurement unit (IMU), consisting of accelerometers and gyroscopes, and then directly integrate the measured accelerations in global coordinate system. Based on the idea of direct integration, Sabatini *et al.* [10] made use of the inertial data collected by an foot-mounted IMU to estimate the average walking speed, while Li *et al.* [11] proposed an algorithm with a shank-mounted IMU. In both studies, the sensor orientation was determined by integrating the angular velocity measurement, and the acceleration measurements were projected to the global coordinate system according to the sensor orientation. As wide range of inertial sensors as well as configurations have been adopted in estimating walking speed, it is certainly of interest to exam how they were utilized and how well they could perform. This systematic review is focused on the use of inertial sensors specifically for walking speed estimation, aiming to analyze and review the existing techniques.

2.2 Methods

2.2.1 Review Questions

We systematically reviewed the literature regarding the inertial sensor-based walking speed estimation methods, and attempted to answer the following questions: (1) What are the existing inertial sensor based walking speed estimation methods? (2) What types of inertial sensors were used in related studies? (3) Where were the inertial sensors attached? (4) How were the experiments conducted? and (5) How was the performance of these studies?

In order to answer all the questions, we reviewed the literatures on inertial sensor based walking speed, step length or walking distance estimation methods.

2.2.2 Article Selection

The research method is graphically depicted in Figure 2.1 for better understanding of the procedure. We systematically searched for published journal articles and papers in proceedings in PubMed (from 1950), ISI Web of Knowledge (Science Citation Index Expanded, from 1899; Social Sciences Citation Index, from 1956; Art & Humanities Citation Index, from 1975), SportDiscus (from 1950) and IEEE Xplore (from 1950) at the first week of July in year 2011. These four electronic engines/databases were chosen because of their popularity and their coverage of literature in engineering, medicine and biomechanics. The searched keyword string was "*(assessment OR estimation OR calculation OR computation OR measurement) AND (inertial sensor OR accelerometer OR gyroscope OR inertial measurement unit) AND (speed OR velocity OR step length OR stride velocity OR stride length) AND (walking)*" appeared in

title, abstract and keyword fields of the articles. The initial total number of identified articles was 344. The title and the abstract of each article was read carefully for the first selection stage, and unrelated and duplicated articles were excluded, which reduced the number of articles to 47. In the second selection stage, these 47 full articles were retrieved from Queen's University library system and completely reviewed. A total of 16 full articles were ultimately included in this review. The inclusion criteria were as follows: (1) The study involved inertial sensors, i.e. accelerometers and/or gyroscopes, and (2) The study reported walking speed, stride length or walking distance estimation results. However, as this review focuss on method development, articles only containing the following contents were excluded: (1) Performance evaluation of commercial products, (2) Performance comparison between existing methods, and (3) Applications based on previous reported methods.

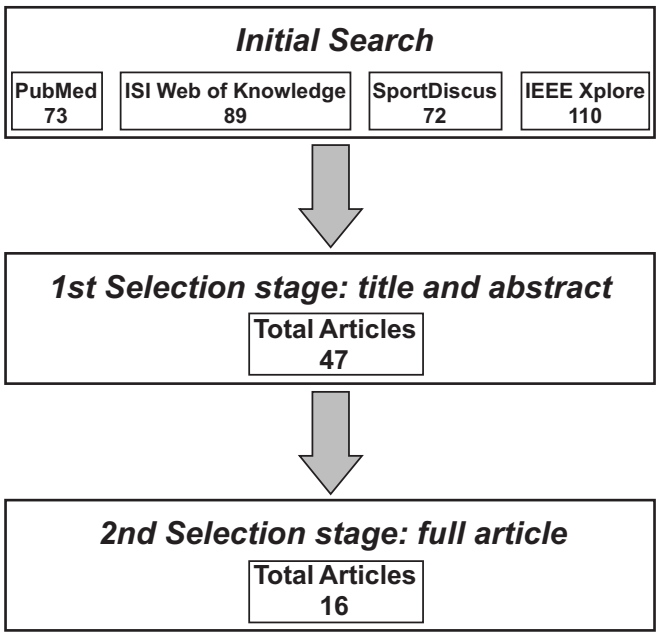

Figure 2.1: Article review procedures. After the initial search, the title and abstract were reviewed first to exclude unrelated articles. The full articles were then retrieved and review with the detailed inclusion/exclusion criteria. 16 articles were finally included in this review.

2.3 Results and Discussion

2.3.1 Sensor Specification

Large varieties of inertial sensors are currently available in the market, ranging from uniaxial accelerometer/gyroscope to IMU with 6 degree of freedom (6DOF). The measuring range of the inertial sensors varies with the specifications, from $\pm 2g$ to $\pm 50g$ for accelerometers and from $\pm 150°/s$ to $\pm 1000°/s$ for gyroscopes, while the inertial sensor measurements were sampled and filtered with different frequencies. Depending on the purpose of the biomechanical study and the system design, different

inertial sensors and sensor configurations were adopted. Table 2.1 shows detailed specifications of the sensors used in these studies.

Table 2.1: Inertial Sensor Specifications in Reviewed Studies

Source	Year	Sensor Model	Number of Sensors	Type and Specification				Sampling Frequency (Hz)	Data Filtering (Hz)
				Accelerometer		Gyroscope			
				Measuring Axes	Measuring Range	Measuring Axes	Measuring Range		
Aminian *et al.* [7]	1995	IC Sensors 3021	4	3				40	16
Miyazaki [8]	1997	ENC-05S, Murata	1			1	$\pm 150°/s$		
Tong and Granat [12]	1999	ENC-05EA, Murata	1			1		50	0.3~4
Aminian *et al.* [13]	2002	ENC-03J, Murata	3			1		200	
Zijlstra and Hof [14]	2003	Kistler	1	3	$\pm 2g$			100	20
Tanaka *et al.* [9]	2004	acc: MC301, Wacoh gyro: ENC-03J, Murata	3			1		25	acc: 3 gyro: 0.3~20
Sabatini *et al.* [10]	2005	acc: ADXL210E, Analog Device gyro: ENC-03J, Murata	1	2	$\pm 10g$	2	$\pm 300°/s$	200	acc: 17 gyro: 15
Alvarez *et al.* [15]	2007	MTx, Xsens	2	3	$\pm 2g$	1		100	
Ojeda and Borenstein [16]	2007	SIMU01, BAE	1	3	$\pm 50g$	3	$\pm 1000°/s$		
Song *et al.* [17]	2007	ADXL330	1	3	$\pm 3g$			200	
Yeoh *et al.* [18]	2007	Crossbow	3	2	$\pm 2g$			25	
Martin *et al.* [19]	2010	MTx, Xsens	2	3		3		50	15
Bebek *et al.* [20]	2010	InertiaCube3, InterSense	1	2	$\pm 6g$	1			
Huang *et al.* [21]	2010		1	3		3			
Li *et al.* [11]	2010	acc: ADXL320 gyro: ADXRS300	1	2		1		1000	
Mariani *et al.* [22]	2010	S-Sense	1	3	$\pm 3g$	3	roll, yaw: $\pm 300°/s$ pitch: $\pm 800°/s$	200	17

* Empty entries indicate variables unspecified by the author.

2.3.2 Sensor Attachment Location

As the nature of human gait, most body motion in walking occurs on lower limbs; therefore, most of the reviewed studies chose to attach the inertial sensors on the thigh and the shank or the feet of the subjects. One study [17] attempted to capture the motion with accelerometer attached to the chest. Four studies [7, 14, 18] utilized trunk sensor to estimate the walking speed. One study additionally used the force/moment sensor [19] as an aiding component in the system. Table 2.2 shows the sensor types and the attachment positions used in the reviewed articles. We followed a similar presentation method as proposed in [23].

Table 2.2: Sensor Type and Attachment Position. Total nine different types of inertial sensors, including uniaxial, biaxial and triaxial accelerometer and gyroscope, were attached to 12 positions, including chest, trunk, thigh, shank and foot.

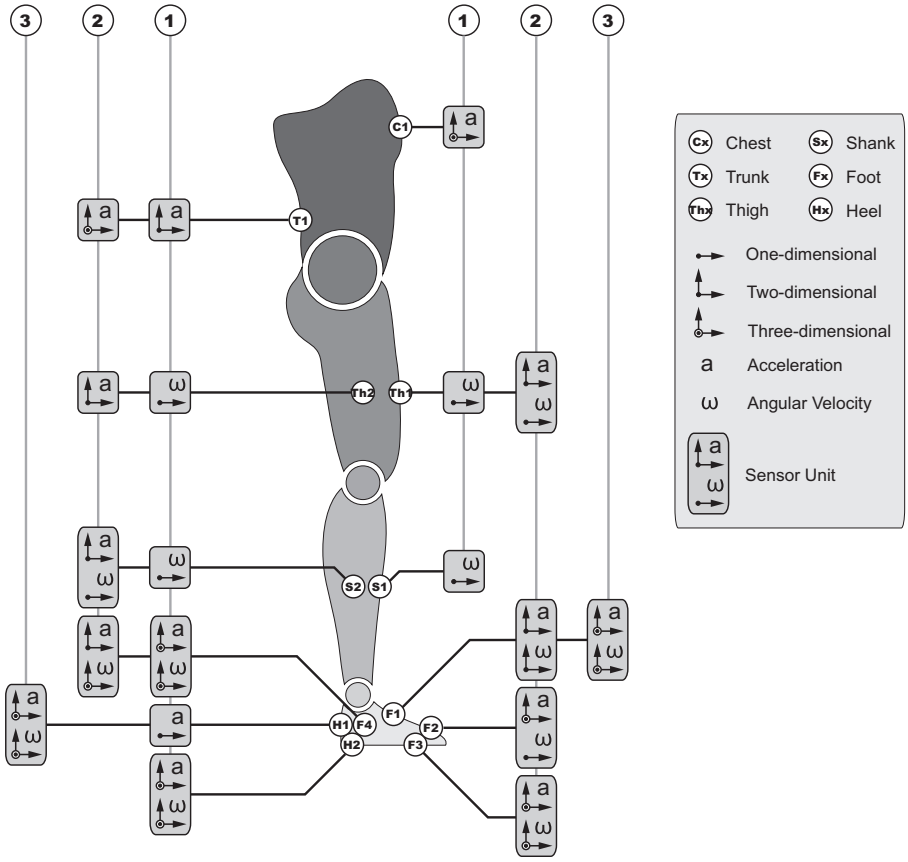

Position	References		
	1	2	3
C1	[17]		
T1	[18]	[14, 7]	
Th1		[8]	
Th2	[13]	[18]	
S1	[12]		
S2	[13]	[11]	
F1		[10]	[21]
F2		[15]	
F3		[19]	
F4	[16]	[20]	
H1	[7]		[22]
H2	[19]		

2.3.3 Experimental Design

Most of the reviewed studies focused on method validation with healthy subjects. Some studies aiming to apply their methods in age-related or pathological gait researches chose to include elderly subjects [13, 22], spinal cord injured subject [12] or patients with prostheses or hemiplegic gait [8] in their experiments. In some studies, the proposed methods were validated with only one subject [12, 15, 16, 20, 21]. Although single subject verification might not be sufficient to demonstrate the robustness of the proposed method, the idea of the proposed method we clearly explained. Two major forms of experiment were treadmill walking and overground walking at either preferred speed or preset speed. For those studies that involved elderly or impaired subjects [12, 8, 13, 22], the experiments were designed with care while providing reasonable comparison with young/healthy subjects. In terms of the motion capturing capability, four out of 16 studies [16, 19, 20, 22] concentrated on inertial sensor based personal navigation systems that were capable of monitoring the subjects walking in 3D environments; 12 out of 16 studies focused on the motion of the subjects in sagittal plane only, which is what most current gait studies are interested in. The detailed experimental design information is shown in Table 2.3.

Table 2.3: Experimental Design in Reviewed Studies

Source	**Subject**	**Experimental Design**
Aminian *et al.* [7]	5 healthy subjects	Treadmill walking at preferred speed.
Miyazaki [8]	18 healthy subjects; 7 patients with above knee prostheses; 10 hemiplegic subjects	Healthy subjects: Overground 25m walking at preferred speed; Patients with above knee prostheses: Overground 25m walking at low, medium and high speed; Hemiplegic subjects: Overground 15m walking at low, medium and high speed.
Tong and Granat [12]	1 incomplete spinal cord injured subject; 1 unimpaired subject	Overground 4.5m walking at preferred speed.
Aminian *et al.* [13]	9 young subjects; 11 elderly subjects	Young subjects: Treadmill walking at preferred speed, under and over preferred speed; Overground 30m walking at preferred speed Elderly subjects: Overground 30m walking at preferred speed.
Zijlstra and Hof [14]	25 healthy subjects	Treadmill walking at 6 speeds ($0.5m/s$, $0.75m/s$, $1.0m/s$, $1.25m/s$, $1.5m/s$ and $1.75m/s$); Overground walking at preferred speed, slow and fast speed.
Tanaka *et al.* [9]	10 healthy subjects	Overground walking at various speeds.
Sabatini *et al.* [10]	5 healthy subjects	Treadmill walking at combinations of 7 speeds ($3km/s$ to $6km/s$ in steps of $0.5km/s$).
Alvarez *et al.* [15]	1 healthy subject	Overground 10m walking at preferred speed.
Ojeda and Borenstein [16]	1 healthy subject	Overground walking at normal and brisk pace; Overground walking along a square-shaped loop path on 1, 2 and 4 floors including stairs; Overground 14-minute and 12-minute walking along city streets.
Song *et al.* [17]	17 healthy subjects	Treadmill walking and running at various speeds from $4.8km/h$ to $15.4km/s$.
Yeoh *et al.* [18]	5 healthy subjects	Treadmill wealking and running at various speed from $1km/h$ to $13km/s$.
Martin *et al.* [19]	10 healthy subjects	Overground 10m walking at preferred speed.
Bebek *et al.* [20]	1 healthy subject	Overground half-hour walking along a loop.
Huang *et al.* [21]	1 healthy subject	Overground walking along the square, rectangle, J-shaped paths and an athletic track.
Li *et al.* [11]	8 healthy subjects	Treadmill walking at 6 speeds ($0.8m/s$, $1.0m/s$, $1.2m/s$, $1.4m/s$, $1.6m/s$ and $1.8m/s$); Overground 100m walking at preferred speed.
Mariani *et al.* [22]	10 young subjects; 10 elderly subjects	Overground 5m "U-turn", 3m "8-turn" and 25m 6-minute walking.

2.3.4 Spatial Parameter Estimation Algorithm

The algorithms of using inertial sensors to estimate walking speed can be grouped into three categories: (1) abstraction model (three studies: [7, 17, 18]), (2) gait model (five studies: [8, 12, 13, 14, 9]) and (3) direct integration (eight studies: [10, 15, 16, 19, 20, 21, 11, 22]).

Abstraction Model

Instead of calculating the gait parameters following certain physical models, some studies decided not to look into the details of the human walking biomechanics, but to abstract the system and construct a hypothetical model for the complex relationship between the inertial sensor data and the resulting walking speed from an information processing point of view.

In 1995, Aminian *et al.* [7] proposed a walking speed estimation algorithm with two artificial neural networks (ANNs) using four acceleration signals. In this study, the system consisted of two two-layer ANNs, in which the input acceleration signals were collected from the trunk (triaxial) and the heel (uniaxial), and the first ANN generated the incline estimation result while the second ANN provided the walking speed estimation result. Before the classification phase (walking speed estimation), the training phase (learning process) of each ANN determined a set of 360 acceleration signal patterns through treadmill walking experiments, and associated the acceleration signals with the actual walking speed by adjusting the weights and biases of the network to minimize the sum squared error. At the end of the training phase, the weights and biases were fixed and later used in the classification phase to

process the acceleration signals for walking speed estimation, which achieved a maximum relative error of 16% from the overground walking experiments at the subjects' preferred speed. Similar method was adopted by Song *et al.* [17] in their study. Song employed a two-stage structure consisting of three ANN's to process the acceleration signals collected from an accelerometer (triaxial) attached to the chest. At the first stage, the walking/running classification network classified the motion, either walking or running; at the second stage, the walking neural network (NNW) and the running neural network (NNR) processed the signals according to the classification to provide speed estimation result. The overall root mean squared error (RMSE) was $0.54km/h$ based on walking/running experiments at various speeds between $4.7km/h$ and $17.14km/h$. Different from the ANNs used in these two studies, Yeoh *et al.* [18] defined the average net acceleration (ANA) of the left and right thighs and estimated the walking speed using a third-order polynomial model. Before the walking experiment, sufficient amount of acceleration signal data at various walking speeds were collected (training phase), and a polynomial model was determined by fitting the mean value of ANA with respect to the walking speed using the least squares approach. This method was derived based on the fact that force exerted by an object is directly proportional to the acceleration and the physical activity intensity (or walking speed) can be expressed as a function of acceleration. The overall mean squared error (MSE) was $1.76km/h$ based on the walking trials at speed ranging from $1km/h$ to $13km/h$.

The implementation and the experimental results of these three studies clearly demonstrated the feasibility of using abstraction model method to estimate walking speed. Both the advantage and the disadvantage of this method are obvious. As the

nature of the abstraction method, the complex biomechanical system is abstracted as a set of parameters with different weights and biases, which guarantees that once the system is successfully established through the training phase, the computation is fast and highly simplified. Additionally, since no physical model is required in this class of methods, a large variety of signals can be used as the input of the abstraction model, which implies that the position and the type of inertial sensor is highly flexible, e.g. attached to trunk and heel in [7] and to chest in [17]. However, due to the fact that the abstraction model is an approximation of the actual physical system, the accuracy of the estimation depends on the type of model and training data set, and the accuracy of the estimation is generally low. Furthermore, the training phase can be very time consuming, because (1) the abstraction model is subject-specific, thus every subject need to go through the training phase, and (2) in order to achieve a better performance, larger amount of training data need to be collected for the system construction, as discussed in [7].

Gait Model

Some researchers chose to make use of the derived kinematic information along with some predefined biomechanical gait models to estimate the spatial parameters, such as stride length, since some aspects of the lower limb kinematics can be derived from the measurements of the inertial sensors attached to the leg.

In early stages, most studies tried to employ a simplified gait model to avoid complicated sensor configuration and to reduce the computation complexity. In 1997, Miyazaki [8] proposed a stride length and walking speed estimation method using a gyroscope (uniaxial) attached to the thigh and a symmetric gait model. In this

method, each leg was modeled as one single segment, and the two legs were assumed symmetrical; thus, at heel-strike, two legs and the distance between the feet formed a isosceles triangle. The angle between the leg segments was calculated by integrating the angular velocity measurement from the gyroscope attached to the thigh, and then the distance between two feet (step length, one half of stride length) was calculated using the properties of isosceles triangle. The overground walking experiment showed that this simple gait model method achieved a relative error of 15%. Similar to Miyazaki, Tong *et al.* [12] also modeled each leg as one segment and attached a gyroscope (uniaxial) on the shank; however, when calculating the stride length, Tong implicitly used a pendulum model in which the one-segment leg swing back and forth about the hip joint during walking. The stride length was simply calculated as the product of the leg segment inclination range (rad) and the leg segment length (m). Another method of using the single segment gait model was proposed by Tanaka *et al.* [9] in 2004; however, one additional accelerometer (biaxial) was attached to the shank along with a gyroscope (uniaxial). The algorithm was basically identical to Miyazaki's method, but used the acceleration measurement to determine initial thigh angle just before starting to walk. In 2002, Aminian *et al.* [13] utilized a foot switch (to monitor temporal parameter) and two gyroscopes (uniaxial) to estimate walking speed. Discarding the simplified gait model reported in [8, 12], Aminian *et al.* chose to solve the complete gait model with separate shank and thigh segments with the same assumption of symmetry between two legs. In this method, the rotation angle of the shank and the thigh were tracked by two gyroscopes, and each stride cycle was divided into stance phase and swing phase using the foot switch, where in each phase the stride length was solved geometrically using the rotation angle and the length of the shank

and thigh. Evaluated from both treadmill and overground walking experiments, the overall RMSE was $0.06m/s(6.7\%)$ for walking speed estimation and $0.07m(7.2\%)$ for stride length estimation. A different model of human gait was introduced by Zijlstra *et al.* [14] in walking speed estimation. The proposed method, rather than using the lower limbs, used the vertical displacement of the center of mass (CoM) to estimate the walking speed. Since the CoM movements in sagittal plane follow a circular trajectory about the foot during each single support phase, upon the determination of the vertical displacement of the CoM, the step length can be derived geometrically. The experimental results showed that the maximum relative error is about 16%.

Using predefined gait model along with inertial sensor measurement in the walking speed estimation algorithm benefits from several aspects: (1) simple sensor setup, (2) ease of use, and (3) relatively consistent accuracy. First, with the support of a gait model, the inertial sensor measurement was usually used to provide only one or two parameters of the whole system, for example, the shank/thigh angle [8, 12, 9, 13] and the vertical displacement of the CoM [14]. Since only one or two sensor measurements were processed in this method, less effort was required to deal with the inevitable sensor errors, i.e. noise and bias. Second, unlike the abstraction model method, the gait model based method followed the physical principle to construct the biomechanical system; thus, no subject-specific training phase was required before the actual application. Third, the accuracy of the gait model based method was very consistent since the results were calculated geometrically using a model constrained by the lower limb segment lengths, which was also effective in correcting subject to subject inconsistence. This method also has some disadvantages. The accuracy of the gait model method highly relied on the validity of the model and meanwhile

the gait model directly affected the complexity of the computation. Comparing the performance of [8] and [13], the estimation error of the simplified gait model was about twice as big as that of the complete gait model; however, for the better accuracy much more complicated calculation procedures were required [13]. Also, subject-specific measurement, i.e. lower limb segment length, must be taken in order to construct the accurate gait model.

Direct Integration

In recent years, more and more studies started to use direct integration method to calculate the sensor velocity/displacement during human walking. The components of a generic direct integration algorithm include: (1) define a starting and ending point of each stride cycle; (2) determine the orientation of the inertial sensor with respect to the global coordinate system; (3) project the acceleration measurement into the global coordinate system based on the instantaneous orientation of the inertial sensor and remove the acceleration due to gravity from the projected sensor acceleration; and (4) integrate the resulting acceleration in global coordinate system from the starting point to obtain sensor velocity and displacement. The direct integration methods have been developed for the purpose of biomechanical research and personal navigation.

Early studies using body-fixed inertial sensors mostly focused on biomechanical research. In the reviewed articles, the first direct integration walking speed estimation method was proposed by Sabatini *et al.* [10] in 2005, which uses an IMU (biaxial accelerometer and biaxial of gyroscope) fixed on the instep of the foot. With a reasonable assumption that the foot (with the shoe) was rigid enough, the estimated sensor velocity could be viewed as the velocity of the foot. The foot flat (FF) was

defined as the starting point of each stride cycle, and the angular velocity data were used to detect the FF event in the stance phase. One important procedure in this algorithm was the zero velocity update (ZUPT), which determined the initial sensor orientation and estimated the sensor measurement offsets during the period of the stride cycle when the sensor velocity is approximately zero, usually at the FF event in the stance phase. This method achieved an overall RMSE of $0.18km/h$ based on the treadmill walking experiments at various speeds ranging from $3km/h$ to $6km/h$. Alvarez *et al.* [15] used the same method to estimate the foot displacement over one stride cycle; however, Alvarez utilized one IMU (triaxial accelerometer and uniaxial gyroscope) on each foot and a data fusion algorithm to reduce the estimation error. Although the experimental results (relative error $10.1 \pm 6.2\%$) showed limited improvement from the results of [10], Alvarez extended Sabatini's study and introduced a method to combine the information obtained from multiple sensors that could potentially increase the estimation accuracy. Attaching the sensor to the foot provided a lot of benefits, such as the possibility to implement ZUPT at foot flat, but the flexibility of the ankle joint brought concerns about the influence of the abnormal gait on the inertial sensor data, such as out of plane motion [24]. To avoid such issue, Li *et al.* [11] attached an IMU (biaxial accelerometer and uniaxial gyroscope) to the lateral side of mid-shank and estimated the walking speed with direct integration method. Different from the sensor attached to the foot, ZUPT technique could not be used for the sensor attached to the shank. Instead, they defined the shank vertical as the starting point of each stride cycle (shank angle is zero), and made use of the inverted pendulum model to assume that the initial sensor velocity was zero. This assumption is based on the fact that the CoM was at its highest point

and the kinetic energy was all transformed into potential energy at the shank vertical event. In their study, a percentage RMSEs of 7% and 4% were obtained from the treadmill and the overground walking experiments, respectively. These methods [10, 15, 11] focused on walking speed estimation in the sagittal plane (or direction of progression) only, since most biomechanical studies used walking speed evaluated along a straight line, e.g. 10-meter walking test (10MWT) [25]. In 2010, Mariani *et al.* [22] attempted to use an IMU (triaxial accelerometer and triaxial gyroscope) attached to the back of the heel to estimate the stride length, stride velocity and turning angle in three-dimensional space. Quaternion representation of the sensor orientation in three-dimensional space was obtained by integrating the angular velocity measurement. The acceleration measurement was then projected to the global coordinate system based on the sensor orientation, and the acceleration due to gravity was removed from the projected sensor acceleration measurement. After the double integration of the projected sensor acceleration, the foot position in each stride was expressed in a 3-dimensional space, while the stride length was the distance between the positions of the foot at two adjacent FF's. The stride length and stride velocity estimation relative error were $1.3 \pm 6.8\%$ and $1.5 \pm 5.8\%$, respectively.

Because of their portability, self-containedness and the capability of working in an indoor environment, the miniature inertial sensors were considered as a potential substitute for satellite based personal navigation system. One attempt was conducted by Ojeda and Borenstein [16]. They developed a navigation system using an IMU (triaxial accelerometer and triaxial gyroscope) attached to the lateral side of the foot. They also used the quaternion representation of the sensor orientation with the triaxial angular velocity measurement to determine the instantaneous sensor orientation. The

overall movement estimation was through a process call dead reckoning, with which the current position was determined by using a previously determined position. The travel distance estimation error was less than 2% as reported in [16]. In 2010, Martin *et al.* [19] used an IMU's (triaxial accelerometer and triaxial gyroscope) and two force sensors attached beneath the heel and the forefoot. The force sensors were used to detect the time instant of heel down (HD) that was defined as the starting point of the stride cycle. The overall stride length estimation error obtained from the 10MWT was $34.1 \pm 2.7mm$. Although the basic estimation procedure was the same, Huang *et al.* [21] used the direction cosines representation to track the orientation of the IMU (triaxial accelerometer and triaxial gyroscope) attached to the arch of the foot, and achieved a walking distance estimation error of about 2%. Moreover, concerning about the effect of the sensor noise in the estimation accuracy, Bebek *et al.* employed extended Kalman filter (EKF) to reduce the sensor noise and bias through the stance phase. A pressure sensor array was place between the heel of the shoe and the shoe insole, and an IMU (triaxial accelerometer and triaxial gyroscope) attached to the lateral side of the foot. The pressure sensor array was used to detect the zero velocity period of the stride cycle, in which the ZUPT with EKF was applied. The relative error of the system was 0.40%, evaluated in the outdoor walking experiments with an average distance of $1215m$.

The direct integration methods benefited from the increasing accuracy of the miniature IMUs and the sophisticated new algorithms. Comparing to the abstraction model based method and the gait model based method, this class of methods is easier to use without the troubles from the training process and subject specific measurement/calibration. Currently, The IMU was attached to the foot or the shank

in order to take the advantage of using the ground as a reference in the algorithm. As discussed in many studies, two important components of the direct integration method were the determination of the sensor orientation and the sensor error correction. Since the direct integration method solely used the IMU measurement in the estimation and very little external information was available on-the-fly, the sensor orientation determination heavily relied the angular velocity measurement and the angle representation, such as Euler angle, quaternion and direction cosines. On the other hand, the sensor noise and bias must be reasonably corrected in the estimation process to ensure the accurate estimation results. One common sensor error correction technique was ZUPT. The sensor noise and bias were evaluated during the zero velocity period of the stride cycle, and then compensated from the calculation. With the direct integration method, three-dimensional motion monitoring was also made possible [16, 22, 19, 20, 21]. Although most age-related or pathological gait research studies still considered the straight line walking speed as the assessment criteria, three-dimensional motion tracking capability significantly will definitely extend the application of the inertial sensors in biomechanical research.

2.4 Conclusion

The development of MEMS highly increased the accuracy and usability of the inertial sensors. For the past 15 years, a large amount of studies have attempted to use inertial sensors for the purpose of estimating gait parameters. Because of their small size, light weight, low cost and ease of use, miniature inertial sensor based human gait analysis systems has been considered as a potential alternative to traditional camera based gait analysis methods. Through this review, the overall experimental results

of the inertial sensor based walking speed estimation methods are promising, even though the performance of some of methods [12, 15, 16, 20, 21] was not clear due to the small sample size. Since this systematic review is developed with a focus on algorithm development, performance evaluation or system validation articles were not included; there have been studies regarding the quantitative evaluation of these developed algorithms [26, 27, 28], which are essential to put these systems eventually into practice. For biomedical application, extended experiments should be conducted to verify the performance of the system with different populations, walking conditions, as well as abnormal gaits.

From the reviewed articles, a clear trend in walking speed estimation algorithm development is that more and more methods rely on direct integration method with 6D IMUs. The integration process amplifies measurement error, leading to the requirement of inertial sensors with higher accuracy. Although the sensor performance has been ramped up dramatically in last 15 years, the inertial senor measurement error is unavoidable, especially for miniature MEMS sensors. As one future research direction, the development should focus on sensor error correction. Noise and bias in the inertial sensor measurement can severely degrade the performance of the direct integration based methods, and the behaviors are complex in nature. Without external reference such as GPS, completely removing the sensor errors is very difficult. Based on some valid assumptions, current methods can somehow reduce the effect of the errors; however, detailed investigation about the sensor error existing in the system is needed in order to increase the speed estimation accuracy. Some studies have already started to analyze the underlying assumption in algorithms, such as zero-velocity assumptions in ZUPT [29, 30]. Another desirable development is the

real-time implementation of the developed algorithms in a portable system. Most of the studies used off line data processing and algorithm implementation while the inertial sensors and associated peripheral devices only performed as the data recorder. Off line data processing definitely presents some inconvenience and requires extra work after the experiment, which hinders its practical applications such as in clinical settings or personal navigation.

References

[1] N. Barbour and G. Schmidt. Inertial sensor technology trends. *IEEE Sensors Journal*, 1(4):332–339, 2001.

[2] A.M. Sabatini. *Computational Intelligence for Movement Sciences: Neural Networks, Support Vecotr Machines and Other Emerging Techniques*, chapter Inertial sensing in biomechanics: a surbey of computational techniques bridging motion analysis and personal nabigation, pages 70–100. Idea Group Inc., 2006.

[3] J.J. Cohen, J.D. Sveen, J.M. Walker, and K. Brummel-Smith. Establishing criteria for community ambulation. *Topics in Geriatric Rehabilitation*, 3(1):71–78, 1987.

[4] CL Richards, F. Malouin, F. Dumas, and D. Tardif. Gait velocity as an outcome measure of locomotor recovery after stroke. In *Gait Analysis: Theory and Application*, pages 355–364. St Louis, Mo: Mosby, 1995.

[5] A. Schmid, P.W. Duncan, S. Studenski, S.M. Lai, L. Richards, S. Perera, and S.S. Wu. Improvements in speed-based gait classifications are meaningful. *Stroke*, 38(7):2096–2100, 2007.

[6] S. Mudge and N.S. Stott. Outcome measures to assess walking ability following stroke: a systematic review of the literature. *Physiotherapy*, 93(3):189–200, 2007.

[7] K. Aminian, P. Robert, E. Jéquier, and Y. Schutz. Estimation of speed and incline of walking using neural network. *IEEE Transactions on Instrumentation and Measurement*, 44(3):743–746, 1995.

[8] S. Miyazaki. Long-term unrestrained measurement of stride length and walking velocity utilizing a piezoelectric gyroscope. *IEEE Transactions on Biomedical Engineering*, 44(8):753–759, 1997.

[9] S. Tanaka, K. Motoi, M. Nogawa, and K. Yamakoshi. A new portable device for ambulatory monitoring of human posture and walking velocity using miniature accelerometers and gyroscope. In *26th Annual International Conference of the IEEE Engineering in Medicine and Biology Society*, volume 1, pages 2283–2286. IEEE, 2004.

[10] A. M. Sabatini, C. Martelloni, S. Scapellato, and F. Cavallo. Assessment of walking features from foot inertial sensing. *IEEE Transactions on Biomedical Engineering*, 52(3):486–94, 2005.

[11] Q. Li, M. Young, V. Naing, and J. M. Donelan. Walking speed estimation using a shank-mounted inertial measurement unit. *Journal of Biomechanics*, 43(8):1640–1643, 2010.

[12] K. Tong and M.H. Granat. A practical gait analysis system using gyroscopes. *Medical Engineering & Physics*, 21(2):87–94, 1999.

[13] K. Aminian, B. Najafi, C. Bula, P.F. Leyvraz, and P. Robert. Spatio-temporal parameters of gait measured by an ambulatory system using miniature gyroscopes. *Journal of Biomechanics*, 35(5):689–699, 2002.

[14] W. Zijlstra and A.L. Hof. Assessment of spatio-temporal gait parameters from trunk accelerations during human walking. *Gait & Posture*, 18(2):1–10, 2003.

[15] J.C. Alvarez, R.C. González, D. Alvarez, A.M. Lóprez, and J. Rodríguez-Uría. Multisensor approach to walking distance estimation with foot inertial sensing. In *29th Annual International Conference of the IEEE Engineering in Medicine and Biology Society*, pages 5719–5722, 2007.

[16] L. Ojeda and J. Borenstein. Non-gps navigation for security personnel and first responders. *Journal of Navigation*, 60(03):391–407, 2007.

[17] Y. Song, S. Shin, S. Kim, D. Lee, and K.H. Lee. Speed estimation from a tri-axial accelerometer using neural networks. In *29th Annual International Conference of the IEEE Engineering in Medicine and Biology Society*, pages 3224–3227, 2007.

[18] W.S. Yeoh, I. Pek, Y.H. Yong, X. Chen, and A.B. Waluyo. Ambulatory monitoring of human posture and walking speed using wearable accelerometer sensors. In *30th Annual International Conference of the IEEE Engineering in Medicine and Biology Society*, pages 5184–5187. IEEE, 2008.

[19] S.H. Martin, E.H.F. van Asseldonk, C. Baten, and P.H. Veltink. Ambulatory estimation of foot placement during walking using inertial sensors. *Journal of Biomechanics*, 43(16):3138–3143, 2010.

[20] O. Bebek, M.A. Suster, S. Rajgopal, M.J. Fu, X. Huang, M.C. Cavusoglu, D.J. Young, M. Mehregany, A.JJ. van den Bogery, and C.H. Mastrangelo. Personal navigation via high-resolution gait-corrected inertial measurement units. *IEEE Transactions on Instrumentation and Measurement*, 59(11):3018–3027, 2010.

[21] C. Huang, Z. Liao, and L. Zhao. Synergism of ins and pdr in self-contained pedestrian tracking with a miniature sensor module. *IEEE Sensors Journal*, 10(8):1349–1359, 2010.

[22] B. Mariani, C. Hoskovec, S. Rochat, C. Büla, J. Penders, and K. Aminian. 3d gait assessment in young and elderly subjects using foot-worn inertial sensors. *Journal of Biomechanics*, 2010.

[23] J. Rueterbories, E.G. Spaich, B. Larsen, and O.K. Andersen. Methods for gait event detection and analysis in ambulatory systems. *Medical Engineering & Physics*, 32(6):545–552, 2010.

[24] J.M. Jasiewicz, J.H.J. Allum, J.W. Middleton, A. Barriskill, P. Condie, B. Purcell, and R.C.T. Li. Gait event detection using linear accelerometers or angular velocity transducers in able-bodied and spinal-cord injured individuals. *Gait & Posture*, 24(4):502–509, 2006.

[25] N.M. Salbach, N.E. Mayo, J. Higgins, S. Ahmed, L.E. Finch, and C.L. Richards. Responsiveness and predictability of gait speed and other disability measures in acute stroke. *Archives of Physical Medicine and Rehabilitation*, 82(9):1204–1212, 2001.

[26] S. Yang and Q. Li. Imu-based ambulatory walking speed estimation in constrained treadmill and overground walking. *Computer Methods in Biomechanics and Biomedical Engineering*, 2011. First published on: 02 February, 2011.

[27] S. Lord, L. Rochester, K. Baker, and A. Nieuwboer. Concurrent validity of accelerometry to measure gait in parkinsons disease. *Gait & Posture*, 27(2):357–359, 2008.

[28] A. Hartmann, S. Luzi, K. Murer, R.A. de Bie, and E.D de Bruin. Concurrent validity of a trunk tri-axial accelerometer system for gait analysis in older adults. *Gait & Posture*, 29:444–448, 2009.

[29] I. Skog, P. Handel, J.O. Nilsson, and J. Rantakokko. Zero-velocity detectionan algorithm evaluation. *IEEE Transactions on Biomedical Engineering*, 57(11):2657–2666, 2010.

[30] A. Peruzzi, U.D. Croce, and A. Cereatti. Estimation of stride length in level walking using an inertial measurement unit attached to the foot: A validation of the zero velocity assumption during stance. *Journal of Biomechanics*, 44(10):1991–1994, 2011.

Chapter 3

IMU-based Ambulatory Walking Speed Estimation in Constrained Treadmill and Overground Walking

Abstract

This study evaluated the performance of a walking speed estimation system based on using an inertial measurement unit (IMU), a combination of accelerometers and gyroscopes. The walking speed estimation algorithm segments the walking sequence into individual stride cycles (two steps) based on the inverted pendulum-like behaviour of the stance leg during walking and integrates the angular velocity and linear accelerations of the shank to determine the displacement of each stride. The evaluation was performed in both treadmill and overground walking experiments with various constraints on walking speed, step length and step frequency to provide a relatively

comprehensive assessment of the system. Promising results were obtained in providing accurate and consistent walking speed/step length estimation in different walking conditions. The overall percentage root mean squared error (%RMSE) of 4.2% and 4.0% was achieved in treadmill and overground walking experiments, respectively. With an increasing interest in understanding human walking biomechanics, the IMU-based ambulatory system could provide a useful walking speed/step length measurement/control tool for constrained walking studies.

3.1 Introduction

Walking is the main form of human locomotion and the most frequently performed daily activity. People choose to use a variety of walking gaits based on their preference and required locomotor tasks. In the past decades, the human gait analysis has proved of great value in the diagnosis of lower limb joint diseases and in the assessment and rehabilitation of pathological gait [1, 2, 3, 4]. Moreover, researchers have conducted different studies to investigate the fundamentals of human walking biomechanics, for example, the analysis of the relationship between the walking speed, step length and step frequency. The combinations of these walking parameters are commonly employed in the studies of the optimal walking gait. Sekiya *et. al* investigated the optimal walking mechanism in terms of the variability in step length at different walking speeds and found that the consistency of the walking gait was optimized at the preferred walking speed with freely chosen step frequency [5]. Bertram *et. al* predicted multiple relations between walking speed and step frequency based on the assumption that people optimized a function of walking speed and step frequency

that has a minimum at the preferred gait [6]. With an increasing interest in understanding human walking biomechanics, the demand for accurate measurement of human walking speed is growing.

The essence of walking speed estimation is to determine the spatial displacement of the human body and the time required for such displacement. Recent years, the development of miniature inertial sensors, i.e. accelerometers and gyroscopes, made it possible to develop ambulatory walking speed estimation system. Because of the low cost and ambulatory capability of inertial sensors, the inertial-sensor-based walking speed estimation method has been considered as an effective alternative to the walking speed measurement methods mentioned above [7, 8, 9, 10, 11, 12, 13]. One of the walking speed measurement methods using inertial sensor is to calculate the displacement of human body segment with direct measurement utilizing accelerometers and gyroscopes. For example, Sabatini *et. al* proposed a method of using a foot-mounted inertial measurement unit (IMU), an electronic device using a combination of accelerometers and gyroscopes, to estimate spatio-temporal gait parameters and obtained walking speed estimation results with an RMSE of 5% [14]. Most recently, Li *et. al* used a shank mounted IMU to estimate walking speed and achieved comparable results with an RMSE of 7% [8]. However, since most of the above mentioned systems were tested under subjects' preferred walking conditions, their performance under constrained walking, as required in fundamental human walking studies or optimal walking [6, 5, 15], was unknown. Therefore, more experiments were desired to provide a comprehensive performance assessment of these inertial-sensor-based walking speed estimation methods.

This paper is focused on the evaluation of a walking speed and step length estimation method, previously developed by Li *et. al* [8] using a shank-mounted IMU. Based on the cyclical pattern exhibited in the characteristics of walking kinematics, the walking speed estimation algorithm segments the walking sequence and analysed each stride cycle individually to reduce the integration error associated with the inaccuracies in the acceleration and angular velocity measurements. To validate the applicability of the system in constrained biomedical experiments [6, 16], the performance evaluation was conducted for both treadmill and overground walking with different constraints on the walking speed, step length and step frequency.

3.2 Methods

3.2.1 Subjects

Sixteen volunteers were recruited for this study. Six female and three male subjects (age: 27.0±8.0 years; height: 167.5±13.5 cm; tibia length: 40.0±5.0 cm) participated in the treadmill walking experiment, and the other three female and four male subjects (age: 23.5±1.5 years; height: 171.0±11.0 cm; tibia length: 40.0±2.0 cm) attended the overground walking experiment. All subjects were healthy and exhibited no clinical gait abnormalities to ensure that they were suitable for the walking exercises in the experiment. All subjects gave their informed consent to participate in accordance with university policy, and the study was approved by the Queen's General Research Ethics Board (GREB).

3.2.2 Apparatus

The Inertia-Link (MicroStrain, Inc., Williston, VT, USA) is a IMU sensor that consists of a triaxial accelerometer ($\pm 5g$, where g is the gravitational acceleration) and a triaxial gyroscope ($\pm 600^{\circ}/sec$) with measurement errors in a range of $\pm 0.005g$ and $\pm 2.0^{\circ}/sec$, respectively, in dynamic conditions. The linear acceleration and angular velocity data were collected at $100Hz$ and sent to a USB base station receiver via a built-in wireless communication system ($2.45GHz$ IEEE 802.15.4). A customized software (MicroStrain, Inc, Williston, VT, USA) was used to record the data in a computer. A treadmill (NordicTrack, Inc., Logan, UT, USA) was used in treadmill walking experiment.

3.2.3 Sensor Configuration

The IMU sensor was attached to the lateral side and located at the midway of the left shank using double sided tape and athletic tape (Figure 3.1). As we only considered the shank motion in sagittal plane, the tangential and normal axes of the accelerometer were pointing to the fore-aft and longitudinal directions of the shank, respectively. One axis of the gyroscope measured the shank angular velocity in sagittal plane (plane of progression). Shank angle, θ, was defined as the angle between the normal axis of the accelerometer and the vertical axis of the world coordinate system. The right hand rule defined the positive angular velocity as the clockwise rotation of the shank in the coordinate system (Figure 3.1).

Before each experiment, the subjects were asked to stand still in the shank vertical position (longitudinal axis of the shank is perpendicular to the floor) with the IMU mounted on the shank, and the IMU was adjusted such that its normal and tangential

axes were aligned to horizontal and vertical directions of the world coordinate system, respectively. As such, the initial measurement of the IMU should showed roughly $0g$ in tangential axis and $1g$ in normal axis.

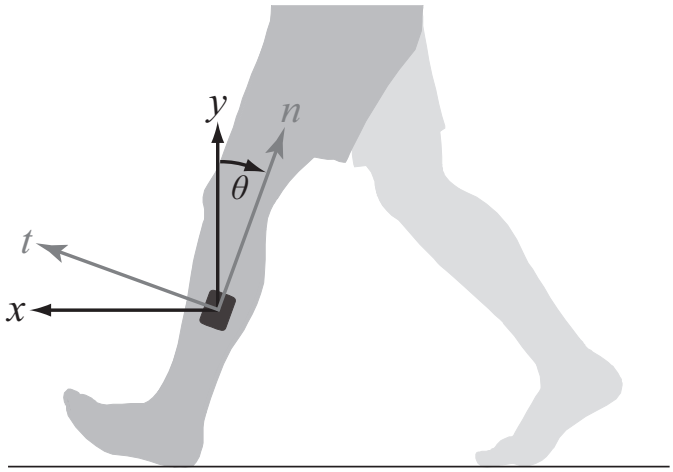

Figure 3.1: Sensor configuration: An IMU was attached to the shank in the sagittal plane on the lateral side. The normal acceleration a_n was measured along the n direction, and the tangential acceleration a_t was measured along the t direction, while the axis of gyroscope was perpendicular to the sagittal plane defined by n and t directions. The arrows indicated positive axes for the corresponding sensor measurements. The world coordinate was defined by the x and y axes, and the vertical axis y extended in a direction parallel to gravity.

3.2.4 Experimental Method and Protocol

The treadmill walking experiment and the overground walking experiment were conducted to evaluate the performance of the IMU-based walking speed and step length estimation method. For each experiment, different constraints were applied to provide a comprehensive assessment. Following the simple relationship between walking speed, step length and step frequency (Equation 3.1), the walking condition could be controlled by constraining any two of these three gait parameters at the same time.

$$walking\ speed = step\ length \times step\ frequency \tag{3.1}$$

In both treadmill and overground walking experiments, step frequency was constrained by requesting the subjects to follow the designated frequency indicated by the beep sounds from a metronome. The walking speed constraint was applied in the treadmill experiment, in which the subjects was instructed to walk on a treadmill at constant pre-defined speeds. As a result, the step length was constrained simultaneously since both step frequency and walking speed were fixed (Equation 3.1). The step length was directly constrained in the overground walking experiment, which was implemented by labeling different distance with yellow adhesive tape markers on the floor with the aid of a tape ruler, and the subjects were instructed to step on the markers during walking trials. Similar walking parameter control techniques have been described in [17] and used in the optimal walking study [6].

Treadmill Walking Experimental Protocol

Walking trials were performed at four different treadmill speeds (1.0, 1.2, 1.4 and 1.6 m/s). For each subject at a selected treadmill speed, we first determined the subject's preferred step frequency using the metronome. Five trials with different step frequencies (80%, 90%, 100%, 110% and 120% of the preferred step frequency) were then performed for each treadmill speed. The treadmill speeds and step frequencies were applied in a random order to prevent subject adapting to a trend. The IMU data in each walking trial were recorded for a duration of 90 seconds.

Overground Walking Experimental Protocol

Four different step lengths ($0.7m$, $0.8m$, $0.9m$ and $1.0m$) were marked on the floor of a flat hallway ($35m$). For each step length, three walking trials with different step frequencies (90%, 100% and 110% of the preferred step frequency) were performed. The reason why we did not apply step frequency at 80% and 120% of the preferred step frequency as the treadmill walking experiment was that the subjects found it difficult to follow the metronome at very low and very high step frequencies while trying to step on markers on the hallway. The controlled step frequencies and step lengths were applied in a random order to prevent the subject adapting to the trend. The IMU data recording started from the $5th$ step to ensure that the subject's walking gait was stable, and ended when the subject reached the end of the marked hallway.

3.2.5 Walking Speed and step length Estimation

The walking speed and step length estimation algorithm was implemented in MATLAB (The MathWorks, Natick, MA, USA). On average, about 5% data loss was present in the wireless transmission. Before the data processing, one-dimensional interpolation was used to reconstruct the missing data points of the IMU acceleration and angular velocity. A second-order butterworth low-pass filter with a cut-off frequency of 2.5 Hz was used to remove the noise from the interpolated data.

A coordinate transformation was used to compute the horizontal and vertical

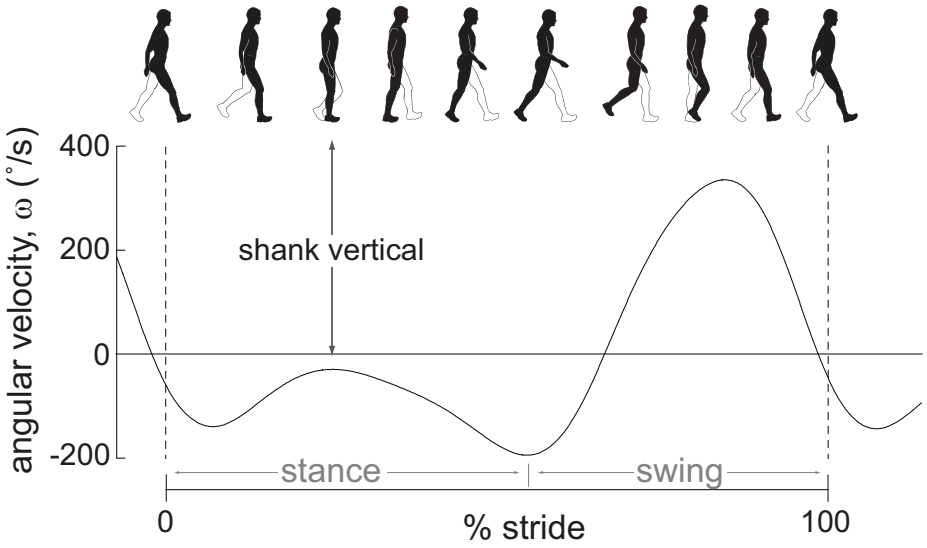

Figure 3.2: Characteristics of angular velocity, ω, during one gait cycle. The curve was filtered by a second order Butterworth filter with a cut-off frequency of $5Hz$. At the mid-stance shank vertical event, the magnitude of the angular velocity of the shank reached a local minimum with a value close to zero. In symmetry, the left shank had the same angular velocity characteristics as the right shank.

accelerations, $a_x(t)$ and $a_y(t)$, in the world coordinate system based on the IMU-measured shank normal, tangential acceleration signals and the resulting instantaneous shank angle, $a_n(t)$, $a_t(t)$ and $\theta(t)$, respectively,

$$\begin{bmatrix} a_x(t) \\ a_y(t) \end{bmatrix} = \begin{bmatrix} -\sin\theta(t) & \cos\theta(t) \\ \cos\theta(t) & \sin\theta(t) \end{bmatrix} \begin{bmatrix} a_n(t) \\ a_t(t) \end{bmatrix} - \begin{bmatrix} 0 \\ g \end{bmatrix}. \tag{3.2}$$

where $\theta(t)$ is the instantaneous shank angle and g is the acceleration due to the gravity.

Our previous work developed the algorithms to segment the walking sequence into a sequence of stride cycles. The segmentation algorithm defined the initial point of each stride cycle as the mid-stance shank vertical event, when the shank was parallel to the direction of gravity (Figure 3.2). Starting from the beginning of each stride cycle,

the instantaneous shank angle θ was calculated by integrating the angular velocity measured by the gyroscope. The horizontal and vertical displacement of the sensor was then calculated by double integration of the resulting horizontal and vertical linear acceleration from Equation 3.2. The average speed of each stride was eventually equal to the vector sum of the displacements in horizontal and vertical directions divided by the time period of the corresponding stride. The step length was one half of the shank displacement over one stride cycle assuming the symmetry of left and right steps. All integrations were reset at the beginning of each stride cycle. As only the motion in the sagittal plane was considered, summing the vertical and horizontal displacements could effectively reduce the error caused by the misalignment between the normal axis of the IMU and the longitudinal direction of the shank. Interested reader may refer to [8] for details.

3.2.6 Data Analysis

Treadmill Walking Experiment Data Analysis

For each treadmill walking trial, the mean walking speed was found by smoothing the stride-to-stride walking speed estimates in a stable period from the 11th to the 45th stride. Estimation error at a given combination of the treadmill speed and step frequency was calculated as the difference between the estimated walking speed and the preset treadmill speed. The mean absolute estimation error (Mean) and standard deviation (SD) were determined by averaging across all trials at each given walking conditions. A root mean squared error (RMSE) was computed as $RMSE = \sqrt{\sum(V_{estimated} - V_{actual})^2/N}$, where N is the number of samples in the calculation. The %RMSE was calculated as the ratio of RMSE and the actual value. For each given

walking speed, a %RMSE was calculated for nine subjects across five different walking frequencies ($N = 45$). For each given step frequency, a %RMSE was calculated for nine subjects across four different walking speeds ($N = 36$). An overall %RMSE was also calculated for nine subjects across all combination of treadmill speed and step frequency ($N = 180$). The effects of the treadmill speed and step frequency on the walking speed estimation error were tested using two-way ANOVA. With the p-values of the two-way ANOVA tests larger than the significance level, 0.05, the effects of walking speed and step frequency on the walking speed estimation error were considered statistically insignificant.

Overground Walking Experiment Data Analysis

For each overground walking trial, about 30 to 40 stride cycles were recorded depending on the designated step length. The mean step length was determined by smoothing the stride-to-stride step length estimates in a stable period from the 12th to 26th stride. Estimation error at a given combination of the step length and step frequency was calculated as the difference between the estimated step length and the designated step length. Similar to the treadmill walking experiment data analysis, the mean absolute estimation error and SD were computed. For each given step length, a %RMSE was calculated for seven subjects across three different step frequencies ($N = 21$). For each given step frequency, a %RMSE was calculated for seven subjects across four different step length ($N = 28$). An overall %RMSE was also calculated for nine subjects across all combinations of step length and step frequency ($N = 84$). The effects of the step length and step frequency on the step length estimation error were tested using two-way ANOVA. With the p-values of the two-way ANOVA tests larger

than the significance level, 0.05, the effects of the step length and step frequency on the step length estimation error were considered statistically insignificant.

Systematic Error Analysis

To find the systematic error of the walking speed/step length estimation algorithm, the relationship of the estimates and the actual values was evaluated by performing linear regression for all combinations of walking speed and step frequency ($N = 180$) in treadmill walking experiment, and for all combinations of step length and step frequency ($N = 84$) in overground walking experiment. The linear regression created a linear model ($y = \beta * x + \varepsilon$) to fit the known data points, where in our experiment y was the estimate and x was the actual value. With the slope of the linear regression curve, β, close to 1.00, the difference between the estimates and the expected values remained constant for all treadmill speeds or step lengths. Thus, the y-intercept, ε, of the linear regression curve was considered as a systematic error and was subtracted from the walking speed estimation results such that the systematic error was removed. The mean absolute estimation error and %RMSE were then calculated again on the adjusted walking speed and step length estimation results.

3.3 Results

Consistent performance of the shank-mounted IMU walking speed/step length estimation algorithm was obtained in the treadmill and overground walking experiments. As shown in Table 3.1 and Table 3.2, the estimation results were with a %RMSE of 14.5% and 17.0% before adjustment and 4.2% and 4.0% after adjustment, respectively.

3.3.1 Treadmill Walking Experiment Result

The walking speed estimation algorithm underestimated the treadmill walking speed. The average walking speed estimates for all subjects at all the combinations of the treadmill speed and step frequency are shown in Figure 3.3. A linear regression function fitting the estimates was plotted to demonstrate the overall trend of the estimation result. The slope (β) of the resulting linear regression function equalled 1.00. The y-intercept (ε) of the linear regression function equalled -0.18, which could be subtracted from the walking speed estimates to obtain the adjusted estimated walking speeds. The largest deviation were observed at the lowest ($1.0m/s$) experiment treadmill speed, and a few extreme outliers (about 40% lower than the treadmill speed) were observed at treadmill speed $1.0m/s$ and $1.6m/s$.

The adjusted average estimated walking speeds across all subjects in all the walking conditions are shown in Figure 3.4. Consistent average walking speed estimations were obtained at all four treadmill speeds, where the overall RMSE between the treadmill speed and the adjusted average estimated walking speed was $0.014m/s$ within the analysed steps (11th to 45th step) across all treadmill speeds. The largest inter-subject variability, quantified by the average standard deviation of the average estimated walking speed of different subjects, was about $0.083m/s$ while the least was less than $0.038m/s$, which occurred at treadmill speed $1.0m/s$ and $1.4m/s$, respectively.

The mean absolute estimation errors and the standard deviations of the estimation error before and after adjustment are summarised in Table 3.1. Relatively large difference was observed in the walking speed %RMSE across different step frequencies, which was in a range from 2.8% to 6.1%, while the walking speed %RMSE across

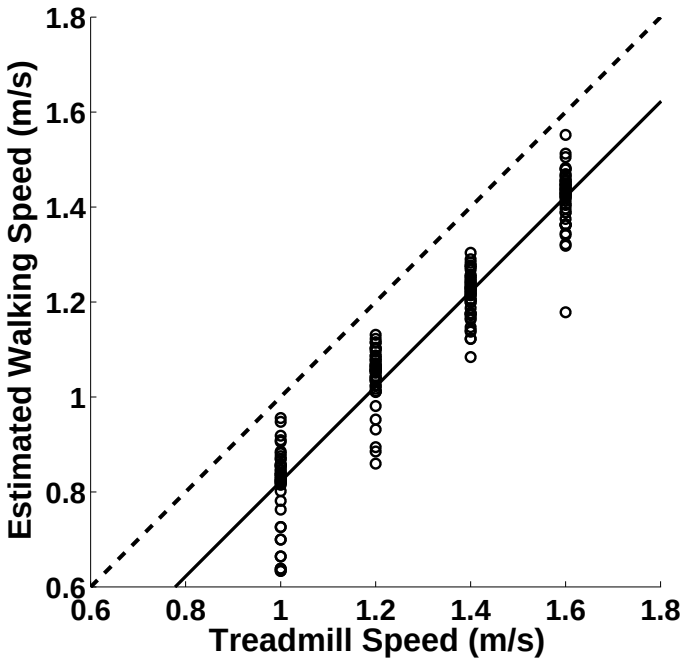

Figure 3.3: Average estimated walking speed (m/s) versus controlled treadmill speed (m/s) during treadmill walking at four treadmill speeds ($1.0m/s$, $1.2m/s$, $1.4m/s$ and $1.6m/s$) and five step frequencies (80%, 90%, 100%, 110% and 120% of the self-chosen step frequency). The solid line is the plot of the linear regression function that fitted the estimates (indicated with circles). The diagonal dash line showes the reference where the estimated walking speed and treadmill speed were equal. Each circle indicates an average walking speed estimate of a subject at a combination of designated treadmill speed and step frequency. Since the treadmill speed (horizontal axis) was controlled, the estimates (indicated with circles) were distributed along vertical lines corresponding to the specific treadmill speeds. In total, 180 estimates were shown in this figure.

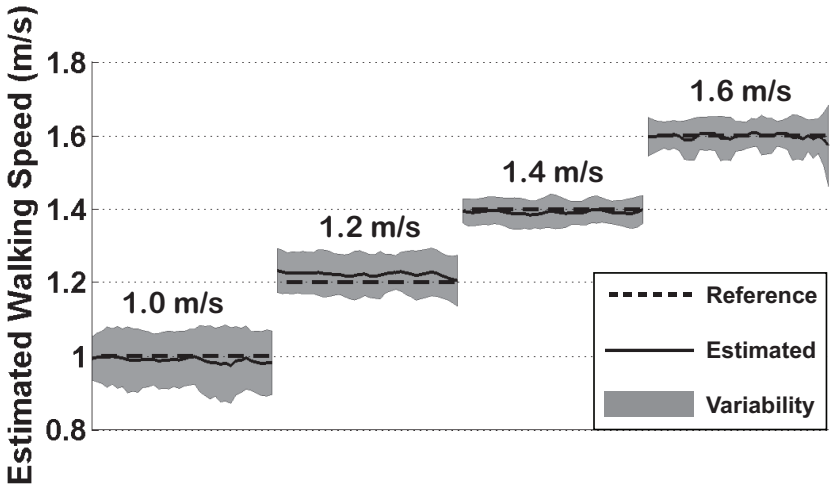

Figure 3.4: Adjusted average estimated walking speed (m/s) during treadmill walking at four treadmill speeds ($1.0m/s$, $1.2m/s$, $1.4m/s$ and $1.6m/s$) across five step frequencies (80%, 90%, 100%, 110% and 120% of the self-chosen step frequency). The solid lines are the average estimated walking speed across all subjects and all step frequencies at the specific treadmill speed. The shadow regions are average estimated walking speed ± one standard deviation of estimates from all subjects, indicating the inter-subject variability of the estimation results.

different treadmill speeds showed less variation in a range from 3.8% to 4.6%. The overall %RMSE of the adjusted walking speed estimation result was 4.2%. However, statistical two-way ANOVA test showed that the estimation errors were not significantly affected by the controlled treadmill speed during treadmill walking experiment ($P > 0.09$) and the step frequency ($P > 0.95$). The joint effect of the treadmill speed and the step frequency also showed insignificant effect on the estimation errors ($P > 0.88$). As such, the performance of the walking speed estimation algorithm could be considered consistent regardless of the tsreadmill speed and the step frequency.

Table 3.1: Treadmill walking speed estimation error and %RMSE at different treadmill speeds and step frequencies

	Frequency	Speed (m/s)				
		1.0	1.2	1.4	1.6	%RMSE
Unadjusted [1]	80% [4]	0.205 ± 0.097[3]	0.155 ± 0.069	0.179 ± 0.045	0.181 ± 0.103	16.1%
	90%	0.197 ± 0.086	0.155 ± 0.053	0.170 ± 0.042	0.159 ± 0.036	15.0%
	100%	0.212 ± 0.091	0.154 ± 0.075	0.185 ± 0.054	0.171 ± 0.042	16.0%
	110%	0.165 ± 0.070	0.162 ± 0.067	0.205 ± 0.061	0.190 ± 0.047	15.1%
	120%	0.168 ± 0.086	0.157 ± 0.048	0.191 ± 0.046	0.199 ± 0.065	15.0%
	%RMSE [5]	20.7%	14.0%	13.7%	11.9%	15.4%
Adjusted [2]	80%	0.065 ± 0.097	0.055 ± 0.069	0.036 ± 0.045	0.062 ± 0.103	4.6%
	90%	0.059 ± 0.086	0.045 ± 0.053	0.030 ± 0.042	0.032 ± 0.036	3.8%
	100%	0.061 ± 0.091	0.059 ± 0.075	0.031 ± 0.054	0.030 ± 0.042	4.2%
	110%	0.055 ± 0.070	0.053 ± 0.067	0.053 ± 0.061	0.051 ± 0.047	4.2%
	120%	0.065 ± 0.086	0.040 ± 0.048	0.040 ± 0.046	0.052 ± 0.065	4.2%
	%RMSE	6.1%	4.2%	2.8%	2.8%	4.2%

* Analysis is based on the data collected from 9 subjects;

[1] Unadjusted section shows the original step length estimation results before adjustment;

[2] Adjusted section shows the step length estimation results adjusted according to the linear regression model;

[3] Entry values are absolute Mean ± SD;

[4] Step frequency is represented by percentage of the self-chosen step frequency;

[5] %RMSE is RMSE divided by actual treadmill speed.

3.3.2 Overground Walking Experiment Result

Similarly, the step length estimation algorithm underestimated the step length. The average step length estimates for all subject at all the combinations of the designated step length and step frequency were shown in Figure 3.5. A linear regression function fitting the estimates was plotted to demonstrate the overall trend of the estimation result. The linear regression function had a slope (β) of 0.99 and a y-intercept (ε)

of -0.13. The y-intercept value of the linear regression function was subtracted from the estimates to obtain the adjusted results. Similar to the treadmill walking speed estimation result, the largest deviation were observed at the shortest ($0.7m$) designated step length while the estimates were less dispersive as the designated step length increases.

The adjusted average estimated step lengths across all subjects in all the walking conditions are shown in Figure 3.6. The overall RMSE between the designated step length and the adjusted average estimated step length was $0.015m$ within the analysed steps (12th to 26th step) across all step lengths. The largest inter-subject variability, quantified by the standard deviation of the average estimated step length of different subjects, was $0.043m$ while the least was $0.034m$, which were corresponding to step length $0.8m$ and $1.0m$, respectively.

Table 3.2 summarises the mean absolute estimation errors and the standard deviations of the estimation error before and after adjustment. Across different step frequencies, smaller variation was observed in the step length %RMSE comparing to the walking speed %RMSE of the treadmill walking experiment, which was in a range from 3.0% to 4.5%. Across different step length, the step length %RMSE was in a range from 3.7% to 4.2%. Two-way ANOVA test showed that the estimation errors were not significantly affected by the step length during overground walking experiment ($P > 0.2$). However, the step frequency was considered to significantly affect the estimation errors ($P < 0.01$), while the joint effect of the step length and the step frequency showed insignificant effect on the estimation errors ($P > 0.99$).

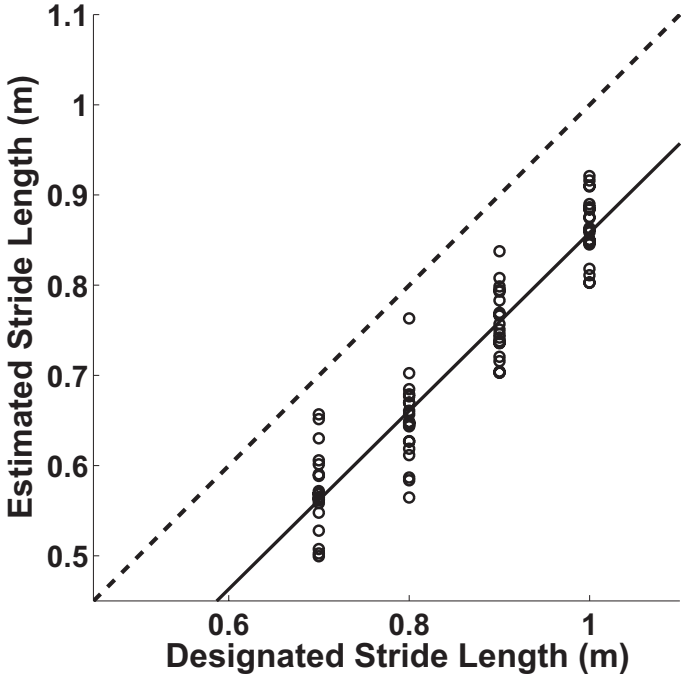

Figure 3.5: Average estimated step length (m) versus controlled step length (m) during overground walking at four designated step length ($0.7m$, $0.8m$, $0.9m$ and $1.0m$) and three step frequencies (90%, 100% and 110% of the self-chosen step frequency). Each circle indicates an average step length estimate of a subject at a combination of designated step length and step frequency. Since the step length (horizontal axis) was controlled, the estimates (indicated with circles) were distributed along lines of specific step length. The solid line is the plot of the linear regression function that fits the estimates (indicated with circles). The diagonal dash line showes the reference where the estimated step length and designated step length are equal.

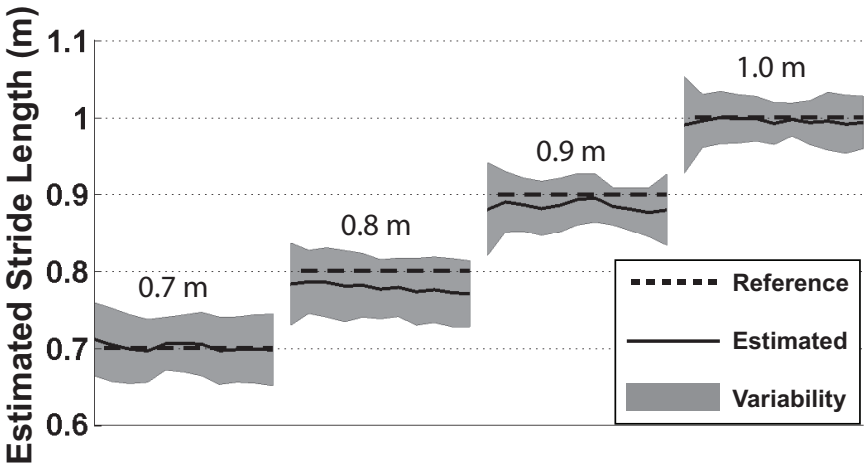

Figure 3.6: Adjusted average estimated step length estimates (m) during overground walking at four designated step length ($0.7m$, $0.8m$, $0.9m$ and $1.0m$) across three step frequencies (90%, 100% and 110% of the self-chosen step frequency). The solid lines are the average estimated step length across all subjects and all step frequencies at the specific designated step length. The shadow regions are average estimated step length $\pm$ one standard deviation of estimates from all subjects, indicating the inter-subject variability of the estimation results.

Table 3.2: Overground Walking Step Length Estimation Error and %RMSE at Different Designated Step Lengths and Step Frequencies

	Frequency	step length (m)				
		0.7	0.8	0.9	1.0	%RMSE
Unadjusted [1]	90% [4]	0.141 ± 0.039[3]	0.172 ± 0.035	0.161 ± 0.031	0.154 ± 0.026	18.9%
	100%	0.132 ± 0.044	0.155 ± 0.035	0.149 ± 0.028	0.135 ± 0.047	17.2%
	110%	0.113 ± 0.047	0.128 ± 0.053	0.123 ± 0.044	0.117 ± 0.026	14.5%
	%RMSE [5]	18.4%	19.1%	16.1%	13.6%	17.0%
Adjusted [2]	90%	0.029 ± 0.039	0.043 ± 0.035	0.038 ± 0.031	0.025 ± 0.026	4.2%
	100%	0.026 ± 0.044	0.035 ± 0.035	0.026 ± 0.028	0.038 ± 0.047	3.7%
	110%	0.038 ± 0.017	0.033 ± 0.053	0.035 ± 0.044	0.024 ± 0.026	4.1%
	%RMSE	4.5%	4.6%	3.7%	3.0%	4.0%

* Analysis is based on the data collected from 7 subjects

[1] Unadjusted section shows the original step length estimation results before adjustment;

[2] Adjusted section shows the step length estimation results adjusted according to the linear regression model;

[3] Entry values are absolute Mean ± SD;

[4] Step frequency is represented by percentage of the self-chosen step frequency;

[5] %RMSE is RMSE divided by actual step length value.

3.4 Discussion

The relationship in Equation 3.1 implies that the walking speed and the step length can be easily derived with known step frequency. The walking speed and step length estimation algorithm is equivalent in nature once the step frequency is fixed; thus, we could compare the step length estimation results from the overground walking experiment with the walking speed estimation results from the treadmill walking experiment. Furthermore, the algorithm estimates the walking speed/step length for each stride. The number of strides does not affect the estimation results and a

minimum number of strides is not required in the estimation process. Underestimation was observed in both treadmill and overground walking experiments for the proposed walking speed/step length estimation algorithm; however, with a proper adjustment, this algorithm could provide one of the most accurate estimations among previous studies [7, 8, 9, 11, 14, 12].

3.4.1 Sources of Error

The main error observed in both treadmill and overground walking experiments is a constant offset between the actual and the estimated values (Figure 3.4 and 3.6). As the constant offset exists for all the subjects in all walking conditions, it could presumably be considered as a systematic error.

The first cause of the systematic error could be the assumption of zero initial conditions in the integrations of the algorithm, referring to [8]. The proposed estimation algorithm uses the mid-stance shank vertical event as the start of each gait cycle, which provides a convenient way to define some of the initial conditions. Zero initial condition assumption were made for the shank linear velocities due to their small amplitude at the mid-stance shank vertical event. However, the shank angular velocity is evidently not exactly zero at the start of each stride cycle (Figure 3.2), which results in a non-zero initial horizontal velocity since the the horizontal velocity can be computed as the product of the angular velocity and the distance between the location of the IMU and the ankle joint. Similar underestimation of the walking speed was observed in [8] due to the same reason. However, higher walking speed does not necessarily result in larger initial walking speed. Since at the shank vertical event, the shank angular velocity reaches a local minimum, the difference between

shank angular velocities under different walking speeds is small at this event. It is reasonable to observe that the average systematic error over all subjects and all trials presents a constant offset.

The second possible cause of the systematic error is related to the orientation of the IMU on the shank. Since the shank is cylinder-like, the IMU cannot be attached steadily on the lateral side of the shank with perfect alignment to the sagittal plane. Our algorithm only considers the sagittal plane kinematics; thus, any misalignment between the IMU axes and the sagittal plane may result in a small IMU tangential acceleration measurement than actual value. Similarly, the angular velocity measurement is smaller than actual value due to the misalignment of the rotation axis with the angular velocity measurement axis. Figure 3.7 depicts the effect of the misalignment on the horizontal acceleration measurement, viewing from the top. To verify the effect, we simulated a simple situation with 10^o misalignment between the sagittal plane and the IMU axes. As a result, about 2.5% walking speed estimation error could be introduced.

3.4.2 Effect of Step Frequency in Overground Walking

Statistical two-way ANOVA test shows that the step frequency constraint significantly affected the step length estimation error in the overground walking experiment, with $P < 0.01$. Since no significant effect of the step frequency constraint on the walking speed estimation error was observed in the treadmill walking experiment, with $P > 0.95$, the difference possibly resulted from the increased attention demands in the overground walking experiment. Compared with the constrained treadmill walking, for which the only constraint that required subjects' attention was the step frequency

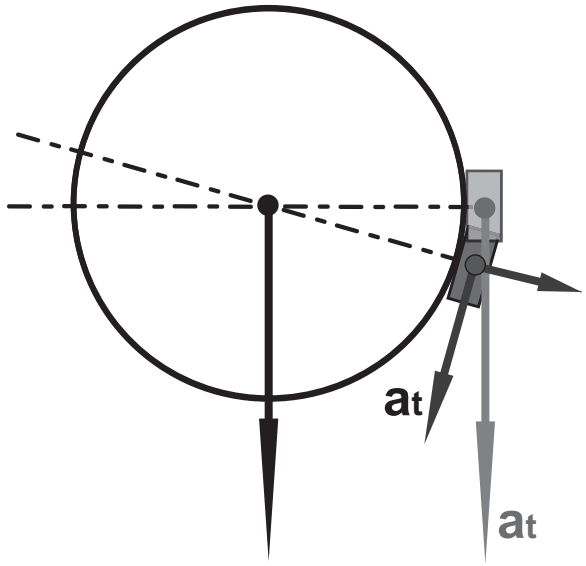

Figure 3.7: The effect of misalignment of the IMU axes with the Sagittal plane on the shank-mounted IMU measurement. The black arrow indicates the progression direction and acceleration magnitude. The circle indicates the top-view of the shank segment, while the light gray rectangle shows the IMU sensor at the designated position and the dark gray rectangle shows the misaligned IMU. a_t in light gray color is the expected tangential acceleration in the sagittal plane, and a_t in dark gray color is the tangential acceleration measurement axis when the IMU is at the misaligned position.

indicated by the beep sounds from the metronome, the constrained overground walking required additional attention from the subjects. The subjects needed to watch for the step markers and listen to the beep sounds from the metronome at the same time during the overground walking trials. As discussed in [18], when the feet placement was constrained the attention demands were greater than unconstrained walking. Furthermore, cognitive tasks, such as listening to the beep sounds from the metronome and watching the step markers on the hallway in our experiments, generally require a certain level of attention during walking [19], which may distract the attention from controlling posture during walking and keeping balance. The subjects in the overground walking experiment also reported that while watching for the step markers during walking it was difficult to follow the step frequencies that were too much lower (-20%) and too much higher ($+20\%$) than their preferred step frequencies. Furthermore, previous studies showed that when attention demanding tasks were performed during walking, a more conservative gait pattern other than natural gait pattern was adopted, implying an increase in the voluntary control of gait [20, 21]. However, since the voluntary gait change is based on the subjects' preference, large variation is expected. Since applying both step length and step frequency constraints was similar to a dual-task paradigm, referring to [19], the attention demands of the visual and auditory tasks is most likely the direct cause of the variation of the step length estimation error in overground walking experiment.

3.4.3 Inter-Subject Variability

The inter-subject variability of the estimation error, quantified by the standard deviation, was observed to be about 2% to 9% of the actual treadmill speed for the

treadmill walking experiment (Figure 3.4), and 2% to 6% the designated step length for the overground walking experiment (Figure 3.6). Depending on the leg length of the subjects, different levels of effort might be required to walking at the controlled treadmill speeds or designated step length. Especially for subjects with a shorter leg length, trying to reach a relatively higher target walking speed or longer target step length might have changed the subjects' natural walking gait patterns and lower limb kinematics. The subject-dependent kinematic changes, including the angular velocity and the linear acceleration, presumably affected the stride-to-stride displacement estimation and consequently introduced differences in the calculation results, which explains, at least partially, the observed inter-subject variability.

3.4.4 Limitations

In our study, the experiments were performed on healthy young subjects, for which the performance is representative for the younger population. As a limitation, the proposed method may not be directly applicable to older population or people with gait deficiencies for two reasons. First, the proposed method underestimated the walking speed/step length by a constant offset and a constant correction is required to improve the accuracy of the estimation. However, the constant offset is possibly different between subject groups, which may introduce inaccuracy to the performance of the proposed method in other populations. Second, the applicability of the algorithm depends on the shank kinematic characteristics. Because the shank kinematic characteristics may not be the same for different subject groups, further experiment is required before applying the method to elderly group or subjects with gait disorder.

The obtained error might be affected by the equipments and control methods we

used in the experiments. When the subject was walking on the treadmill, certain level of treadmill speed fluctuations were inevitable. As direct quantification of the stride-to-stride treadmill speed fluctuations of a commercial treadmill is difficult, we attempted to indirectly quantify the average treadmill speed fluctuations. We performed a treadmill calibration procedure proposed by NASA [22] and found that the maximum average treadmill speed variation over a period of time was around $\pm 0.035 m/s$ when a young subject (weight $75 kg$) was walking on the treadmill. This fluctuation would at most account for 0.08% of the overall RMSE% observed in this study, which is negligible. On the other hand, it was assumed that subjects in the overground walking experiment stepped on the designated markers for each step; however, the actual step length in each step may fluctuate as well. We expect the variation of the actual step length to be $\pm 2 cm$ at maximum. At the worst case, the fluctuation of the actual step length would account for 1.14% of the overall RMSE%. Methods or equipments that can directly measure the instantaneous actual treadmill speed/step length will be employed to eliminate associated error related to the experimental equipment. For example, we could apply a sensor mat, such as GAITRite system (CIR System Inc. Havertown, USA), on the floor to track the exact position of each step. A concurrent validation procedure similar to [23] could be used to evaluate the performance of our method.

3.5 Conclusion

This study thoroughly evaluated the performance of an IMU-based ambulatory walking speed estimation system in both treadmill and overground walking experiments under different combinations of walking conditions. Consistent walking speed/step

length estimation results were achieved, and the estimation accuracy is comparable with other inertial-sensor-based walking speed estimation systems. Moreover, since the algorithm estimates the stride-to-stride walking speed and step length, in application there is no learning process or requirement for a minimum number of strides for the walking speed/step length estimation if the subject is from the same test population. Although a certain level systematic error was found in the proposed walking speed/step length estimation algorithm, it could be removed with a simple adjustment. The inter-subject variability of the estimation error indicates that a subject-specific calibration might be considered to improve the performance of the system. Overall, the application of the system in constrained walking studies, including optimal walking study, is promising.

3.6 Acknowledgements

This study was partially supported by NSERC discovery grant and a Queen's ARC grant to Q. Li. I would also like to gratefully acknowledge the contribution of Martin Eriksson and Emily Bishop in the experiment of this study.

References

[1] Kenton R. Kaufman, Christine Hughes, Bernard F. Morrey, Michael Morrey, and Kai-Nan An. Gait characteristics of patients with knee osteoarthritis. *Journal of Biomechanics*, 34(7):907 – 915, 2001.

[2] J. Perry. *Gait analysis: normal and pathological function*. SLACK incorporated, 1992.

[3] CL Richards, F. Malouin, and C. Dean. Gait in stroke: assessment and rehabilitation. *Clinics in Geriatric Medicine*, 15(4), 1999.

[4] T. P. Andriacchi, J. A. Ogle, and J. O. Galante. Walking speed as a basis for normal and abnormal gait measurements. *Journal of Biomechanics*, 10(4):261–268, 1977.

[5] N. Sekiya, H. Nagasaki, H. Ito, and T. Furuna. Optimal walking in terms of variability in step length. *The Journal of Orthopaedic and Sports Physical Therapy*, 26(5):266, 1997.

[6] J.E.A. Bertram and A. Ruina. Multiple walking speed–frequency relations are predicted by constrained optimization. *Journal of Theoretical Biology*, 209(4):445–453, 2001.

[7] K. Aminian, B. Najafi, C. Bula, P.F. Leyvraz, and P. Robert. Spatio-temporal parameters of gait measured by an ambulatory system using miniature gyroscopes. *Journal of Biomechanics*, 35(5):689–699, 2002.

[8] Q. Li, M. Young, V. Naing, and J. M. Donelan. Walking speed estimation using a shank-mounted inertial measurement unit. *Journal of Biomechanics*, 43(8):1640–1643, 2010.

[9] S. Miyazaki. Long-term unrestrained measurement of stride length and walking velocity utilizing a piezoelectric gyroscope. *IEEE Transactions on Biomedical Engineering*, 44(8):753–759, 1997.

[10] R.E. Mayagoitia, A.V. Nene, and P.H. Veltink. Accelerometer and rate gyroscope measurement of kinematics: an inexpensive alternative to optical motion analysis systems. *Journal of Biomechanics*, 35(4):537–542, 2002.

[11] RC González, D. Alvarez, AM López, and JC Alvarez. Ambulatory estimation of mean step length during unconstrained walking by means of cog accelerometry. *Computer Methods in Biomechanics and Biomedical Engineering*, 12(6):721–726, 2009.

[12] W. Zijlstra and A.L. Hof. Assessment of spatio-temporal gait parameters from trunk accelerations during human walking. *Gait & Posture*, 18(2):1–10, 2003.

[13] A. Zijlstra, E. D. de Bruin, N. Bruins, and W. Zijlstra. The step length-frequency relationship in physically active community-dwelling older women. *Europeam Journal of Applied Physiology*, 104(3):427–434, 2008.

[14] A. M. Sabatini, C. Martelloni, S. Scapellato, and F. Cavallo. Assessment of walking features from foot inertial sensing. *IEEE Transactions on Biomedical Engineering*, 52(3):486–94, 2005.

[15] K. Jordan, J.H. Challis, and K.M. Newell. Walking speed influences on gait cycle variability. *Gait & Posture*, 26(1):128–134, 2007.

[16] J.E.A. Bertram. Constrained optimization in human walking: cost minimization and gait plasticity. *Journal of Experimental Biology*, 208(6):979, 2005.

[17] J.E.A. Bertram. Hypothesis testing as a laboratory exercise: A simple analysis of human walking, with a physiological surprise. *Advances in Physiology Education*, 26(2):110, 2002.

[18] W.A. Sparrow, E.J. Bradshaw, E. Lamoureux, and O. Tirosh. Ageing effects on the attention demands of walking. *Human Movement Science*, 21(5-6):961–972, 2002.

[19] M. Woollacott and A. Shumway-Cook. Attention and the control of posture and gait: a review of an emerging area of research. *Gait & Posture*, 16(1):1–14, 2002.

[20] M.D. Grabiner and K.L. Troy. Attention demanding tasks during treadmill walking reduce step width variability in young adults. *Journal of NeuroEngineering and Rehabilitation*, 2(1):25, 2005.

[21] J.B. Dingwell, R.T. Robb, K.L. Troy, and M.D. Grabiner. Effects of an attention demanding task on dynamic stability during treadmill walking. *Journal of NeuroEngineering and Rehabilitation*, 5(1):12, 2008.

[22] P. A. Bishop, M. M. Bamman, S. Fortnet, M. Greenisen, Jr. A. D. Moore, S. F. Siconolfi, and W. Squires. Procedures for exercise physiology laboratories. Technical report, NASA, 1998.

[23] A. Hartmann, S. Luzi, K. Murer, R.A. de Bie, and E.D de Bruin. Concurrent validity of a trunk tri-axial accelerometer system for gait analysis in older adults. *Gait & Posture*, 29:444–448, 2009.

Chapter 4

An Ambulatory Spatio-Temporal Analysis System for Post-Stroke Hemiparetic Gait using Shank-Attached IMUs

Abstract

Clinical gait analysis is an important component of the post-stroke rehabilitation process. In this study we investigated the performance of an ambulatory spaio-temporal analysis system for hemiparetic gait after stroke using inertial measurement units (IMUs) attached to the shanks. For general clinical interest, two aspects of the hemiparetic gait were analyzed: walking speed and gait asymmetry. The walking

speed algorithm is based on the fact that walking is a cyclical motion with a distinguishable pattern. The shank kinematics provide sufficient information to assess the spatio-temporal characteristics of hemiparetic gait. According to the kinematic characteristics exhibited, the walking speed estimation algorithm used the shank angular velocity to determine initial conditions for the integration and correct integration drift errors. Gait asymmetry was quantified in terms of stride length ratio (SLR) and the comparison of stance/swing ratio (SSR). The system evaluation was carried out over the standardized 10 meter walking test (10MWT). The Bland-Altman method showed good agreement between the mean walking speed measured by the IMU-based system and a stopwatch method, with a mean difference of $0.01m/s$ and $0.00m/s$ and limit of agreement of $\pm 0.09m/s$ and $\pm 0.10m/s$ for the non-paretic and the paretic legs, respectively. The gait asymmetry analysis produced results that were comparable with previous reports.

4.1 Introduction

Stroke is a leading cause of adult disability in Western countries [1]. According to World Health Organization estimates, 15 million people suffer stroke each year, of which 5 million are permanently disabled [2]. A common disability after stroke is hemiparesis: weakness on one side of the body. Due to muscle weakness, stroke survivors either unintentionally or intentionally tend to limit the use of the paretic leg, which consequently leads to asymmetrical gait and reduced mobility. Since gait impairments and mobility disorders can negatively impact independence, assisting the restoration of a normal gait and enabling safe community ambulation has been considered a primary goal for stroke rehabilitation [3]. During the rehabilitation

process, clinical gait analysis generally provides valuable outcome measures to assess post-stroke recovery [4].

Both gait speed and gait asymmetry have been widely used in assessing post-stroke gait [5, 6]. Self-selected walking speed has long been recognized as a proxy measure of ambulation quality and is used to quantify the progress of gait rehabilitation [7, 8, 9, 4]. A widely accepted clinical ambulation assessment of short duration walking speed (m/s) is the standardized 10-Meter Walking Test (10MWT) [10, 11], which makes use of a stopwatch and reflects general physical function [12]. On the other hand, the degree of asymmetry of spatio-temporal gait parameters has been considered as a valuable indicator of hemiparetic gait recovery, since it is directly related to the disturbances in motor coordination [13, 14]. Common spatio-temporal parameters used in the evaluation of gait asymmetry include the relative stance/swing ratio (SSR) and the paretic/non-paretic leg stride length ratio (SLR) at preferred walking speed [15, 16, 17, 18]. Recently, the GAITRite system, a portable instrumented electronic walkway, has been commonly utilized to record the spatio-temporal parameters, such as stride length, swing time and stance time [16, 19, 18]. The use of this system however is restricted by its limited length and it is costly. An inexpensive and easy-to-use system capable of assessing both walking speed and gait asymmetry could be a cost-effective means of monitoring progressive changes during post-stroke rehabilitation.

Previous studies have demonstrated that miniature inertial sensors are well suited to evaluating the spatio-temporal parameters of human gait. They are lightweight, very portable and easy to use. The walking speed estimation for healthy people using inertial sensors has been developed and validated in the past several years

[20, 21, 22, 23]; however, their application in post-stroke hemiparetic gait analysis is mostly limited to using raw inertial information to detect gait events or count steps [24, 25, 26, 27, 28, 29].

The objective of this study is to test an inertial sensor-based portable gait analysis system that is capable of providing walking speed and quantifying gait asymmetries of people with stroke simultaneously. A shank-attached IMU-based walking speed estimation algorithm was previously reported by Li *et. al* [22] for healthy individuals; however, because the algorithm requires a linear regression on the test data to correct the systematic error [23], it may not be suited for stroke gait if the inter-subject variability of the data is high. A novel walking speed estimation algorithm was therefore developed in this study by considering the initial speed and compensating the sensor drift error to minimize systematic error. The gait asymmetry quantification is based on the stride length and swing/stance time associated with the non-paretic and paretic legs. The gait events (heel-strike and toe-off) are determined from the characteristics of the shank angular velocity of both legs, measured by gyroscopes.

4.2 Methods

4.2.1 Apparatus

The Inertia-Link (MicroStrain, Inc., Williston, VT, USA) is an IMU sensor that consists of a triaxial accelerometer ($\pm 5g$, where g is the gravitational acceleration) and a triaxial gyroscope ($\pm 600^\circ/sec$) with measurement errors in a range of $\pm 0.005g$ and $\pm 2.0^\circ/sec$, respectively, in dynamic conditions. Only two accelerometer axes and one gyroscope axis were used as our focus was motion in the plane of progression (ie.

sagittal plane). The linear acceleration and angular velocity data were collected at $100Hz$ and sent to a USB base station receiver via a built-in wireless communication system ($2.45GHz$ IEEE 802.15.4). Modified data acquisition software (MicroStrain, Inc., Williston, VT, USA) was used to record the raw data for off-line analysis.

4.2.2 Sensor Configuration

An IMU sensor was attached at the midpoint of each shank on the lateral side using athletic tape. Before each experiment, subjects were asked to stand still with the shank vertical (longitudinal axis perpendicular to the floor) and the IMU was adjusted such that its normal and tangential axes were aligned to vertical and horizontal directions of the world coordinate system, respectively (Figure 4.1). As such, the initial measurement from the IMU showed approximately $0g$ in the tangential axis and $1g$ in the normal axis of the IMU sensor.

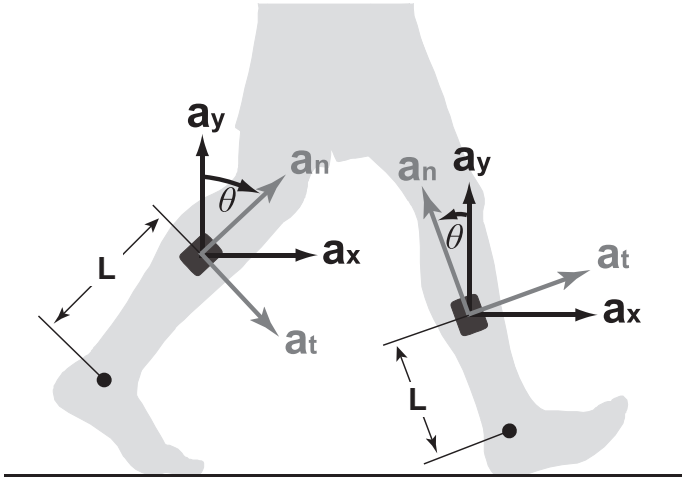

Figure 4.1: Sensor configuration: An IMU is attached to the shank in the sagittal plane on the lateral side. Since only the shank motion in sagittal plane was considered in the method, the normal acceleration a_n is measured along the n direction, the tangential acceleration a_t is measured along the t direction, and the axis of the gyroscope is perpendicular to the sagittal plane defined by n and t directions. The arrows indicate positive axes for the corresponding sensor measurements. L is the sensor-to-ankle distance. The world coordinate system is defined by the x and y axes, and the vertical axis y extends in a direction parallel to gravity.

4.2.3 Signal Conditioning

Signal processing was performed using MATLAB (The MathWorks, Natick, MA, USA). On average, 5% of data loss was present in the wireless transmission between the IMUs and the computer. Before data processing, one-dimensional interpolation was used to reconstruct the missing data points. For the walking speed estimation and the gait events detection algorithm, a second-order Butterworth low-pass filter with cut-off frequency of $10Hz$ was used to remove noise from the raw acceleration and angular velocity measurements. The cut-off frequency was selected to maximize the resolution of the gyroscope characteristics for the gait events detection while

removing the signal noise resulting both from sensor electronics and skin motion. For the gait segmentation for walking speed estimation, a second-order Butterworth low-pass filter with cut-off frequency of $2.5Hz$ was applied to the gyroscope signals. The gait segmentation process was less time sensitive than the gait event detection and the resultant smoothed signal reduced the complexity of the algorithm.

4.2.4 Walking Speed Estimation

Gait segmentation algorithm was implemented to divide the walking sequence into stride cycles, and the average walking speed for each stride cycle was calculated individually. Therefore, integrations of the acceleration and angular velocity data over time would cause large drift errors in the velocity and position estimation due to a small offset in acceleration measurements. The use of gait segmentation effectively avoided such drift errors and enabled stride-to-stride velocity drift error correction. The starting point of each stride cycle was defined as the shank vertical event, when the longitudinal direction of the shank was parallel to the direction of gravity [22]. This specific gait event could be determined by the characteristics of the shank angular velocity (Figure 4.2). Starting from the beginning of each stride cycle, the instantaneous shank angle was computed by integrating the gyroscope measured angular velocity. The shank angle was then used to transform the accelerometer measured accelerations from the local coordinate system (sensor) to the global coordinate system. The instantaneous shank velocities were calculated through direct time integration of the accelerations in the global coordinate system, and then the walking speed was calculated for the corresponding stride cycle (see [22] for details). Walking speed estimation performed in this way yielded relatively high accuracy in treadmill and

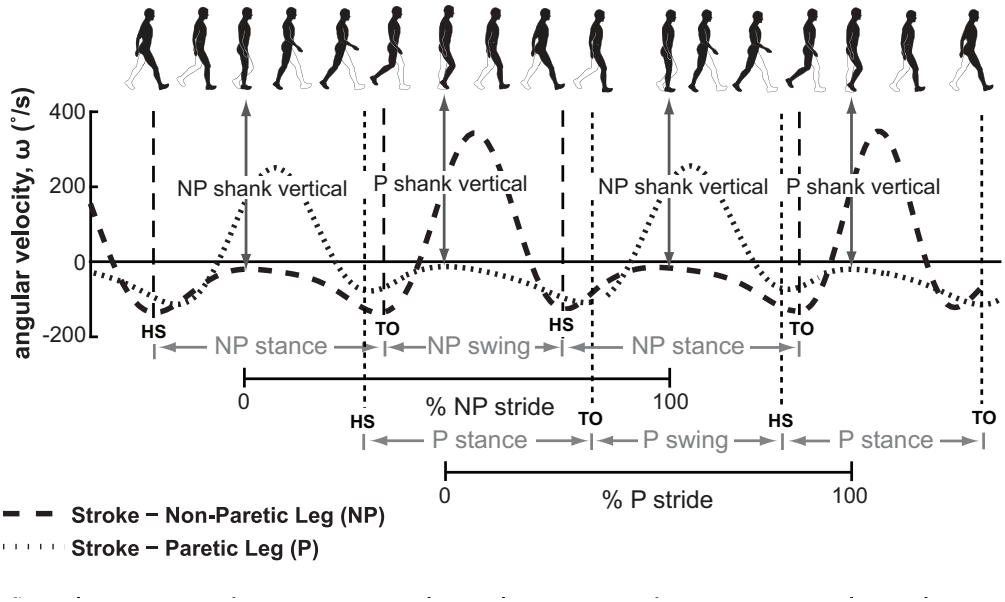

Figure 4.2: Characteristic of shank angular velocity, ω, during two consecutive stride cycles. The angular velocity of the non-paretic leg (NP) is indicated by the thick dashed curve, and the paretic leg (P) is indicatd by the thin dashed curve. The stride cycle of the NP leg and the P leg was was determined by the mid-stance shank vertical event, at which point the magnitude of the angular velocity approached zero. The swing phase and the stance phase of each leg were determined by the heel-strike (HS) and toe-off (TO) gait events, which were identified by the negative peaks of the shank angular velocity. The segmented stride cycles, the gait events and gait phases were labeled according to the aforementioned criteria.

overground walking experiments [22]. However, further experiments identified systematic errors requiring a calibration process using linear regression to compensate the error for a given subject population [23]. The calibration process required to determine the appropriate correction constant hinders the practicability of the system. Furthermore, the less fluid gait of stroke subjects and inter-subject variability render the linear regression method of correction less useful. Hence, we have developed two new strategies to compensate the systematic error and the sensor errors.

First, the initial speed at the beginning of each stride cycle was taken into consideration in the algorithm. At shank vertical event, although the shank angular velocity is minimal, it is not exactly zero (Figure 4.2). As an observation, the shank could be modeled as an inverted pendulum rotating about the ankle joint; thus, the inertial sensor velocity could be calculated as product of the rotation radius and the shank angular velocity. The initial sensor velocity at shank vertical event ($\theta(0) = 0$) is calculated as

$$v_t(0) = \omega(0) \cdot L, \tag{4.1}$$

$$\begin{bmatrix} v_x(0) \\ v_y(0) \end{bmatrix} = \begin{bmatrix} \cos\theta(0) \\ -\sin\theta(0) \end{bmatrix} \cdot v_t(0) = \begin{bmatrix} v_t(0) \\ 0 \end{bmatrix}, \tag{4.2}$$

where $v_t(0)$ is the initial sensor velocity tangential to the shank, $\theta(0)$ is the shank angle when vertical, $v_x(0)$ and $v_y(0)$ are the initial sensor horizontal and vertical velocities in the global coordinate system, respectively. L is the distance from the sensor to the ankle joint, which is approximately half of the total shank length (Figure 4.1). These initial conditions, $v_x(0)$ and $v_y(0)$, are added to the calculation of instantaneous sensor velocities,

$$\begin{aligned} v'_x(t) &= \textstyle\int_0^t a_x(\tau)d\tau + v_x(0) \\ v'_y(t) &= \textstyle\int_0^t a_y(\tau)d\tau + v_y(0), \end{aligned} \tag{4.3}$$

where $v'_x(t)$ and $v'_y(t)$ are the instantaneous horizonal and vertical velocities obtained from integrating the sensor accelerations. a_x and a_y are the horizontal and vertical accelerations in the global coordinate system, transformed from the sensor accelerations, a_t and a_n (Figure 4.1).

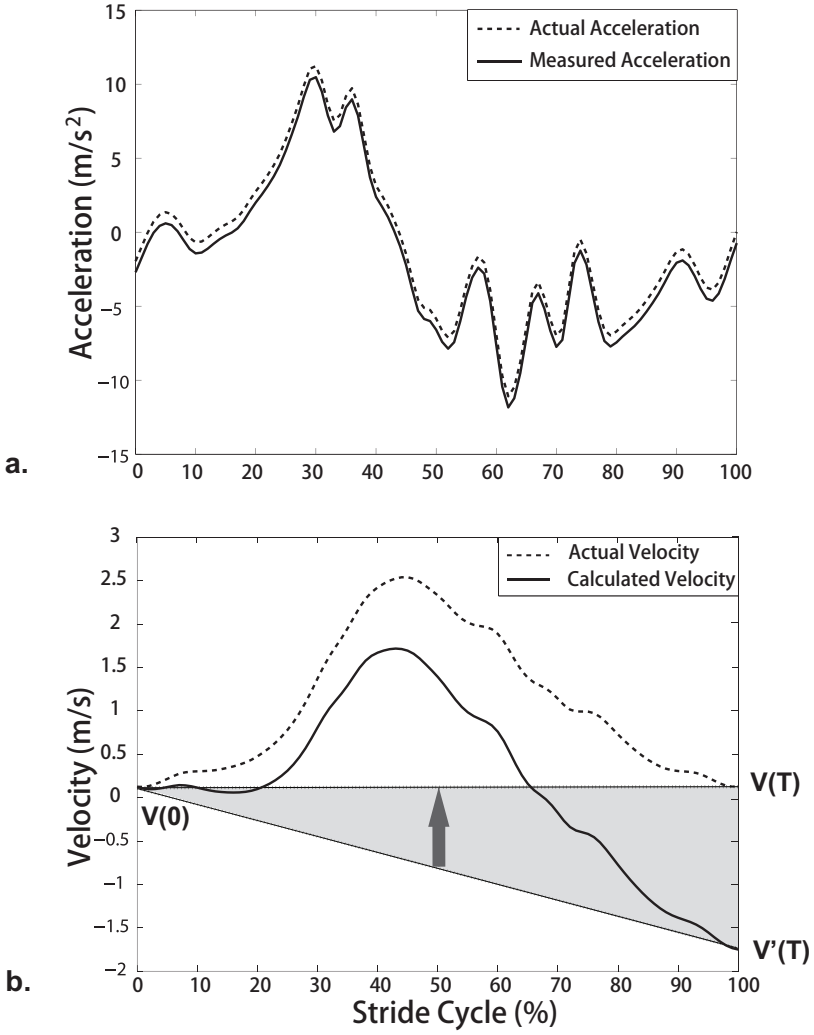

Figure 4.3: a). A constant acceleration bias in global coordinate system observed in the IMU acceleration measurement (solid line) in comparison with the acceleration measurement (dashed line) with OptoTrak motion capture system (OptoTrak, NDI, ON, Canada). The constant bias might vary upon each reset of the IMU. This figure shows the shank acceleration measurement for an entire stride cycle beginning with the mid-stance shank vertical events. b). Velocity integrated from the measured acceleration with a constant acceleration bias. The gray area indicates the drifts of the velocity calculation due to the acceleration bias. A correction is therefore required to obtain the actual shank velocity. $V(0)$ is the initial sensor velocity, $V'(T)$ is the calculated sensor velocity in the end of the stride cycle with drift error, and $V(T)$ is the corrected sensor velocity.

Second, the shank angular velocity measurement was utilized to correct the walking speed estimation error associated with the acceleration measurement bias. The accelerometer measurement bias is inevitable for low-cost IMU sensors [30], and the direct consequence is velocity drift, resulting from the integration of biased acceleration data over a period of time (Figure 4.3b). Although the long-term behavior of the accelerometer measurement bias is difficult to predict, the bias can be approximated as a constant in a relatively short time interval. We confirmed this assumption through a comparison between the accelerometer measured acceleration with a motion capture system measured acceleration (Figure 4.3a). To determine the constant accelerometer bias, it requires a known reference velocity at the end of the stride cycle. Given the angular velocity measurement and the inverted pendulum model at the end of the stride cycle, the reference velocities are calculated as

$$\begin{aligned} v_{xref}(T) &= \omega(T) \cdot L \\ v_{yref}(T) &= 0, \end{aligned} \tag{4.4}$$

By comparing these reference velocities with the sensor velocities calculated from Equation (4.3), $v'_x(t)$ and $v'_y(t)$, we calculated the constant accelerometer biases as

$$\begin{aligned} a_{xbias} &= \tfrac{v_x(T)-v'_x(T)}{T} \\ a_{ybias} &= \tfrac{v_y(T)-v'_y(T)}{T}, \end{aligned} \tag{4.5}$$

The corrected sensor velocity was calculated by subtracting the velocity drift caused by the constant accelerometer bias from the calculated instantaneous sensor velocities,

$$\begin{aligned} v_x(t) &= v'_x(t) - a_{xbias} \cdot t \\ v_y(t) &= v'_y(t) - a_{ybias} \cdot t, \end{aligned} \tag{4.6}$$

where $v_x(t)$, $v_y(t)$ are the corrected instantaneous sensor horizontal and vertical velocities in global coordinate system, respectively.

After calculating the instantaneous shank velocity through Equations (4.1)-(4.6), the stride length and time average of the shank velocity in horizontal and vertical directions could be calculated over any selected stride cycle as

$$\begin{aligned} \bar{v}_x &= \frac{1}{T} \cdot \int_0^T v_x(t)dt \\ \bar{v}_y &= \frac{1}{T} \cdot \int_0^T v_y(t)dt, \end{aligned} \tag{4.7}$$

where $\bar{v}_x$ and $\bar{v}_y$ are the average horizontal and vertical velocities over the corresponding stride cycle in $(0, T]$, as defined by gait segmentation.

The walking speed over the stride was then calculated as $\bar{v} = \sqrt{\bar{v}_x^2 + \bar{v}_y^2}$. The vector calculation eliminated error resulting from the misalignment of the accelerometer normal and tangential axes with the shank longitudinal and fore-aft directions. The stride length was defined as the shank displacement over one stride cycle starting from initial shank vertical event to the next of the same leg. Thus, the stride length (SL) of each stride cycle was calculated as $SL = \bar{v} \cdot T$.

4.2.5 Gait Asymmetry

The temporal parameters and gait phases of hemiparetic gait were determined based on the toe-off (TO) and the heel-strike (HS) gait events within a stride cycle, which correspond to the start and the end of the swing phase, respectively (Figure 4.2). Thus, the swing phase time is the time difference between TO and HS, and the stance phase is the rest of the cycle. Using a shank mounted gyroscope to detect these gait events has proven to be accurate and presents some advantages over foot mounted inertial sensors due to the simplicity of the detecting algorithm [31, 27, 26]. The characteristics of the shank angular velocity and the gait phase definitions are shown in Figure 4.2, where two negative peaks represent the TO and HS gait events

[20, 31, 27, 26].

Upon the detection of TO and HS gait events, the swing phase and the stance phase of each stride were determined for both paretic and non-paretic legs. The percentage stance time ($\%T_{st}$) and the percentage swing time ($\%T_{sw}$) were defined as the stance time (T_{st}) and the swing time (T_{sw}) divided by the total stride cycle (T_{sc}) time, $\%T_{st} = T_{st}/T_{sc}$ and $\%T_{sw} = T_{sw}/T_{sc}$, respectively. The stance/swing ratio (SSR) was defined as the stance phase time divided by the swing phase time of a stride cycle, $SSR = T_{st}/T_{sw}$. As the stride length has been estimated by the proposed walking speed estimation algorithm, the stride length ratio (SLR) for each subject was defined as the paretic stride length (SL_P) divided by the non-paretic stride length (SL_{NP}), $SLR = SL_P/SL_{NP}$. The farther the ratio from 1, the more severe the asymmetry.

4.2.6 Experimental Method

Subjects

Thirteen stroke subjects were recruited from the community forming a sample of convenience including ten males and three females (age: 59.5 ± 10.3 years; height: 168.1 ± 8.1 cm; weight: 73.7 ± 16.1 kg; shank length: 37.0 ± 2.2 cm; time post-stroke: 23.4 ± 15.1 months). Eight had left hemiparesis and five had right hemiparesis. All subjects were screened to ensure they: (1) had residual unilateral lower limb weakness, (2) were able to walk independently, and (3) could follow instructions. All subjects gave their informed consent to participate in accordance with university policy, and the study was approved by the Queen's Health Science Research Ethics Board (HSREB).

Protocol

Subjects were instructed to walk at a comfortable speed along a straight hallway with yellow adhesive tape marking the 10-meter distance on the floor. Three trials were performed and the time to cover the 10-meter distance was recorded using a stopwatch. The average walking speed was calculated across the trials and was used as the reference in the analysis. During the walking trials, IMU sensors were attached laterally on each shank and data recorded for the entire walking trial.

4.2.7 Data Analysis

The Bland-Altman method was used to compare the walking speed measured with a stopwatch to that estimated by the algorithm. A Bland-Altman plot visually demonstrated the agreement between the measurements made by two different methods, in which each data point is represented by the mean of two measurements (x-axis) and the difference between two measurements (y-axis) [32], $V_{StopWatch} - V_{IMU}$. The mean of the difference (Mean) and ± 2 Standard Deviations (SD) were plotted to illustrate the bias and the limits of agreement between the two methods. Since the stopwatch could not provide the stride-to-stride walking speed, the mean estimated walking speed for each walking trial was calculated by averaging the estimated stride-to-stride walking speed. The spatio-temporal asymmetries were quantified using the stance phase, swing phase and the stride length of the paretic and the non-paretic legs. The stance/swing ratio (SSR) and the stride length ratio (SLR) were calculated to provide direct comparison between the legs. Student's t-tests were applied to the spatio-temporal parameters to examine difference between paretic and non-paretic sides, with $p < 0.05$ indicating the statistical significance. The mean and standard

deviation (SD) of all the parameters described the inter-subject variability.

4.3 Results

The data from twelve subjects were included in the walking speed estimation analysis and gait asymmetry analysis. One subject's data were excluded due to the inability of the algorithm to detect the gait events correctly. The mean self-selected 10MWT speed ($\pm 1SD$) was 0.93±0.20 m/s, which compares to other studies investigating mild to moderately affected people with stroke [33, 18, 25]. Using the proposed walking speed estimation algorithm, the systematic errors found in the original walking speed estimation algorithm [23] were effectively removed as shown in the Bland-Altman plot (Figure 4.4). Strong agreement between the walking speed estimated from the IMU sensors and the reference walking speed from the 10MWT was clearly evident. The mean difference was 0.01 m/s with limits of agreement from −0.08 to 0.09 m/s for the non-paretic leg (Figure 4.4a), indicating that ±2SD of the measurements estimated from the algorithm and by the stopwatch would correspond within −0.08 and 0.09 m/s for the population. Similarly, for the paretic leg, the mean difference was 0.00 m/s with limits of agreement from −0.10 to 0.10 m/s (Figure 4.4b).

The details of the gait asymmetry analysis results are summarized in Table 4.1. The measured stride length from the paretic and the non-paretic legs were comparable, and the SLR of 1.02 ± 0.03 reflected minimal asymmetry ($p > 0.25$). On the other hand, the stance and swing phase times were significantly different between the non-paretic leg ($\%T_{st} = 59.46 \pm 2.86\%$; $\%T_{sw} = 40.54 \pm 2.86\%$) and the paretic leg ($\%T_{st} = 53.28 \pm 3.70\%$; $\%T_{sw} = 46.72 \pm 3.70\%$), $p < 0.01$. The stance/swing ratios (SSR) were also different between the two legs ($SSR_{NP} = 1.48 \pm 0.18$; $SSR_P =$

1.15 ± 0.16), $p < 0.01$.

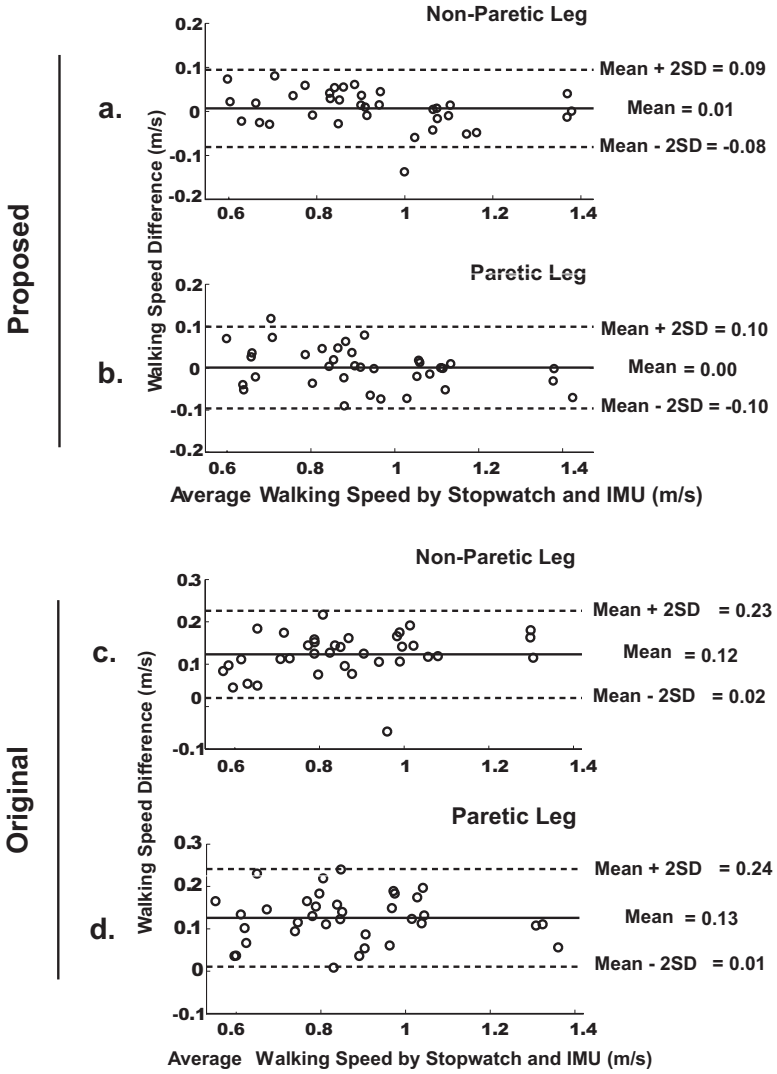

Figure 4.4: Bland-Altman plots for the proposed walking speed estimation algorithm and the original walking speed estimation algorithm [23]. (a). and (b).: estimation results from the proposed algorithm; (c). and (d).: estimation results from the original algorithm. The x-axis depicts the average walking speed (m/s) determined from the IMU sensor and stopwatch, and the y-axis depicts the mean difference in average walking speed determined using both methods. Each circle represents one data point from a single walking trial. The solid lines indicate the overall mean of the measurement difference, and the dashed lines show the limits of agreement (±2SD).

Table 4.1: Asymmetry Analysis of Hemiparetic Gait

Variable	Non-Paretic Leg[1]	Paretic Leg[2]	Mean
SL (m)	1.07 ± 0.19	1.08 ± 0.20	1.08 ± 0.20
SLR	1.02 ± 0.03		
$\%T_{st}$ (%)	59.46 ± 2.86	$53.28 \pm 3.70^{\dagger}$	
$\%T_{sw}$ (%)	40.54 ± 2.86	$46.72 \pm 3.70^{\dagger}$	
SSR	1.48 ± 0.18	$1.15 \pm 0.16^{\dagger}$	

* Analysis is based on the data collected from 12 subjects;
** All results are presented as Mean±SD;
[1] Analysis based on the IMU attached on the non-paretic leg;
[2] Analysis based on the IMU attached on the paretic leg;
† $p < 0.05$; significant difference between NP and P legs.

4.4 Discussion

For both non-paretic and paretic legs, the walking speed estimated by the IMU ambulatory system showed strong agreement with the same measurement obtained with a stopwatch over the standard 10MWT. For our study population very small bias (non-paretic leg: 0.01 m/s; paretic leg: 0.00 m/s) was found as illustrated in the Bland-Altman plots (Figure 4.4a and b), thus confirming that no offset adjustment was required. The Bland-Altman plots also showed us that for about 95% of cases, the measurement difference between the two methods would lie within the limits of agreement (±2SD). In practice, clinical assessment based on self-selected walking speed uses broadly defined categories to classify the abilities of people with stroke. For example, Schmid *et. al* classified the ambulation ability (post-stroke) into household ambulation, community ambulation and full community ambulation categories using walking speed thresholds of $0.4m/s$ and $0.8m/s$ [9]. Other reported community ambulation classification thresholds vary from $0.8m/s$ to $1.3m/s$ [34]. Further, changes

in walking speed averaging $0.14m/s$ have been associated with significant gains in walking efficiency and improved gait kinetics [35, 36]. Therefore, the measurement differences, within the limits of agreement ($0.01 \pm 0.08m/s$ for non-paretic leg and $0.00 \pm 0.10m/s$ for paretic leg), was considered not clinically important, and the proposed system could be used in place of the stopwatch in walking speed measurement for post-stroke subjects.

The walking speed estimation algorithm took initial speed and drift error correction into consideration to enable accurate speed estimation. As a comparison, the original walking speed estimation algorithm proposed in [23] showed a consistent underestimation of speed with a systematic error (bias) of $0.12m/s$ for the non-paretic leg and $0.13m/s$ for the paretic leg (Figure 4.4c and d). The bias could be corrected by subtracting a constant, but additional measurements and calibrations are required to determine the population-dependent constant. The acquisition of these additional measurements would limit the clinical value of the ambulatory gait analysis system.

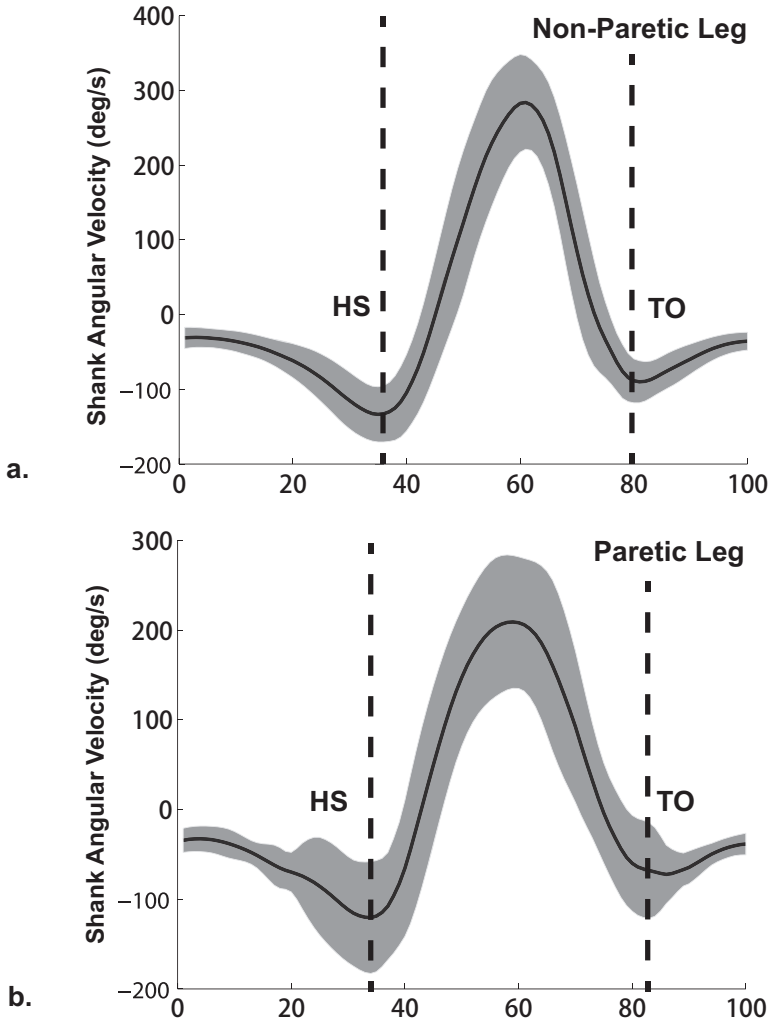

Figure 4.5: Summary of shank angular velocity characteristics for non-paretic leg (a) and paretic leg (b). The solid curves are the average shank angular velocity over a complete stride cycle for all walking trials across all subjects. The shadow regions are the average shank angular velocity ± one standard deviation, indicating the inter-subject variability of the shank angular velocity characteristics. Two negative peaks of the shank angular velocity correspond to the toe-off (TO) and heel-strike (HS) gait events.

Although the biomechanics of hemiparetic gait differ from healthy gait, the consistency in the pattern of the shank angular velocity [37] (Figure 4.2) ensures the

applicability of the gait segmentation and the walking speed estimation algorithm. The shank angular velocity characteristics of the paretic leg showed a lower amplitude peak during swing compared to the non-paretic leg and greater inter-subject variability (Figure 4.5). Despite this, the algorithm appropriately recognized key events (shank vertical, TO and HS). Thus, the application of the algorithm from healthy adults [22] to stroke subjects did not affect its performance. However, the gait segmentation algorithm failed when the shank angular velocity characteristics deviated markedly from the healthy group profile and the typical stroke profile (Figure 4.6). Since the gait segmentation algorithm uses the negative peak of the shank angular velocity in stance to determine the shank vertical event, the multiple negative peaks present on both sides of this stroke subject prevented the algorithm from correctly identifying key gait events. Observationally, this subject walked with a "stiff gait" with limited knee mobility.

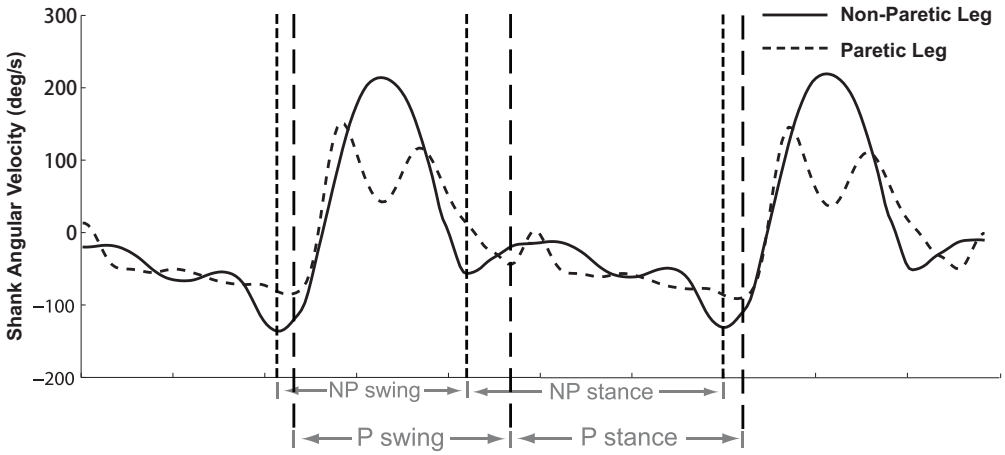

Figure 4.6: Shank angular velocity characteristics for one subject for whom the gait segmentation algorithm failed to recognize the correct shank vertical event in the corresponding stride cycle. The double positive peaks exhibited in the shank angular velocity trace during the swing phase of the paretic leg prevented the gait event detection algorithm from locating the midpoint of the swing phase. The non-paretic leg showed a near normal pattern compared to the paretic leg, while more oscillations were observed during the stance phase.

Gait asymmetry measurements obtained with the ambulatory gait analysis system revealed that the temporal parameters showed more asymmetry than spatial parameters. These findings are consistent with previous studies [38, 39, 37]. Olney *et. al* found that people with hemiparesis compensated for the weakness of the paretic leg by spending significantly less time in stance on the paretic leg than on the non-paretic leg [38]. The $\%T_{st}$, $\%T_{sw}$ and SSR measured using IMUs (Table 4.1) provided a quantitative evaluation of the temporal asymmetry in hemiparetic gait without the need for motion capture systems or costly commercially available gait analysis systems. A normal SSR (1.48 ± 0.18) was observed for the non-paretic leg, while the percentage of stride spent in stance on the paretic leg ($53.28 \pm 3.70\%$) was less than non-paretic leg ($59.46 \pm 2.86\%$). This degree of inter-limb discrepancy is consistent with other

studies [40]. On the other hand, the SLR exhibited greater symmetry than reported elsewhere [41, 42]. This may be attributed to the degree of impairment amongst our subjects since our results were comparable with those presented by Balasubramanian *et. al* and Patterson *et. al*, in which subjects with mild or moderate hemiparesis showed less spatial asymmetry than those more severely affected [18, 17]. Patterson *et. al* also suggested that spatial step asymmetry was more likely to occur in stroke subjects who exhibited severe temporal asymmetry [17], which is not the case for our subject population.

The present study makes two major contributions. First, the proposed walking speed estimation method abandoned the assumption of zero initial and end shank velocities and utilized the sensor measured shank angular velocity to correct the effect of accelerometer measurement bias on the walking speed estimation. The new method effectively minimized systematic error without the requirement for population-based calibration prior to the gait evaluation and/or systematic error correction after the experiment. Second, the applicability of the proposed system in people with stroke has been demonstrated in this study. To the best of our knowledge, no previous study has proposed such a comprehensive ambulatory gait analysis system to assess post-stroke hemiparetic gait in terms of walking speed and gait asymmetry.

One of the limitations of the study was that the actual stride-to-stride walking speed variability was unknown because the reference walking speed was determined over a distance of 10 meters (10MWT) and a gold standard measure of stance and swing time and SL was not available in this study. It is the case that the values obtained are consistent with the literatures; however, a validation study would confirm the accuracy of the algorithm. Another limitation is that the applicability of the

method has been demonstrated in people with mild to moderate hemiparesis only. The test results from twelve of thirteen people with stroke were promising, but further study involving a wide range of stroke-related mobility deficits would be desirable.

4.5 Acknowledgements

I would like to gratefully acknowledge the support from NSERC discovery grant.

References

[1] KT Khaw. Journal of Neurology, Neurosurgery, and Psychiatry. *British Medical Journal*, 61(4):333–338, 1996.

[2] J. Mackay, G.A. Mensah, S. Mendis, and K. Greenlund. *The atlas of heart disease and stroke*. World Health Organization, 2004.

[3] C.L. Richards and S.J. Olney. Hemiparetic gait following stroke. part ii: Recovery and physical therapy. *Gait & Posture*, 4(2):149–162, 1996.

[4] S. Mudge and N.S. Stott. Outcome measures to assess walking ability following stroke: a systematic review of the literature. *Physiotherapy*, 93(3):189–200, 2007.

[5] S Hesse. Rehabilitation of Gait After Stroke. *Topics in Geriatric Rehabilitation*, 19(2):111–131, 2002.

[6] S.M. Woolley. Characteristics of gait in hemiplegia. *Topics in Stroke Rehabilitation*, 7(4):1–18, 2001.

[7] J.J. Cohen, J.D. Sveen, J.M. Walker, and K. Brummel-Smith. Establishing criteria for community ambulation. *Topics in Geriatric Rehabilitation*, 3(1):71–78, 1987.

[8] CL Richards, F. Malouin, F. Dumas, and D. Tardif. Gait velocity as an outcome measure of locomotor recovery after stroke. In *Gait Analysis: Theory and Application*, pages 355–364. St Louis, Mo: Mosby, 1995.

[9] A. Schmid, P.W. Duncan, S. Studenski, S.M. Lai, L. Richards, S. Perera, and S.S. Wu. Improvements in speed-based gait classifications are meaningful. *Stroke*, 38(7):2096–2100, 2007.

[10] N.M. Salbach, N.E. Mayo, J. Higgins, S. Ahmed, L.E. Finch, and C.L. Richards. Responsiveness and predictability of gait speed and other disability measures in acute stroke. *Archives of Physical Medicine and Rehabilitation*, 82(9):1204–1212, 2001.

[11] J.R. Jorgensen, D.T. Bech-Pedersen, P. Zeeman, J. Sorensen, L.L. Andersen, and M. Schonberger. Effect of Intensive Outpatient Physical Training on Gait Performance and Cardiovascular Health in People With Hemiparesis After Stroke. *Physical Therapy*, 90(4):527–537, 2010.

[12] D.M. Buchner, M.E. Cress, P.C. Esselman, A.J. Margherita, B.J. De Lateur, A.J. Campbell, and E.H. Wagner. Factors associated with changes in gait speed in older adults. *The Journals of Gerontology Series A: Biological Sciences and Medical Sciences*, 51(6):297–302, 1996.

[13] S.J. Olney and C. Richards. Hemiparetic gait following stroke. Part I: Characteristics. *Gait & Posture*, 4(2):136–148, 1996.

[14] EB Titianova and IM Tarkka. Asymmetry in walking performance and postural sway in patients with chronic unilateral cerebral infarction. *Journal of Rehabilitation Research and Development*, 32(3):236–244, 1995.

[15] ME Dewar and G. Judge. Temporal asymmetry as a gait quality indicator. *Medical and Biological Engineering and Computing*, 18(5):689–693, 1980.

[16] M.L. Harris-Love, L.W. Forrester, R.F. Macko, K.H.C. Silver, and G.V. Smith. Hemiparetic gait parameters in overground versus treadmill walking. *Neurorehabilitation and Neural Repair*, 15(2):105–112, 2001.

[17] K.K. Patterson, I. Parafianowicz, C.J. Danells, V. Closson, M.C. Verrier, W.R. Staines, S.E. Black, and W.E. McIlroy. Gait asymmetry in community-ambulating stroke survivors. *Archives of Physical Medicine and Rehabilitation*, 89(2):304–310, 2008.

[18] C.K. Balasubramanian, M.G. Bowden, R.R. Neptune, and S.A. Kautz. Relationship between step length asymmetry and walking performance in subjects with chronic hemiparesis. *Archives of Physical Medicine and Rehabilitation*, 88(1):43–49, 2007.

[19] A.L. McDonough, M. Batavia, F.C. Chen, S. Kwon, and J. Ziai. The validity and reliability of the GAITRite system's measurements: a preliminary evaluation. *Archives of Physical Medicine and Rehabilitation*, 82(3):419–425, 2001.

[20] K. Aminian, B. Najafi, C. Bula, P.F. Leyvraz, and P. Robert. Spatio-temporal parameters of gait measured by an ambulatory system using miniature gyroscopes. *Journal of Biomechanics*, 35(5):689–699, 2002.

[21] A. Hartmann, K. Murer, R.A. de Bie, and E.D. de Bruin. Reproducibility of spatio-temporal gait parameters under different conditions in older adults using a trunk tri-axial accelerometer system. *Gait & Posture*, 30(3):351–355, 2009.

[22] Q. Li, M. Young, V. Naing, and J. M. Donelan. Walking speed estimation using a shank-mounted inertial measurement unit. *Journal of Biomechanics*, 43(8):1640–1643, 2010.

[23] S. Yang and Q. Li. Imu-based ambulatory walking speed estimation in constrained treadmill and overground walking. *Computer Methods in Biomechanics and Biomedical Engineering*, 2011. First published on: 02 February, 2011.

[24] K. Tong and M.H. Granat. A practical gait analysis system using gyroscopes. *Medical Engineering & Physics*, 21(2):87–94, 1999.

[25] C. Mizuike, S. Ohgi, and S. Morita. Analysis of stroke patient walking dynamics using a tri-axial accelerometer. *Gait & Posture*, 30:60–64, 2009.

[26] P. Catalfamo, S. Ghoussayni, and D. Ewins. Gait event detection on level ground and incline walking using a rate gyroscope. *Sensors*, 10(6):5683–5702, 2010.

[27] H. Lau and K. Tong. The reliability of using accelerometer and gyroscope for gait event identification on persons with dropped foot. *Gait & Posture*, 27(2):248–257, 2008.

[28] J. Rueterbories, E.G. Spaich, B. Larsen, and O.K. Andersen. Methods for gait event detection and analysis in ambulatory systems. *Medical Engineering & Physics*, 32(6):545–552, 2010.

[29] A. Mansfield and G.M. Lyons. The use of accelerometry to detect heel contact events for use as a sensor in FES assisted walking. *Medical Engineering & Physics*, 25(10):879–885, 2003.

[30] YK Thong, MS Woolfson, JA Crowe, BR Hayes-Gill, and RE Challis. Dependence of inertial measurements of distance on accelerometer noise. *Measurement Science and Technology*, 13:1163–1172, 2002.

[31] J.M. Jasiewicz, J.H.J. Allum, J.W. Middleton, A. Barriskill, P. Condie, B. Purcell, and R.C.T. Li. Gait event detection using linear accelerometers or angular velocity transducers in able-bodied and spinal-cord injured individuals. *Gait & Posture*, 24(4):502–509, 2006.

[32] J.M. Bland and D.G. Altman. Statistical methods for assessing agreement between two methods of clinical measurement. *International Journal of Nursing Studies*, 47(8):931–936, 2010.

[33] H.P. von Schroeder, R.D. Coutts, P.D. Lyden, E. Billings Jr, and V.L. Nickel. Gait parameters following stroke: a practical assessment. *Journal of Rehabilitation Research and Development*, 32(1):25–31, 1995.

[34] S.E. Lord and L. Rochester. Measurement of community ambulation after stroke: current status and future developments. *Stroke*, 36(7):1457, 2005.

[35] S.K. Sabut, P.K. Lenka, R. Kumar, and M. Mahadevappa. Effect of functional electrical stimulation on the effort and walking speed, surface electromyography activity, and metabolic responses in stroke subjects. *Journal of Electromyography*

and Kinesiology: Official Journal of the International Society of Electrophysiological Kinesiology, 2010.

[36] K. Parvataneni, S.J. Olney, and B. Brouwer. Changes in muscle group work associated with changes in gait speed of persons with stroke. *Clinical Biomechanics*, 22(7):813–820, 2007.

[37] J. Stein. *Stroke Recovery and Rehabilitation*. Demos Medical Pub, 2009.

[38] S.J. Olney, M.P. Griffin, T.N. Monga, and I.D. MacBride. Work and power in gait of stroke patients. *Archives of Physical Medicine and Rehabilitation*, 72(5):309–314, 1991.

[39] IA De Quervain, SR Simon, S. Leurgans, WS Pease, and D. McAllister. Gait pattern in the early recovery period after stroke. *The Journal of Bone and Joint Surgery. American Volume*, 78(10):1506–1514, 1996.

[40] K. Parvataneni, L. Ploeg, S.J. Olney, and B. Brouwer. Kinematic, kinetic and metabolic parameters of treadmill versus overground walking in healthy older adults. *Clinical Biomechanics*, 24(1):95–100, 2009.

[41] G. Chen, C. Patten, D.H. Kothari, and F.E. Zajac. Gait differences between individuals with post-stroke hemiparesis and non-disabled controls at matched speeds. *Gait & Posture*, 22(1):51–56, 2005.

[42] G. Yavuzer, F. Eser, D. Karakus, B. Karaoglan, and H.J. Stam. The effects of balance training on gait late after stroke: a randomized controlled trial. *Clinical Rehabilitation*, 20(11):960–969, 2006.

Chapter 5

Inertial Sensors in Estimating Walking Speed and Inclination: An Evaluation of Sensor Error Models

Abstract

With the increasing interest of using inertial measurement units (IMU) in human biomechanics studies, methods dealing with inertial sensor measurement errors become more and more important. Pre-test calibration and in-test error compensation are commonly used to minimize the sensor errors and improve the accuracy of the estimation results. However, the performance of a given sensor error compensation method does not only depend on the accuracy of the calibration or the sensor error evaluation, but also strongly relies on the selected sensor error model. The best performance could be achieved only when the essential components of sensor errors are included and compensated. Three sensor error models, with the concerns about

sensor acceleration measurement biases and sensor attachment misalignment, were evaluated in the shank-mounted IMU-based walking speed/inclination estimation algorithm. With the treadmill walking experiment conducted at both level and incline conditions, the comparison between these three sensor error models demonstrated the importance of sensor error model on the spatio-temporal gait parameter estimation performance. Accurate walking inclination estimation was also achieved using a newly developed sensor error model.

5.1 Introduction

Microelectromechanical (MEMS) inertial sensors have long been used as an aiding component in the navigation and control applications and offered promising performance [1]. As the MEMS technology development, the application of miniature inertial sensors has been gradually explored in the field of biomechanics. Conventional camera-based motion tracking systems used in human mobility studies accurately measure position and orientation information in a small area but inevitably suffer from the range restriction, the complex laboratory setup and the lack of long-term monitoring capability. In any case, the use of miniature MEMS inertial sensors has become very attractive in human mobility studies due to their low-cost, small-size features and capability of sensing the motion without additional equipments [2, 3]. The orientation and position of any given body segment can be derived based on the measurements from a body-fixed inertial measurement unit (IMU), a combination of accelerometers and gyroscopes. Over the past decade, different algorithms using the inertial data have been developed to estimate the spatio-temporal gait parameters of human gait, such as walking speed, stride length and stride frequency

[4, 5, 6, 7, 8, 9, 10]. However, a common issue of utilizing low-cost IMU is the cumulative calculation error resulting from sensor errors, such as the integration drift caused by acceleration measurement bias, and considerable effort has been devoted looking for ways to reduce such errors.

Two common methods to compensate the sensor errors in inertial sensor based gait analysis systems are pre-test static/dynamic calibration and in-test compensation based on a specific sensor error model that describe the possible sensor error involved in the data collection and algorithm implementation. With pre-test calibration approach, a off-line static (stand still) or a dynamic (standardized movement) calibration process is carried out before each trial of an experiment in order to obtain the sensor error characteristics [11, 12, 13], which is then corrected in the calculation. An in-test sensor error compensation is implemented in the algorithm and the sensor errors are updated during a specific period of time, such as the zero-velocity duration of the foot in the mid-stance phase, so called zero-velocity update (ZUPT) [14, 10, 15], or the shank vertical event, when the shank segment is perpendicular to the floor [6, 16]. However, no matter which compensation method is used and how accurately the sensor error is evaluated, the performance of the inertial sensor based system strongly relies on the sensor error model, the description of the sensor error components in the system. For example, some studies made the assumption in their sensor error model that the acceleration measurement bias was constant in the global coordinate system [6, 15]. Although algorithms with this sensor error model achieved accurate estimation results for some gait parameters, such as walking speed, stride length and etc., it failed in estimating other gait parameters such as inclination of walking. Therefore, it is important to understand the effect of sensor error model on

the gait parameter estimation performance.

This study compared three sensor error models in estimating walking speed and inclination using inertial sensors. Of the three models, one has been used in a shank-mounted IMU-based walking speed estimation algorithm, previously reported by Li *et. al* [6]. Two new sensor error compensation models were developed in this paper for comparison. Treadmill walking experiments were conducted to evaluate the performance of these three sensor error models.

5.2 Methods

5.2.1 IMU-based Walking Speed Estimation

The walking speed estimation method using shank-mounted IMU sensor was first proposed by Li *et. al* [6]. This method is based on the fact that human walking is a cyclic motion with distinct patterns in the inertial data that characterize shank kinematics and could be further used to determine spatio-temporal parameters including stride cycle, stride length, stride frequency, walking speed and etc.. In particular, the shank angular velocity characteristics clearly define several important gait events, such as heel-strike, toe-off, shank vertical and etc. [4, 17, 18, 19]. The measured sensor accelerations, $a_n(t)$ in normal direction and $a_t(t)$ in tangential direction of the shank rotation, are first projected to the global coordinate system, $a_x(t)$ in horizontal direction and $a_y(t)$ in vertical direction:

$$\begin{bmatrix} a_x(t) \\ a_y(t) \end{bmatrix} = \begin{bmatrix} \cos\theta(t) & -\sin\theta(t) \\ \sin\theta(t) & \cos\theta(t) \end{bmatrix} \begin{bmatrix} a_t(t) \\ a_n(t) \end{bmatrix} - \begin{bmatrix} 0 \\ g \end{bmatrix}, \tag{5.1}$$

where g is the acceleration due to gravity. $\theta(t)$ is the sensor orientation angle, which is integrated from the measured shank angular velocity, $\omega(t)$ (Fig. 5.1).

The accelerations in the global coordinate systems are then integrated to determine the instantaneous sensor velocity in each axis of the global coordinate system, $v_x(t)$ and $v_y(t)$. The average sensor velocities are the average of the instantaneous sensor velocities over the corresponding stride cycle, while the walking speed is the magnitude of the vector sum of the the averaged sensor velocities. Detailed description of the walking speed estimation method can be found in [6].

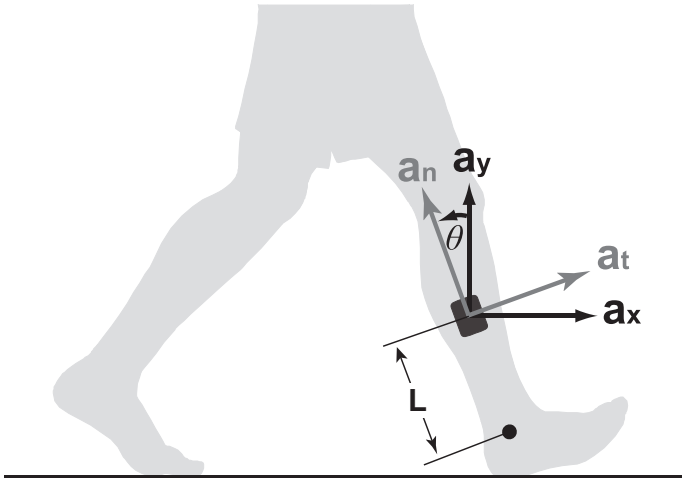

Figure 5.1: Sensor configuration (sagittal view): An IMU is attached to the midway of the shank on the lateral side. The acceleration a_n is measured along the normal direction, a_t is measured along the tangential direction, and the angular velocity ($\omega(t)$) is measured about the rotation of the shank in the sagittal plane. The arrows indicate positive axes for the corresponding sensor measurements. L is the sensor-to-ankle distance. θ is the shank angle with respect to the vertical direction. The world coordinate system is defined by the x and y axes.

Two strategies have been implemented to reduce the speed estimation errors resulted from sensor measurement uncertainty. First, a walking sequence was segmented

into a sequence of stride cycles. Specifically, in [6] the shank vertical event, when the longitudinal direction of the shank is vertical to the floor, was used to segment the walking sequence into stride cycles. Within each stride cycle, the walking speed was estimated in order to reduce drift errors caused by long time integrations of sensor measurement biases. Second, acceleration measurement bias-induced integration drifts were further compensated in a given stride cycle by the aid of known reference velocities. Li *et. al* [6] assumed that the initial and the final sensor velocities are equal and both zero, which provided the reference boundary conditions for correcting integration drifts. The compensated sensor velocities, $v_{x\_comp}(t)$ and $v_{y\_comp}(t)$, are then used to calculate the average sensor velocities over one stride cycle,

$$\begin{aligned} \bar{v}_x &= \tfrac{1}{T}\int_0^T v_{x\_comp}(\tau)d\tau, \\ \bar{v}_y &= \tfrac{1}{T}\int_0^T v_{y\_comp}(\tau)d\tau. \end{aligned} \tag{5.2}$$

Thus, the estimated walking speed, $\bar{V}_{estimated}$, and inclination in percentage of grade, Φ, can be calculated as

$$\bar{V}_{estimated} = \sqrt{\bar{v}_x^2 + \bar{v}_y^2}\ , \tag{5.3}$$

$$\Phi_{estimated} = \tfrac{\bar{v}_y}{\bar{v}_x}100\ . \tag{5.4}$$

5.2.2 Sensor Measurement Error Compensation

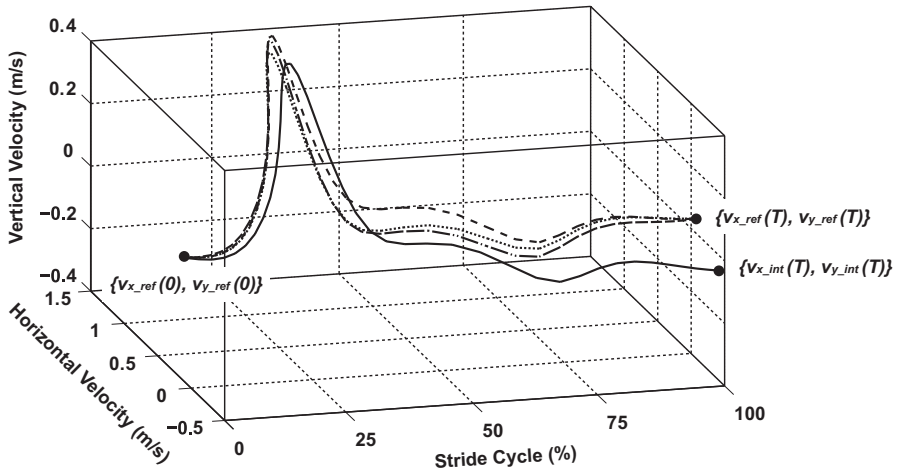

Figure 5.2: Instantaneous sensor velocities for different sensor error models over one stride cycle. The solid curve is the sensor velocity calculated by direct sensor acceleration integration without any sensor error compensation starting from the reference initial sensor velocities ($v_{x\_ref}(0)$ and $v_{y\_ref}(0)$), which ends up with the final sensor velocities ($v_{x\_int}(T)$ and $v_{y\_int}(T)$), which are different from the reference final sensor velocities ($v_{x\_ref}(T)$ and $v_{y\_ref}(T)$). The dashed, dotted and dash-dot curves represent three different sensor error compensation methods (CABGCS, CABSCS and CABSCS plus SM). All methods attains the final reference sensor velocities but with different instantaneous velocities in the middle of the stride cycle.

The goal of the compensation is to reduce the effect of the sensor measurement error on the estimated walking speed and achieve an accurate estimation. There are two main sources of sensor measurement error: (1) Sensor uncertainty including accelerometer bias and gyroscope drift. (2) Uncertainty related to the procedure and algorithm such as initial sensor orientation: it is unavoidable that there is a discrepancy between the actual sensor orientation and the initial orientation used in the algorithm.

To achieve error compensation, it requires reference measurements which could

be used to correct estimation error in the algorithm. There are two prerequisites for the reference measurement. First, it should be available for each stride cycle. Second, it should be relatively accurate and can be directly compared with results from integration of the sensor accelerations. For the shank-mounted IMU-based walking speed estimation algorithm [6], It used zero initial/final sensor velocities as reference measurements for correcting integration drifts. However, a follow-up evaluation experiment and analysis identified a systematic error associated with the zero velocity assumption, which resulted in an underestimation of walking speed [7]. This is due to the facts that initial and final velocities are not exactly zero. One remedy to achieve accurate reference is to use the shank angular velocity measurements, $\omega(t)$, to calculate initial/final velocities. During the mid-stance shank vertical events (i.e. the beginning and the end of the stride cycle), the shank rotates around the ankle joint as an inverted pendulum. Therefore, the sensor velocities can be accurately estimated as the product of angular velocities and rotation radius,

$$\begin{aligned} v_{x\_ref}(t) &= \omega(t) \cdot L \\ v_{y\_ref}(t) &= 0, \end{aligned} \qquad t = 0, T \tag{5.5}$$

where $v_{x\_ref}(t)$ and $v_{y\_ref}(t)$ are the initial (when $t = 0$) and final (when $t = T$) sensor horizontal and vertical velocities in the global coordinate system, respectively, and T is the period of the corresponding stride cycle. L is the distance from the sensor to the ankle joint (Fig. 5.1).

As the reference measurements (sensor instantaneous velocities) are only available at limited time instants (e.g. the beginning and the end of a stride cycle), it is not possible to compare the estimated instantaneous velocities from acceleration integration with the reference velocities continuously. Instead, a sensor error model

needs to be developed to account for the sensor measurement error compensation in the middle of a stride cycle when the reference is not available. Even though the end velocities are the same, the compensated sensor instantaneous velocities in the middle of a stride cycle are determined by the sensor measurement error compensation model (Fig. 5.2). As the stride-by-stride velocities are calculated as the average of the compensated sensor instantaneous velocities over one stride cycle (Eq. 5.2), the difference between the instantaneous velocity paths in the middle of a stride will have an impact on the estimated speed and inclination.

To determine the effects of sensor measurement error compensation model on the estimated speed and inclination, three models are evaluated in this study:

- *CABGCS* - constant acceleration measurement biases in global coordinate system
- *CABSCS* - constant acceleration measurement biases in sensor coordinate system
- *CABSCS plus SM* - constant acceleration measurement biases in sensor coordinate system plus sensor misalignment

CABGCS

CABGCS has been used in the previous studies [6, 7, 16] and achieved reasonable accuracy in estimating walking speeds but unsatisfactory inclination estimation. This sensor error model assumes a constant acceleration measurement bias in each axis of the global coordinate system, a_{x_bias} and a_{y_bias}, such that the compensated sensor acceleration in global coordinate system can be expressed as the original sensor

acceleration (Eq. (5.1)) with added biases,

$$\begin{bmatrix} a_x(t) \\ a_y(t) \end{bmatrix} = \begin{bmatrix} \cos\theta(t) & -\sin\theta(t) \\ \sin\theta(t) & \cos\theta(t) \end{bmatrix} \begin{bmatrix} a_t(t) \\ a_n(t) \end{bmatrix} - \begin{bmatrix} a_{x\_bias} \\ a_{y\_bias} \end{bmatrix} - \begin{bmatrix} 0 \\ g \end{bmatrix}. \tag{5.6}$$

The constant biases, a_{x_bias} and a_{y_bias}, in the sensor measurement model could be determined using the reference end velocities,$v_{x\_ref}(T)$ and $v_{y\_ref}(T)$, obtained from Eq. (5.5). The biases should be selected such that the velocities, integrating Eq. (5.6) from time 0 to T reaches the reference end velocities,

$$\begin{bmatrix} v_{x\_ref}(T) \\ v_{y\_ref}(T) \end{bmatrix} = \int_0^T \left(\begin{bmatrix} \cos\theta(\tau) & -\sin\theta(\tau) \\ \sin\theta(\tau) & \cos\theta(\tau) \end{bmatrix} \begin{bmatrix} a_t(\tau) \\ a_n(\tau) \end{bmatrix} - \begin{bmatrix} 0 \\ g \end{bmatrix} \right) d\tau + \begin{bmatrix} v_{x\_ref}(0) \\ v_{y\_ref}(0) \end{bmatrix} - \begin{bmatrix} \hat{a}_{x\_bias} \\ \hat{a}_{y\_bias} \end{bmatrix} T \ , \tag{5.7}$$

where $v_{x\_ref}(0)$ and $v_{y\_ref}(0)$ are the initial velocities determined using Eq. (5.5), and $\hat{a}_{x\_bias}$ and $\hat{a}_{y\_bias}$ are the estimated sensor acceleration measurement biases in the global coordinate system. To simplify the expression, the sensor velocities calculated from direct integration without considering the acceleration measurement biases, $v_{x\_int}(t)$ and $v_{y\_int}(t)$, are defined as,

$$\begin{bmatrix} v_{x\_int}(t) \\ v_{y\_int}(t) \end{bmatrix} = \int_0^t \left(\begin{bmatrix} \cos\theta(\tau) & -\sin\theta(\tau) \\ \sin\theta(\tau) & \cos\theta(\tau) \end{bmatrix} \begin{bmatrix} a_t(\tau) \\ a_n(\tau) \end{bmatrix} - \begin{bmatrix} 0 \\ g \end{bmatrix} \right) d\tau + \begin{bmatrix} v_{x\_ref}(0) \\ v_{y\_ref}(0) \end{bmatrix}. \tag{5.8}$$

Combining Eq. (5.7) and (5.8),

$$\begin{bmatrix} v_{x\_ref}(T) \\ v_{y\_ref}(T) \end{bmatrix} = \begin{bmatrix} v_{x\_int}(T) \\ v_{y\_int}(T) \end{bmatrix} - \begin{bmatrix} \hat{a}_{x\_bias} \\ \hat{a}_{y\_bias} \end{bmatrix} T \ . \tag{5.9}$$

Thus, the constant biases are calculated as

$$\begin{bmatrix} \hat{a}_{x\_bias} \\ \hat{a}_{y\_bias} \end{bmatrix} = \frac{1}{T} \left(\begin{bmatrix} v_{x\_int}(T) \\ v_{y\_int}(T) \end{bmatrix} - \begin{bmatrix} v_{x\_ref}(T) \\ v_{y\_ref}(T) \end{bmatrix} \right) . \tag{5.10}$$

Upon the determination of biases, the effect of the biases are compensated by subtracting the velocity integration drift from the instantaneous sensor velocities over the corresponding stride cycle,

$$\begin{bmatrix} v_{x\_comp}(t) \\ v_{y\_comp}(t) \end{bmatrix} = \int_0^t \left(\begin{bmatrix} \cos\theta(\tau) & -\sin\theta(\tau) \\ \sin\theta(\tau) & \cos\theta(\tau) \end{bmatrix} \begin{bmatrix} a_t(\tau) \\ a_n(\tau) \end{bmatrix} - \begin{bmatrix} 0 \\ g \end{bmatrix} \right) d\tau + \begin{bmatrix} v_{x\_ref}(0) \\ v_{y\_ref}(0) \end{bmatrix} - \begin{bmatrix} \hat{a}_{x\_bias} \\ \hat{a}_{y\_bias} \end{bmatrix} t \ . \tag{5.11}$$

The implementation of this compensation algorithm benefits from its simplicity, and has been reported in inertial sensor based gait analysis studies [15, 6].

CABSCS

Although *CABGCS* significantly improved the performance in estimating walking speeds, we mush realize that accelerometer biases are physically with respect to the measurement axes of the accelerometer, a_n and a_t, but not the global coordinate axes, a_x and a_y.

Therefore, it makes better sense to develop a sensor error model that considers the accelerometer biases in the measurement axes, a_{t_bias} and a_{n_bias}. The new sensor error model, *CABSCS*, is developed as

$$\begin{bmatrix} a_x(t) \\ a_y(t) \end{bmatrix} = \begin{bmatrix} \cos\theta(t) & -\sin\theta(t) \\ \sin\theta(t) & \cos\theta(t) \end{bmatrix} \begin{bmatrix} a_t(t) - a_{t\_bias} \\ a_n(t) - a_{n\_bias} \end{bmatrix} - \begin{bmatrix} 0 \\ g \end{bmatrix}. \tag{5.12}$$

The acceleration measurement biases in global coordinate system can then be isolated and written as functions of time, t,

$$\begin{bmatrix} a_x(t) \\ a_y(t) \end{bmatrix} = \begin{bmatrix} \cos\theta(t) & -\sin\theta(t) \\ \sin\theta(t) & \cos\theta(t) \end{bmatrix} \begin{bmatrix} a_t(t) \\ a_n(t) \end{bmatrix} - \begin{bmatrix} a_{x\_bias}(t) \\ a_{y\_bias}(t) \end{bmatrix} - \begin{bmatrix} 0 \\ g \end{bmatrix}, \tag{5.13}$$

where

$$\begin{bmatrix} a_{x\_bias}(t) \\ a_{y\_bias}(t) \end{bmatrix} = \begin{bmatrix} \cos\theta(t) & -\sin\theta(t) \\ \sin\theta(t) & \cos\theta(t) \end{bmatrix} \begin{bmatrix} a_{t\_bias} \\ a_{n\_bias} \end{bmatrix}. \tag{5.14}$$

Thus, at the end of the stride cycle when $t = T$,

$$\begin{bmatrix} v_{x\_ref}(T) \\ v_{y\_ref}(T) \end{bmatrix} = \int_0^T \left(\begin{bmatrix} \cos\theta(\tau) & -\sin\theta(\tau) \\ \sin\theta(\tau) & \cos\theta(\tau) \end{bmatrix} \begin{bmatrix} a_t(\tau) \\ a_n(\tau) \end{bmatrix} - \begin{bmatrix} 0 \\ g \end{bmatrix} \right) d\tau + \begin{bmatrix} v_{x\_ref}(0) \\ v_{y\_ref}(0) \end{bmatrix} - \int_0^T \left(\begin{bmatrix} \hat{a}_{x\_bias}(\tau) \\ \hat{a}_{y\_bias}(\tau) \end{bmatrix} \right) d\tau \ , \tag{5.15}$$

where $\hat{a}_{x\_bias}$ and $\hat{a}_{y\_bias}$ are the estimated sensor accelerometer biases projected in the global coordinate system. Similar to Eq. (5.6)-(5.10), the differences between the reference velocities and the velocities through integration can be expressed as

$$\begin{aligned} \begin{bmatrix} v_{x\_ref}(T) - v_{x\_int}(T) \\ v_{y\_ref}(T) - v_{y\_int}(T) \end{bmatrix} &= \begin{bmatrix} \int_0^T \hat{a}_{x\_bias}(\tau)d\tau \\ \int_0^T \hat{a}_{y\_bias}(\tau)d\tau \end{bmatrix} \\ &= \begin{bmatrix} \int_0^T cos(\tau)d\tau & -\int_0^T sin(\tau)d\tau \\ \int_0^T sin(\tau)d\tau & \int_0^T cos(\tau)d\tau \end{bmatrix} \begin{bmatrix} \hat{a}_{t\_bias} \\ \hat{a}_{n\_bias} \end{bmatrix}, \end{aligned} \tag{5.16}$$

where $v_{x\_ref}(T)$, $v_{y\_ref}(T)$, $v_{x\_int}(T)$ and $v_{y\_int}(T)$ are respectively calculated using Eq. (5.5) and (5.8), and $\hat{a}_{t\_bias}$ and $\hat{a}_{n\_bias}$ are the estimated sensor acceleration measurement biases in the sensor coordinate system.

Thus, the constant acceleration measurement biases can be calculated by solving Eq. (5.15),

$$\begin{bmatrix} \hat{a}_{t\_bias} \\ \hat{a}_{n\_bias} \end{bmatrix} = \begin{bmatrix} \int_0^T cos(\tau)d\tau & -\int_0^T sin(\tau)d\tau \\ \int_0^T sin(\tau)d\tau & \int_0^T cos(\tau)d\tau \end{bmatrix}^{-1} \begin{bmatrix} v_{x\_ref}(T) - v_{x\_int}(T) \\ v_{y\_ref}(T) - v_{y\_int}(T) \end{bmatrix}. \tag{5.17}$$

Therefore, similar to Eq. (5.11), the compensated instantaneous sensor velocities over

the corresponding stride cycle are calculated as

$$\begin{bmatrix} v_{x\_comp}(t) \\ v_{y\_comp}(t) \end{bmatrix} = \int_0^t \left(\begin{bmatrix} \cos\theta(\tau) & -\sin\theta(\tau) \\ \sin\theta(\tau) & \cos\theta(\tau) \end{bmatrix} \begin{bmatrix} a_t(\tau) - \hat{a}_{t\_bias} \\ a_n(\tau) - \hat{a}_{n\_bias} \end{bmatrix} - \begin{bmatrix} 0 \\ g \end{bmatrix} \right) d\tau \ . \tag{5.18}$$

CABSCS plus SM

Both the *CABGCS* and *CABSCS* are developed based on the assumption that the sensor is perfectly aligned with the global coordinate system at the shank vertical event with no error, i.e. $\theta(0) = 0$; however, the exact orientation of the sensor, $\theta(0)$, at the beginning of a stride cycle, most likely does not equal to zero. To account for the measurement error in the sensor orientation angle, we developed the sensor measurement model *CABSCS plus SM*. In the new sensor error model, we introduce a constant bias to the measured sensor orientation angle, $\theta(0) = \theta_0$, which describes the sensor misalignment at the shank vertical event. In the mean time, we preserve the fact that sensor acceleration measurement biases are in sensor coordinate system (*CABSCS*). With the initial sensor misalignment angle, θ_0, the *CABSCS plus SM* is given by

$$\begin{bmatrix} a_x(t) \\ a_y(t) \end{bmatrix} = \begin{bmatrix} \cos\theta_0 & -\sin\theta_0 \\ \sin\theta_0 & \cos\theta_0 \end{bmatrix} \begin{bmatrix} \cos\theta(t) & -\sin\theta(t) \\ \sin\theta(t) & \cos\theta(t) \end{bmatrix} \begin{bmatrix} a_t(t) - a_{t\_bias} \\ a_n(t) - a_{n\_bias} \end{bmatrix} - \begin{bmatrix} 0 \\ g \end{bmatrix}. \tag{5.19}$$

In this sensor error model, there are three constants, a_{t_bias}, a_{n_bias} and θ_0, need to be determined using the end reference velocity measurements. Because we only have two equations with two reference end velocity measurements, we could only determine two of the three constants. As the two acceleration measurement biases are small and close to each other, we make a reasonable assumption as $a_{t\_bias} = a_{n\_bias} = a_{bias}$ to

reduce the number of unknowns to two as the accelerometer bias and the sensor misalignment angle, a_{bias} and θ_0. Integrating Eq. (5.19), and comparing with the reference end velocities,

$$\begin{bmatrix} v_{x\_ref}(T) \\ v_{x\_ref}(T) \end{bmatrix} = \int_0^T \left(\begin{bmatrix} \cos\hat{\theta}_0 & -\sin\hat{\theta}_0 \\ \sin\hat{\theta}_0 & \cos\hat{\theta}_0 \end{bmatrix} \begin{bmatrix} cos(\tau) & -sin(\tau) \\ sin(\tau) & cos(\tau) \end{bmatrix} \begin{bmatrix} a_t(\tau) - \hat{a}_{bias} \\ a_n(\tau) - \hat{a}_{bias} \end{bmatrix} - \begin{bmatrix} 0 \\ g \end{bmatrix} \right) d\tau, \tag{5.20}$$

where $v_{x\_ref}(T)$, $v_{y\_ref}(T)$ are calculated using Eq. (5.5), and $\hat{\theta}_0$ and $\hat{a}_{bias}$ are the estimated sensor misalignment angle and sensor accelerometer measurement bias. To solve Eq. (5.20), two methods, analytical and numerical, have been developed.

Analytical Solution In order to simplify and analytically solve the non-linear equation, the small angle approximation was utilized based on the assumption that the sensor misalignment angle is very small ($< 5°$), such that Eq. (5.20) can be re-written as

$$\begin{bmatrix} v_{x\_ref}(T) \\ v_{x\_ref}(T) \end{bmatrix} = \int_0^T \left(\begin{bmatrix} 1 & -\hat{\theta}_0 \\ \hat{\theta}_0 & 1 \end{bmatrix} \begin{bmatrix} cos(\tau) & -sin(\tau) \\ sin(\tau) & cos(\tau) \end{bmatrix} \begin{bmatrix} a_t(\tau) - \hat{a}_{bias} \\ a_n(\tau) - \hat{a}_{bias} \end{bmatrix} - \begin{bmatrix} 0 \\ g \end{bmatrix} \right) d\tau. \tag{5.21}$$

Isolating the acceleration measurement bias and rearrange the equation, we get

$$\begin{aligned} \begin{bmatrix} v_{x\_ref}(T) \\ v_{x\_ref}(T) \end{bmatrix} &= \int_0^T \left(\begin{bmatrix} 1 & -\hat{\theta}_0 \\ \hat{\theta}_0 & 1 \end{bmatrix} \begin{bmatrix} cos(\tau) & -sin(\tau) \\ sin(\tau) & cos(\tau) \end{bmatrix} \begin{bmatrix} a_t(\tau) \\ a_n(\tau) \end{bmatrix} - \begin{bmatrix} 0 \\ g \end{bmatrix} \right) d\tau \\ &\quad - \int_0^T \left(\begin{bmatrix} 1 & -\hat{\theta}_0 \\ \hat{\theta}_0 & 1 \end{bmatrix} \begin{bmatrix} cos(\tau) & -sin(\tau) \\ sin(\tau) & cos(\tau) \end{bmatrix} \begin{bmatrix} \hat{a}_{bias} \\ \hat{a}_{bias} \end{bmatrix} \right) d\tau \end{aligned} . \tag{5.22}$$

Further, we decompose the approximated misalignment angle transformation matrix into an identity matrix and an anti-diagonal matrix about $\hat{\theta}_0$,

$$\begin{aligned}\begin{bmatrix} v_{x\_ref}(T) \\ v_{x\_ref}(T) \end{bmatrix} &= \int_0^T \left(\begin{bmatrix} 1 & 0 \\ 0 & 1 \end{bmatrix} \begin{bmatrix} cos(\tau) & -sin(\tau) \\ sin(\tau) & cos(\tau) \end{bmatrix} \begin{bmatrix} a_t(\tau) \\ a_n(\tau) \end{bmatrix} - \begin{bmatrix} 0 \\ g \end{bmatrix} \right) d\tau \\ &+ \int_0^T \left(\begin{bmatrix} 0 & -\hat{\theta}_0 \\ \hat{\theta}_0 & 0 \end{bmatrix} \begin{bmatrix} cos(\tau) & -sin(\tau) \\ sin(\tau) & cos(\tau) \end{bmatrix} \begin{bmatrix} a_t(\tau) \\ a_n(\tau) \end{bmatrix} \right) d\tau \\ &- \int_0^T \left(\begin{bmatrix} 1 & 0 \\ 0 & 1 \end{bmatrix} \begin{bmatrix} cos(\tau) & -sin(\tau) \\ sin(\tau) & cos(\tau) \end{bmatrix} \begin{bmatrix} \hat{a}_{bias} \\ \hat{a}_{bias} \end{bmatrix} \right) d\tau \\ &- \int_0^T \left(\begin{bmatrix} 0 & -\hat{\theta}_0 \\ \hat{\theta}_0 & 0 \end{bmatrix} \begin{bmatrix} cos(\tau) & -sin(\tau) \\ sin(\tau) & cos(\tau) \end{bmatrix} \begin{bmatrix} \hat{a}_{bias} \\ \hat{a}_{bias} \end{bmatrix} \right) d\tau \end{aligned} . \tag{5.23}$$

Note that the first term of Eq. (5.23) is the same as the right side of Eq. (5.8), while the last term can be rewritten as

$$\int_0^T \left(\begin{bmatrix} sin(\tau) + cos(\tau) \\ cos(\tau) - sin(\tau) \end{bmatrix} \right) d\tau \cdot \hat{\theta}_0 \cdot \hat{a}_{bias}, \tag{5.24}$$

which can be omitted since the magnitude of $\hat{\theta}_0$ and $\hat{a}_{bias}$ is very small and the product of them is negligible. Thus, Eq. (5.23) is simplified to

$$\begin{aligned}\begin{bmatrix} v_{x\_ref}(T) \\ v_{x\_ref}(T) \end{bmatrix} &= \begin{bmatrix} v_{x\_int}(T) \\ v_{y\_int}(T) \end{bmatrix} \\ &+ \int_0^T \left(\begin{bmatrix} 0 & -\hat{\theta}_0 \\ \hat{\theta}_0 & 0 \end{bmatrix} \begin{bmatrix} cos(\tau) & -sin(\tau) \\ sin(\tau) & cos(\tau) \end{bmatrix} \begin{bmatrix} a_t(\tau) \\ a_n(\tau) \end{bmatrix} \right) d\tau \\ &- \int_0^T \left(\begin{bmatrix} 1 & 0 \\ 0 & 1 \end{bmatrix} \begin{bmatrix} cos(\tau) & -sin(\tau) \\ sin(\tau) & cos(\tau) \end{bmatrix} \begin{bmatrix} \hat{a}_{bias} \\ \hat{a}_{bias} \end{bmatrix} \right) d\tau \end{aligned} . \tag{5.25}$$

We rearranged the equation such that $\hat{\theta_0}$ and $\hat{a}_{bias}$ are isolated,

$$\begin{aligned}\begin{bmatrix} v_{x\_ref}(T) - v_{x\_int}(T) \\ v_{x\_ref}(T) - v_{y\_int}(T) \end{bmatrix} &= \int_0^T \left(\begin{bmatrix} -a_t(\tau)sin(\tau) - a_n(\tau)cos(\tau) \\ a_t(\tau)cos(\tau) - a_n(\tau)sin(\tau) \end{bmatrix} \right) d\tau \cdot \hat{\theta_0} \\ &\quad - \int_0^T \left(\begin{bmatrix} cos(\tau) - sin(\tau) \\ sin(\tau) + cos(\tau) \end{bmatrix} \right) d\tau \cdot \hat{a}_{bias} \\ &= \begin{bmatrix} \int_0^T (-a_t(\tau)sin(\tau) - a_n(\tau)cos(\tau))d\tau & \int_0^T (cos(\tau) - sin(\tau))d\tau \\ \int_0^T (a_t(\tau)cos(\tau) - a_n(\tau)sin(\tau))d\tau & \int_0^T (sin(\tau) + cos(\tau))d\tau \end{bmatrix} \begin{bmatrix} \hat{\theta_0} \\ \hat{a}_{bias} \end{bmatrix}\end{aligned} \tag{5.26}$$

Thus, we solved $\hat{\theta_0}$ and $\hat{a}_{bias}$ as

$$\begin{bmatrix} \hat{\theta_0} \\ \hat{a}_{bias} \end{bmatrix} = \begin{bmatrix} \int_0^T (-a_t(\tau)sin(\tau) - a_n(\tau)cos(\tau))d\tau & \int_0^T (cos(\tau) - sin(\tau))d\tau \\ \int_0^T (a_t(\tau)cos(\tau) - a_n(\tau)sin(\tau))d\tau & \int_0^T (sin(\tau) + cos(\tau))d\tau \end{bmatrix}^{-1} \begin{bmatrix} v_{x\_ref}(T) - v_{x\_int}(T) \\ v_{x\_ref}(T) - v_{y\_int}(T) \end{bmatrix}. \tag{5.27}$$

Numerical Solution Instead of determine the constants in the nonlinear equation of Eq. (5.20) analytically based on first-order approximation, we solve the constants numerically using MATLAB optimization routine FMINUNC. We first rearrange Eq. (5.20) and form two functions (f_x and f_y) with respect to $\hat{\theta_0}$ and $\hat{a}_{bias}$:

$$\begin{bmatrix} f_x(\hat{\theta_0}, \hat{a}_{bias}) \\ f_y(\hat{\theta_0}, \hat{a}_{bias}) \end{bmatrix} = \begin{bmatrix} v_{x\_ref}(T) \\ v_{x\_ref}(T) \end{bmatrix} - \int_0^T \left(\begin{bmatrix} \cos\hat{\theta_0} & -\sin\hat{\theta_0} \\ \sin\hat{\theta_0} & \cos\hat{\theta_0} \end{bmatrix} \begin{bmatrix} cos(\tau) & -sin(\tau) \\ sin(\tau) & cos(\tau) \end{bmatrix} \begin{bmatrix} a_t(\tau) - \hat{a}_{bias} \\ a_n(\tau) - \hat{a}_{bias} \end{bmatrix} + \begin{bmatrix} 0 \\ g \end{bmatrix} \right) d\tau. \tag{5.28}$$

Ideally, f_x and f_y should be zero when the exact value of θ_0 and a_{bias} is found. We use another function f_{err} as the criteria for the MATLAB optimization routine,

$$f_{err}(\hat{\theta_0}, \hat{a}_{bias}) = f_x^2(\hat{\theta_0}, \hat{a}_{bias}) + f_y^2(\hat{\theta_0}, \hat{a}_{bias}). \tag{5.29}$$

To start the optimization routine, an initial value is provided for the unknown misalignment angle ($\hat{\theta_0}$) and sensor acceleration measurement bias ($\hat{a}_{bias}$), and then FMINUNC searches for the best value of $\hat{\theta_0}$ and $\hat{a}_{bias}$ such that f_{err} is minimized. The resulting $\hat{\theta_0}$ and $\hat{a}_{bias}$ are the numerical solution for Eq. (5.20).

Upon the determination of $\hat{\theta_0}$ and $\hat{a}_{bias}$, the compensated instantaneous sensor velocities in the stride cycle are simply calculated by plugging $\hat{\theta_0}$ and $\hat{a}_{bias}$ back to Eq. (5.19) and integrating both sides,

$$\begin{bmatrix} v_{x\_comp}(t) \\ v_{y\_comp}(t) \end{bmatrix} = \int_0^T \left(\begin{bmatrix} \cos\hat{\theta_0} & -\sin\hat{\theta_0} \\ \sin\hat{\theta_0} & \cos\hat{\theta_0} \end{bmatrix} \begin{bmatrix} \cos\theta(\tau) & -\sin\theta(\tau) \\ \sin\theta(\tau) & \cos\theta(\tau) \end{bmatrix} \begin{bmatrix} a_t(\tau) - \hat{a}_{bias} \\ a_n(\tau) - \hat{a}_{bias} \end{bmatrix} - \begin{bmatrix} 0 \\ g \end{bmatrix} \right) d\tau \ . \tag{5.30}$$

With the compensated instantaneous sensor velocities, $v_{x\_comp}(t)$ and $v_{y\_comp}(t)$, from each sensor error model, the stride-by-stride walking speed and inclination are calculated according to Eq. (5.3) and (5.5).

5.2.3 Experimental Method

An IMU sensor was attached to the midway of the right shank on the lateral side. The IMU sensor (Xsens Technology B.V., Netherlands) consists of a triaxial accelerometer ($\pm 18g$, where g is the gravitational acceleration) and a triaxial gyroscope ($\pm 1200°/sec$). Since we are only interested in the shank movement in the progression plane (sagittal plane), only the measurements from two accelerometer axes and one gyroscope axis were used in the calculation. The acceleration and angular velocity data were collected at $120Hz$ with MVN Studio (Xsens Technology B.V., Netherlands). The raw sensor acceleration measurement data were filtered using a second order Butterworth low-pass filter with cut-off frequency $3Hz$. The sensor-to-ankle distance (L) was measured and recorded for the off-line algorithm implementation. Before each walking trial, the subject was asked to stand still with the shank in vertical direction and the IMU was adjusted such that its normal and tangential axes were aligned as closely as possible to vertical and horizontal directions of the world coordinate system, respectively (Fig. 5.1).

Two sets of experiments have been conducted to evaluate the performance of the three sensor error models in estimating walking speeds and slopes. The first experiment aims at the walking speed estimation performance comparison. Ten healthy subjects without any history of orthopedic impairments were recruited from the university community, including five males and five females (age: 21.0 ± 0.5 years; height: 172.9 ± 10.0 cm; weight: 68.9 ± 12.4Kg; sensor-to-ankle distance: 27.6 ± 3.2 cm). Five different preset treadmill speeds (0.8, 1.0, 1.2, 1.4 and $1.6 m/s$) with 0% inclination were performed. The second experiment aims at evaluating the performance in estimating inclination of walking. Four healthy subjects without any history of orthopedic impairments were recruited, including 3 males and 1 female (age: 22.5 ± 3.3 years; height: 178.4 ± 13.5 cm; weight: 72.4 ± 16.6Kg; sensor-to-ankle distance: 30.9 ± 2.9 cm). The subjects were instructed to walk at three different preset treadmill inclines (0%, 5% and 10%) with $1.0 m/s$ treadmill speed. For each trial, the IMU data were recorded for a duration of 60 seconds. The stride-by-stride walking speed and inclination were estimated off-line with different sensor measurement error compensation methods implemented in MATLAB (The MathWorks, Natick, MA, USA). Twenty strides from the steady walking period of each trial were used in the error analysis. Before experiment, subjects gave their informed consent to participate in accordance with university policy, and the study was approved by the Queen's General Research Ethics Board (GREB).

5.2.4 Data Analysis

For the walking speed estimation performance comparison, estimation error of each trial (20 strides from the steady walking period) was calculated as the difference

between the average estimated stride-by-stride walking speed over 20 strides and the corresponding preset treadmill speed. The mean absolute estimation error (Mean) and standard deviation (SD) were determined for each treadmill speed across all the subjects. A percentage root mean squared error (%RMSE) for each treadmill speed was also computed by averaging the results over all subjects,

$$\%RMSE = \frac{\sqrt{\sum(\bar{V}_{estimated} - V_{treadmill})^2/N}}{V_{treadmill}} 100\%, \tag{5.31}$$

where $N = 10$ for each walking speed, $\bar{V}_{estimated}$ is the average estimated walking speed for each treadmill speed across all subjects, and $V_{treadmill}$ is the corresponding preset treadmill speed. At each walking speed, the walking speed estimation error difference between different sensor error models were tested using the one-way ANOVA. With the p-values smaller than the significance level, 0.05, the performances of sensor error models were considered different. The estimated horizontal, vertical sensor velocities and estimated inclination were also analyzed separately using the one-way ANOVA. For the walking inclination estimation performance comparison, the one-way ANOVA was used to test the difference between the estimated inclination of different sensor error models.

5.3 Results

Both *CABSCS* and *CABSCS plus SM* based walking speed estimation methods achieved smaller absolute error and %RMSE than the previously used *CABGCS*, as shown in Table 5.1. An improvement of overall %RMSE from *CABSCS* (3.7%) and *CABSCS plus SM* (3.4% from numerical solution and 3.5% from analytical solution) could be observed in comparison with that from *CABGCS* (4.1%). One-way

Table 5.1: Walking Speed Estimation Errors Comparison between Methods

		Walking Speed (m/s)					Overall %RMSE[2]
		0.8	1.0	1.2	1.4	1.6	
CABGCS	Error[1]	0.02 ± 0.01	0.06 ± 0.04	0.03 ± 0.02	0.05 ± 0.03	0.04 ± 0.03	4.1%
	%RMSE	3.4%	7.2%	2.8%	3.9%	2.9%	
CABSCS	Error	0.02 ± 0.01	0.06 ± 0.04	0.02 ± 0.02	0.04 ± 0.03	0.03 ± 0.03	3.7%
	%RMSE	3.2%	6.9%	2.5%	3.5%	2.6%	
CABSCS plus SM (numerical)	Error	0.02 ± 0.01	0.05 ± 0.04	0.02 ± 0.02	0.04 ± 0.03	0.03 ± 0.02	3.4%
	%RMSE	2.8%	6.3%	2.3%	3.2%	2.3%	
CABSCS plus SM (analytical)	Error	0.02 ± 0.01	0.05 ± 0.04	0.02 ± 0.02	0.04 ± 0.03	0.03 ± 0.02	3.5%
	%RMSE	2.9%	6.5%	2.3%	3.3%	2.5%	
p[3]		0.74	0.89	0.94	0.76	0.92	

[1] Entry values are absolute Mean ± SD of the average walking speed estimates of each treadmill walking trial;
[2] %RMSE is RMSE divided by preset treadmill speed;
[3] One-way ANOVA results between different methods, with $p > 0.05$ the difference is not statistically significant.

ANOVA showed that the estimation error difference between three error models were not statistically significant.

The comparisons between estimated average horizontal and vertical sensor velocities with different sensor error models are shown in Fig. 5.3a. As the experiment was carried out on the treadmill with 0° inclination, the horizontal sensor velocities estimated with all three sensor error models approach the preset treadmill speeds; however, much smaller vertical sensor velocities are obtained from *CABSCS* and *CABSCS plus SM*, which are significantly different from *CABGCS*, where the ideal estimated vertical sensor velocity should be zero. The estimated vertical velocities in *CABSCS plus SM* are slightly better than those by *CABSCS* at lower walking speeds (0.8m/s and 1.0m/s). However, as the treadmill speed increases, the difference becomes significant and *CABSCS* shows larger errors while *CABSCS plus SM* still provides accurate estimates of vertical velocities. On the other hand, the comparison between numerical and analytical solutions for *CABSCS plus SM* in Fig. 5.3b indicates that the numerical method provided a better vertical sensor velocity estimate. Significant difference is observed in the vertical sensor velocity estimation under two out of five treadmill speeds, and the estimation variability is larger for the

analytical solution.

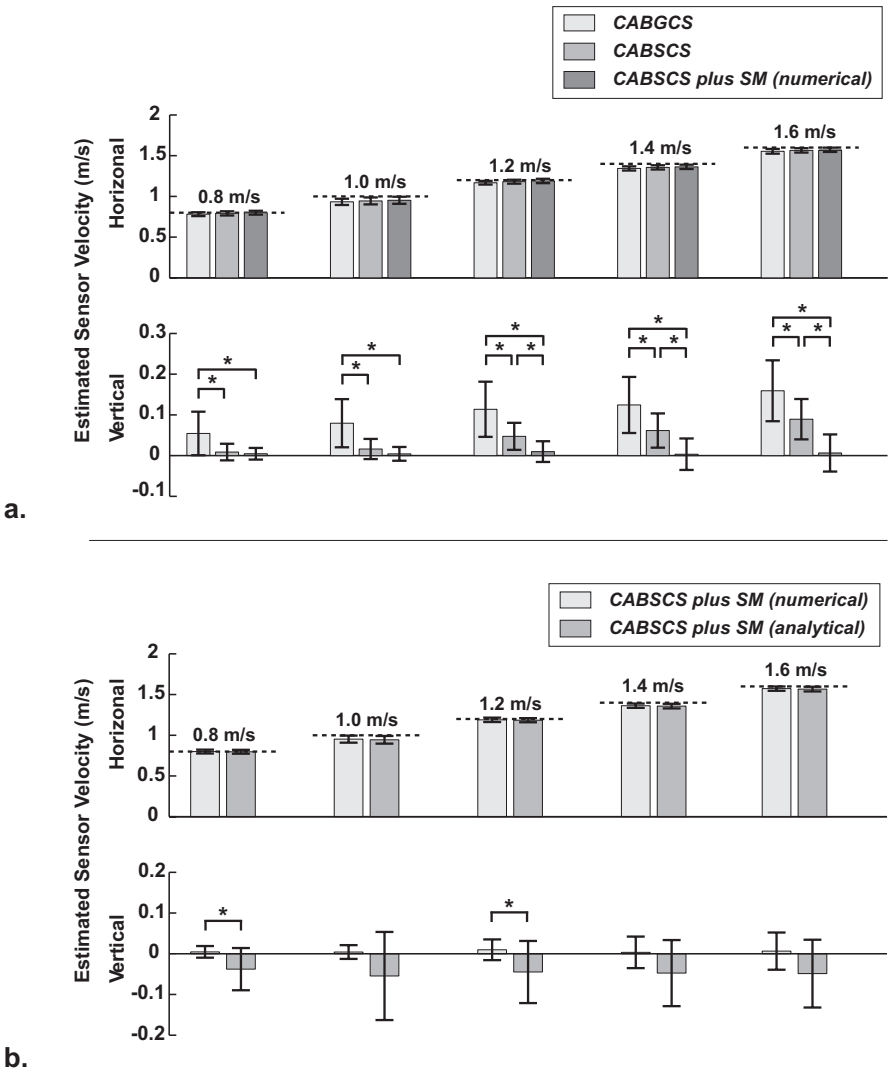

Figure 5.3: a). Estimated average sensor velocities (global coordinate system) under different sensor error models. The light grey bars indicate the results with *CABGCS*. The mid-grey bars show the results with *CABSCS*. The dark grey bars show the results from *CABSCS plus SM*. The error bars represent ± one standard deviation, indicating the estimation inter-subject variability. The asterisks (∗) indicate that the results are significantly different between pairs. b). Comparison between the numerical and analytical solution of *CABSCS plus SM* method. The light grey bars indicate the numerical solution, while the mid-grey bars represent the analytical solution.

In the inclination estimation experiment, the estimated inclination between any two of the three sensor error models are significantly different, as shown in Fig. 5.4a, where *CABSCS plus SM* provides the most accurate inclination estimates and the performance of *CABSCS* is better than *CABGCS*. Significant difference is observed in the inclination estimation results between the numerical and analytical solutions for *CABSCS plus SM*, as depicted in Fig. 5.4b.

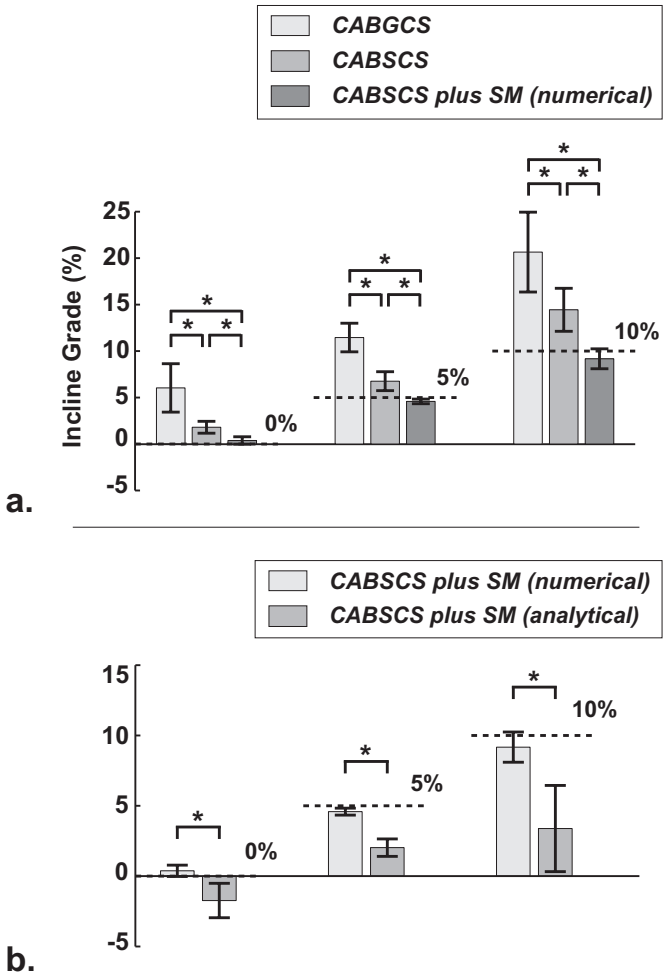

Figure 5.4: a). Estimated inclinations between different sensor error models. The light grey bars indicate the estimated average inclination with *CABGCS*. The mid-grey bars show the estimated inclination with *CABSCS*. The dark grey bars show the estimated inclination with *CABSCS plus SM*. The error bars represent ± one standard deviation, indicating the estimation inter-subject variability. The asterisks (∗) indicate that the results are significantly different between pairs. b). Comparison between the numerical and analytical solution of *CABSCS plus SM* method. The light grey bars indicate the numerical solution, while the mid-grey bars represent the analytical solution.

5.4 Discussion

Although accurate in estimating walking speeds for all three sensor error models, only *CABSCS plus SM* with numerical implementation achieved accurate results in estimating inclination. In the original shank-mounted IMU walking speed estimation [6], the initial shank angle at the shank vertical event was assumed to be zero, $\theta(0) = 0°$; however, this requires perfect sensor initial sensor angle at the beginning of each stride cycle, which can not be guaranteed. Although the walking speed estimation results are accurate because of the small amplitude of the estimated vertical sensor velocity, the walking inclination estimation is severely affected. Previous studies with IMU attached to human body have attempted to estimate inclination during inclined walking, but failed to provide accurate results [6, 15]. The unsuccessful estimation of inclination is most likely due to the use of an sensor error model that is insufficient to describe the sensor errors involved in the system. In Fig. 5.3a, *CABSCS* and *CABSCS plus SM* do not present significant difference in the sensor vertical velocity estimation; however, as the walking speed increases, the difference becomes significant, which to some extent indicates that using shank angular velocity characteristics to determine shank vertical event in high walking speed may not be as accurate as in low walking speed. Comparing *CABSCS* and *CABSCS plus SM* in Fig. 5.5, it is obvious that the vertical sensor velocity profile is very sensitive to shank angle changes and even the small sensor misalignment angle ($< 5°$) will make a big discrepancy. Therefore, the inclusion of the misalignment angle in the sensor error model is essential for the walking inclination estimation.

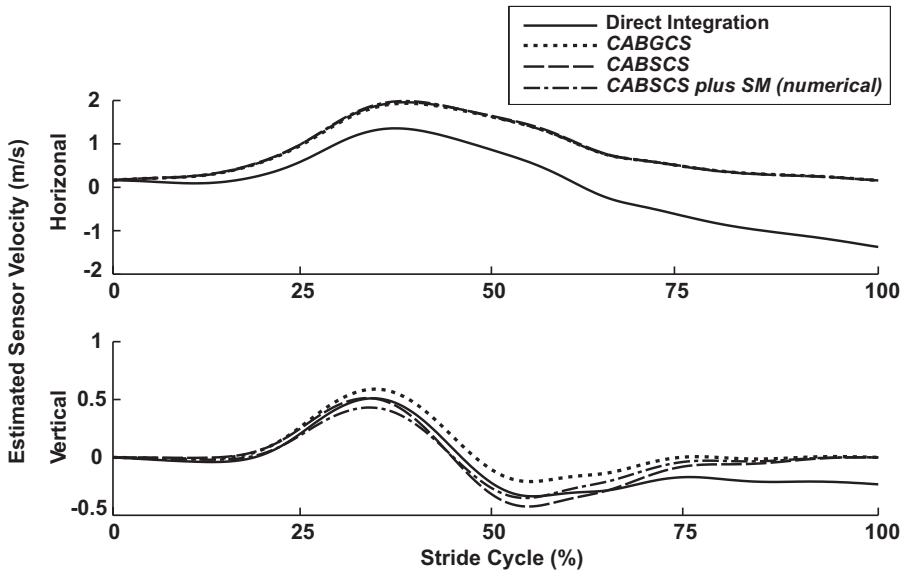

Figure 5.5: Estimated sensor velocity comparison (global coordinate system) over one stride cycle between different sensor error models. The solid curves represent the estimated horizontal and vertical sensor velocities without any compensation. The dotted curves show the estimated velocities corrected with *CABGCS*, the dashed curves represent the estimated velocities corrected with *CABSCS*, and the dash-dot curves represent the estimated velocities corrected with *CABSCS plus SM*.

The main difference between sensor error models lied in the instantaneous vertical velocities between 25% and 80% of the stride cycle (Fig. 5.5). This duration corresponds to the swing phase of a stride cycle when the accelerations of the shank-mounted sensor becomes large. Since the sensor acceleration measurement biases are independent of the orientation of the sensor and the direction of the acceleration, the effect of the acceleration measurement biases in global coordinate system strongly relies on the shank angle that is used in the acceleration projection. The constant acceleration measurement bias model in global coordinate system applied in *CABGCS* ignores such fact and uses a rough approximation in the calculation, *CABSCS* senses

the shank angle changes and realistically model the projection of the biases in horizontal and vertical directions, and *CABSCS plus SM* further takes care of the sensor misalignment angle. Meanwhile, the contribution of the gravity on sensor coordinate system also influences the calculated sensor acceleration measurement biases if the shank angle is not accurate. Due to the consideration of relationship between the shank angle and sensor error in global coordinate system, *CABSCS* observably corrects the sensor velocity estimation in vertical direction, and *CABSCS plus SM* significantly minimizes such error (Fig. 5.3a).

All in-test sensor error correction methods require some reference measurements to determine the sensor acceleration measurement bias. For example, the ZUPT has been used in foot-mounted IMU based algorithm [14, 10] and shank-mounted IMU based algorithm [6] to correct sensor measurement error. *CABGCS*, *CABSCS* and *CABSCS plus SM* all use the angular velocities measured during the end of stride cycle to generate the reference measurements, which is easy to implement and much simpler than other sensor fusion algorithms, e.g. Kalman filtering [10]. In comparison with *CABGCS* [6, 15], *CABSCS* and *CABSCS plus SM* require the consideration of sensor acceleration measurement biases for every sample collected in the walking trial, i.e. describing the sensor errors in global coordinate system as a function of time, and a relatively more complicated implementation is needed. We developed numerical and analytical methods for *CABSCS plus SM*. Both methods obtained accurate walking speed estimation results; however, the numerical solution performed better in terms of the inclination estimation. The small angle approximations we used in the derivation for the analytical solution are the main reason for the discrepancy found between numerical and analytical methods. The omission of the term in (Eq.

(5.24)) also accounts for part of the estimation error. As the vertical displacement is relatively small, these approximations could introduce a small absolute error in the estimated vertical displacement but relatively large percentage error. This will ultimately cause the wrong inclination estimation. On the other hand, the numerically implemented *CABSCS plus SM* solve the nonlinear equation directly without approximation, achieving accurate inclination estimation. One shortcoming of this implementation is the computational complexity because it involves solving a nonlinear equation in each stride cycle. In this study, we only conducted inclined walking due to the limitation of treadmill, which can only be adjusted to positive inclinations. The performance of these three sensor measurement error compensation methods under declined walking conditions deserves further evaluation.

In summary, this study proposed two new sensor error models and evaluated the performance in comparison with one sensor error model from previous study ([6]). The results suggested that either method (*CABSCS*, *CABGCS*, or *CABSCS plus SM*) could be used to estimate walking speeds accurately. In the case of estimating walking inclination, *CABSCS plus SM* with a numerical implementation will be the best choice.

5.5 Acknowledgements

We would like to gratefully acknowledge the support from NSERC discovery grant.

References

[1] N. Barbour and G. Schmidt. Inertial sensor technology trends. *IEEE Sensors Journal*, 1(4):332–339, 2001.

[2] A.M. Sabatini. *Computational Intelligence for Movement Sciences: Neural Networks, Support Vecotr Machines and Other Emerging Techniques*, chapter Inertial sensing in biomechanics: a surbey of computational techniques bridging motion analysis and personal nabigation, pages 70–100. Idea Group Inc., 2006.

[3] R.E. Mayagoitia, A.V. Nene, and P.H. Veltink. Accelerometer and rate gyroscope measurement of kinematics: an inexpensive alternative to optical motion analysis systems. *Journal of Biomechanics*, 35(4):537–542, 2002.

[4] K. Aminian, B. Najafi, C. Bula, P.F. Leyvraz, and P. Robert. Spatio-temporal parameters of gait measured by an ambulatory system using miniature gyroscopes. *Journal of Biomechanics*, 35(5):689–699, 2002.

[5] A. Hartmann, K. Murer, R.A. de Bie, and E.D. de Bruin. Reproducibility of spatio-temporal gait parameters under different conditions in older adults using a trunk tri-axial accelerometer system. *Gait & Posture*, 30(3):351–355, 2009.

[6] Q. Li, M. Young, V. Naing, and J. M. Donelan. Walking speed estimation using a shank-mounted inertial measurement unit. *Journal of Biomechanics*, 43(8):1640–1643, 2010.

[7] S. Yang and Q. Li. Imu-based ambulatory walking speed estimation in constrained treadmill and overground walking. *Computer Methods in Biomechanics and Biomedical Engineering*, 2011. First published on: 02 February, 2011.

[8] S. Miyazaki. Long-term unrestrained measurement of stride length and walking velocity utilizing a piezoelectric gyroscope. *IEEE Transactions on Biomedical Engineering*, 44(8):753–759, 1997.

[9] M. Henriksen, H. Lund, R. Moe-Nilssen, H. Bliddal, and B. Danneskiod-Samsře. Test-retest reliability of trunk accelerometric gait analysis. *Gait & Posture*, 19(3):288–297, 2004.

[10] O. Bebek, M.A. Suster, S. Rajgopal, M.J. Fu, X. Huang, M.C. Cavusoglu, D.J. Young, M. Mehregany, A.JJ. van den Bogery, and C.H. Mastrangelo. Personal navigation via high-resolution gait-corrected inertial measurement units. *IEEE Transactions on Instrumentation and Measurement*, 59(11):3018–3027, 2010.

[11] S. Scapellato, F. Cavallo, C. Martelloni, and A.M. Sabatini. In-use calibration of body-mounted gyroscopes for applications in gait analysis. *Sensors and Actuators A: Physical*, 123:418–422, 2005.

[12] JC Lotters, J. Schipper, PH Veltink, W. Olthuis, and P. Bergveld. Procedure for in-use calibration of triaxial accelerometers in medical applications. *Sensors and Actuators A: Physical*, 68(1-3):221–228, 1998.

[13] F. Ferraris, U. Grimaldi, and M. Parvis. Procedure for effortless in-field calibration of three-axis rate gyros and accelerometers. *Sensors and Materials*, 7(5):311–311, 1995.

[14] L. Ojeda and J. Borenstein. Non-gps navigation for security personnel and first responders. *Journal of Navigation*, 60(03):391–407, 2007.

[15] A. M. Sabatini, C. Martelloni, S. Scapellato, and F. Cavallo. Assessment of walking features from foot inertial sensing. *IEEE Transactions on Biomedical Engineering*, 52(3):486–94, 2005.

[16] S. Yang, J.T. Zhang, A.C. Novak, B. Brouwer, and Q Li. An ambulatory spatio-temporal analysis system for post-stroke hemiparetic gait using shank-attached imus. *Medical Engineering & Physics (Submitted)*, 2011.

[17] J.M. Jasiewicz, J.H.J. Allum, J.W. Middleton, A. Barriskill, P. Condie, B. Purcell, and R.C.T. Li. Gait event detection using linear accelerometers or angular velocity transducers in able-bodied and spinal-cord injured individuals. *Gait & Posture*, 24(4):502–509, 2006.

[18] H. Lau and K. Tong. The reliability of using accelerometer and gyroscope for gait event identification on persons with dropped foot. *Gait & Posture*, 27(2):248–257, 2008.

[19] P. Catalfamo, S. Ghoussayni, and D. Ewins. Gait event detection on level ground and incline walking using a rate gyroscope. *Sensors*, 10(6):5683–5702, 2010.

Chapter 6

Conclusions & Future Work

6.1 Conclusions

Capturing human movement is a common task in biomedical and biomechanical studies; however, the complex laboratory setting required for accurate measurement makes it a headache to conduct the experiment. For recent years, miniature inertial sensors have become widely adopted in an effort to simplify the equipments and procedures required in biomedical and biomechanical experiments. This thesis fully investigates the feasibility and the performance of using a shank-mounted IMU to estimate walking speed for both the people with healthy gait and the people with post-stroke hemiparetic gait, where promising results have been obtained. In addition, a complete error analysis is made to understand the aspects of the estimation errors, which can help the future development of walking speed estimation methods.

6.2 Future Work

In order to make the shank-mounted IMU based walking speed estimation method a practical system, further research and engineering work is required. To achieve such goal, simplification and optimization of the current algorithm is needed and a proper hardware system platform is desired to implement the algorithm.

On the other hand, as discussed in Chapter 2, although most biomedical and biomechanical studies still focused on the measurement of the walking speed from straight line walking trials, such as treadmill walking and 10MWT, the research should start to focus on enabling the three-dimensional motion monitoring capability, for which some of the tools are already available, e.g. Euler angles, quaternion and direction cosine rotation representations for inertial sensor orientation determination. This improvement will significantly extend the biomedical and biomechanical researches and provide more accurate and comprehensive measurement, such as stride width and walking path.

Appendix A

Experimental Procedure

The research experiments presented in this thesis were carried out with two different IMUs: Inertia-Link from MicroStrain and Xsens MVN from Xsens Technology. As we only care about the raw inertial data provided by the IMUs, a simple calibration procedure was implemented:

- The subject was instructed to stand still with the shank segment perpendicular to the level floor;
- The IMU was attached to the mid-way of the shank on the lateral side using rubber stripe or athletic tape (Figure A.1);
- The data acquisition program was running to provide the instantaneous IMU measurement, and The IMU was adjusted such that the horizonal acceleration measurement was approximately $0g$ and the vertical acceleration measurement was approximately $1g$.

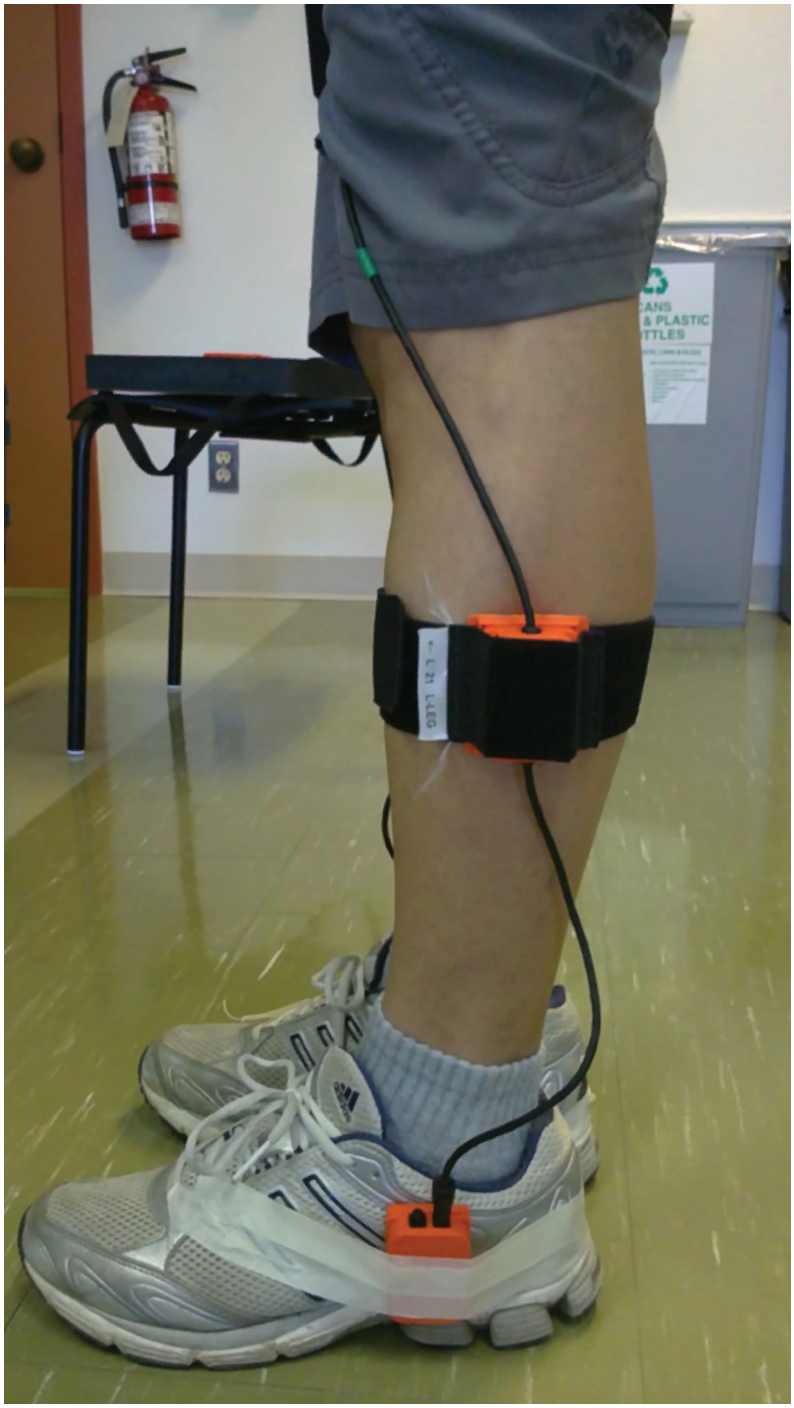

Figure A.1: Shank-mounted IMU based walking speed estimation method sensor configuration.

Appendix B

Signal Processing

The sensor signal conditioning and data processing were all implemented in MATLAB (The MathWorks, Natick, MA, USA). In general, the processing method was selected as follows.

Table B.1: Signal Conditioning and Data processing.

Sampling rate	$100Hz$
Interpolation	One-dimensional linear interpolation
Filtering	Second order low-pass Butterworth filter with cut-off frequency $2.5 \sim 10Hz^*$
Integration	Trapezoidal numerical integration
Optimization	Unconstrained nonlinear minimization (FMINUNC)

* Cut-off frequencies are selected based on the fact that the human walking gait follow a stride frequency of 1 to $2Hz$, while the sensor noise is much high than that.

Appendix C

Estimation Algorithm

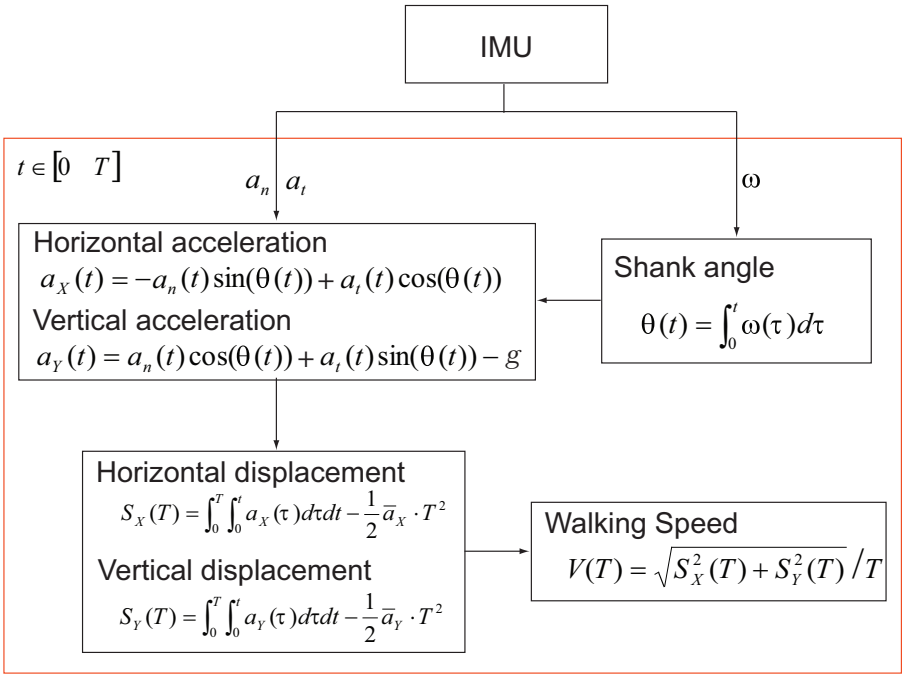

Figure C.1: Shank-mounted IMU based walking speed estimation algorithm flowchart.

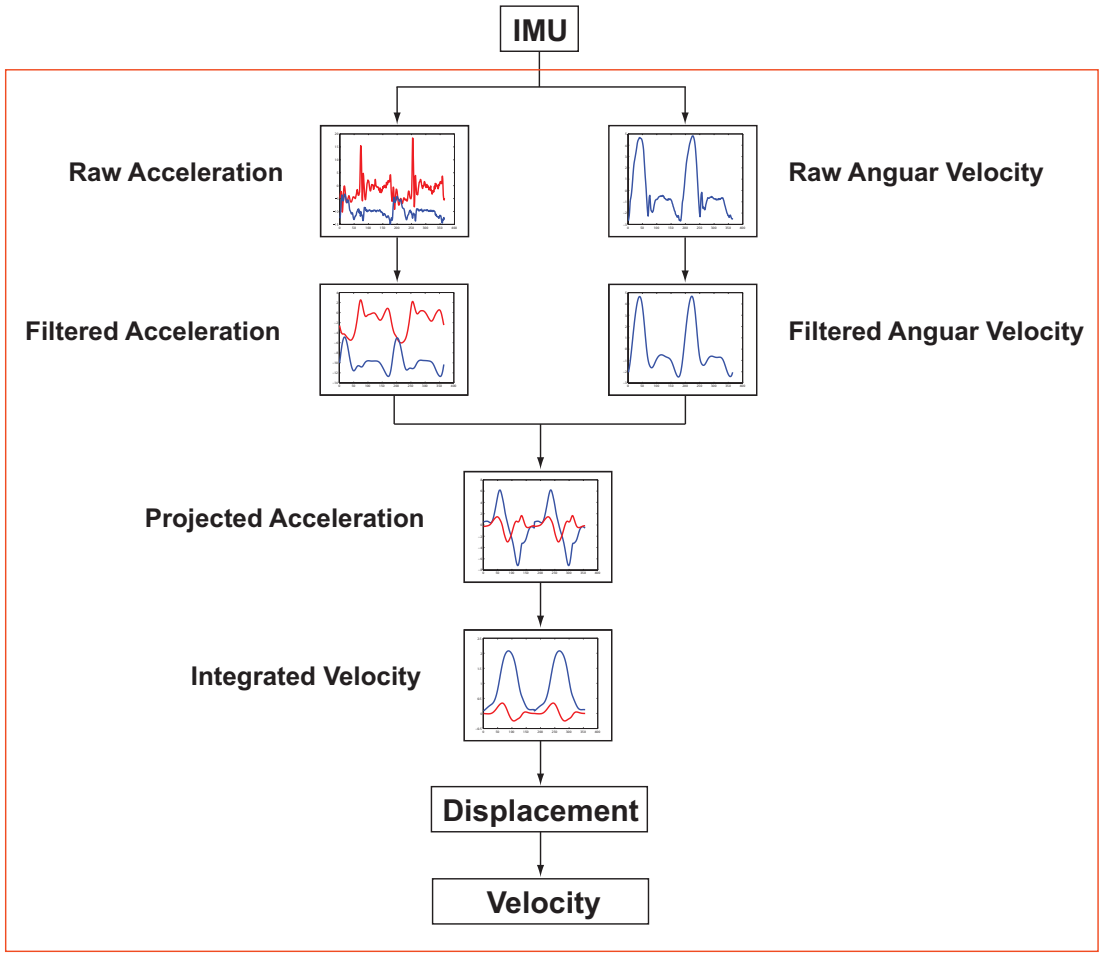

Figure C.2: Shank-mounted IMU based walking speed estimation signal processing flowchart.